

Search for Particles with Anomalous Charge in the IceCube Detector

Ward Van Driessche



Search for Particles with Anomalous Charge in the IceCube Detector

Ward Van Driessche

Auteur

DATUM

Goedgekeurd door

prof. dr. D. Ryckbosch
Thesis Promotor

Aanvaard door

???

Hoofd Examenjury

Promotor: prof. dr. D. Ryckbosch

Proefschrift ingediend tot het verkrijgen van de academische graad van
Doctor in de Wetenschappen: Fysica en Sterrenkunde

Leden van de examenjury:

Prof. dr ... (Universiteit ???)

Vakgroep Fysica en Sterrenkunde
Faculteit Wetenschappen
Universiteit Gent
Academiejaar 2018-2019



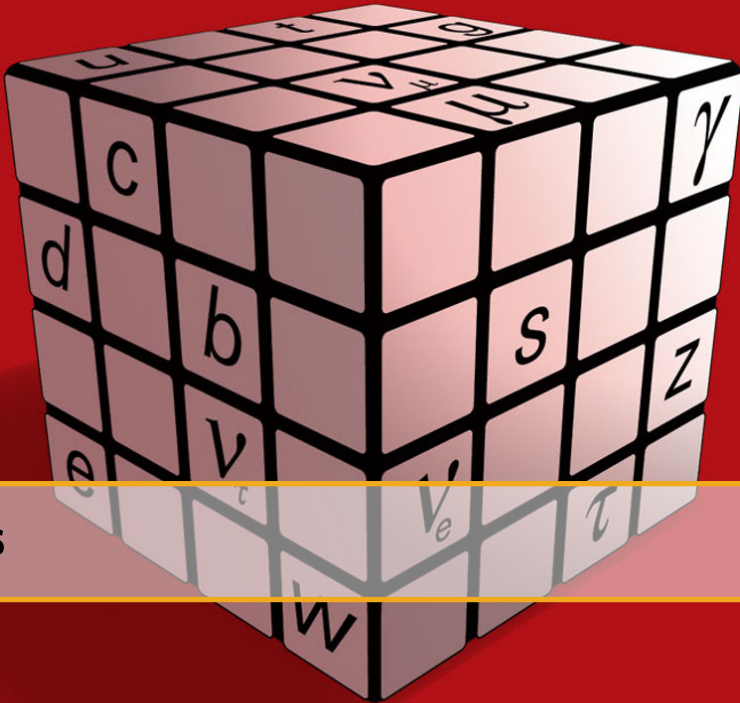


Table of Contents

Nederlandstalige samenvatting 5

Introduction 7

I

Theory and Experiment

1	The Standard Model of Particle Physics	11
1.1	What we call matter: fermions	11
1.1.1	Leptons	12
1.1.2	Quarks	13
1.2	How particles communicate: interactions	13
1.2.1	Gravity	13
1.2.2	Electromagnetism	14
1.2.3	Weak force	15
1.2.4	Strong force	15
1.2.5	A note about bosons	15
1.3	The Standard Model in theory	16
1.3.1	SU(3): quantum chromodynamics	17
1.3.2	SU(2) \times U(1): electroweak	17
1.3.3	Brout-Englert-Higgs mechanism	18
1.3.4	Particle mixing	21
1.4	A success story	23
1.4.1	Predictions	24
1.4.2	Precision tests	24
1.5	The need for physics beyond the Standard Model	25
1.5.1	Unifying theories	28
1.5.2	How to look for new physics	29
2	Motivation of the Analysis	31
2.1	Introduction	31

2.2	Theory	31
2.3	Previous searches	32
2.3.1	Searches with accelerators and fixed targets	32
2.3.2	Colliders	33
2.3.3	Searches for particles with telescopes	33
2.4	Properties of the signal	34
3	Cosmic Rays and Neutrinos	37
3.1	Cosmic rays	37
3.1.1	Discovery of cosmic rays	37
3.1.2	What are cosmic rays?	38
3.1.3	Acceleration mechanism	43
3.1.4	Propagation	48
3.2	Air showers	49
3.2.1	Hadronic component	49
3.2.2	Muonic component	50
3.2.3	Electromagnetic component	50
3.3	Neutrinos	51
3.3.1	Conventional	51
3.3.2	Prompt	52
3.3.3	Astrophysical	53
3.3.4	Other neutrino sources	53
4	Relativistic Particles in Matter	55
4.1	Cherenkov effect	55
4.2	Neutrino interactions	57
4.3	Propagation	58
4.3.1	Cascades	58
4.3.2	Muon tracks	59
4.4	Energy loss formulae	61
4.4.1	Ionization	61
4.4.2	Bremsstrahlung	62
4.4.3	Inelastic component	63
4.4.4	Photonuclear	63
4.4.5	Pair production	63
4.4.6	Conclusion	64
5	The IceCube Experiment	65
5.1	Geometry	65
5.1.1	In-ice array	67
5.1.2	DeepCore	67
5.1.3	IceTop	67
5.1.4	IceCube coordinate system	68
5.2	Hardware components	69
5.2.1	Digital optical modules	69
5.2.2	Calibration	71
5.2.3	Cable systems	71
5.2.4	IceCube laboratory	71

5.3	Deployment	73
5.4	Data taking	73
5.4.1	Triggers	73
5.4.2	Filters	75
5.4.3	Data handling	76
5.5	Antarctic ice	76
5.5.1	Ice simulation	76
5.5.2	Systematic uncertainties	77
5.6	IceCube event topology	78
5.7	Future upgrades	78
5.7.1	IceCube Upgrade	79
5.7.2	IceCube Gen2	79
5.8	Beyond the Standard Model searches	81
5.8.1	Lorentz invariance violation	82
5.8.2	Dark matter	82
5.8.3	Magnetic monopoles	83
5.9	Discussion	84
	Bibliography	85

Nederlandstalige Samenvatting

Denkt aleer gij doende zijt en doende, denk dan nog ~ Guido Gezelle

De aanpak om nieuwe dingen te ontdekken binnen de fysica is de laatste eeuwen sterk geëvolueerd. De overgang van eenvoudige verklaringen naar theorieën die fenomenen niet alleen konden uitleggen, maar ook experimenteel konden reproduceren, bleek een cruciale stap naar een nieuwe methode in fysisch onderzoek. Als gevolg bracht deze methode nieuwe voorspellingen met zich mee; een theorie kon iets verklaren maar ook fenomenen beschrijven die tot dan toe nog niet werden geobserveerd. Deze fenomenen werden nadien ofwel waargenomen ofwel werd de theorie weerlegd. Hieruit volgde een natuurlijke evolutie in aanpak waarbij theorie en experiment elkaar horen te bevestigen.

In de loop van de 20ste eeuw viel er door de technologische ontwikkelingen veel te ontdekken. Men begon langzamerhand beter te begrijpen hoe de wereld in elkaar zit en hoe de wetten van de fysica neergeschreven konden worden. Wiskunde was daarin de taal van fysici om een theorie te ontwikkelen en experimenten te beschrijven. Experimentele deeltjesfysica kende zijn (eerste) hoogdagen in de jaren '60 waarbij deeltjesversnellers het ene na het andere nieuwe deeltje ontdekten: de "particle zoo". Fysici drongen aan op een theorie die een beter beeld kon geven; een handvol basisstenen (fundamentele deeltjes) en regels hoe deze deeltjes zich gedragen en hoe ze tot uiting komen. Die theorie werd de daaropvolgende jaren ontwikkeld en is gekend als het *standaardmodel van de deeltjesfysica*. Het blijkt tot op heden een van de meest succesvolle ooit binnen het vakdomein van de fysica.

Met de ontdekking van het Brout-Engler-Higgs deeltje in 2012 werd de laatste bouwsteen, die door het standaardmodel voorspeld was, gevonden. Het model verklaart echter niet alles. We hebben bijvoorbeeld nog geen idee wat donkere materie precies is, waarom er zoveel minder antimaterie is in vergelijking met materie, enzovoort. Ook de schijnbaar wiskundige willekeur in het standaardmodel roept tot op heden nog steeds vragen op. Er lijken drie types leptonen te zijn. Waarom drie? En waarom zijn er welbepaalde symmetrieën die het standaardmodel beschrijven terwijl er ontelbaar veel andere symmetrieën mogelijk zijn? Waarom deze niet? Om deze redenen proberen fysici in experimenten op zoek te gaan naar processen die met de huidige, aanvaardde modellen nog niet beschreven kunnen worden. Dit zou ons een betere controle kunnen geven welk soort nieuwe theorie - waar er honderden van zijn - de juiste is. Deze experimenten worden steeds complexer: ze worden groter of miniteuzer en veelal een combinatie van beide. Deze complexiteit brengt een groter kostenplaatje met zich mee waardoor deze projecten goed beargumenteerbaar moeten zijn: ze zijn een gerichte tast in het duister.

Er zijn ook andere experimenten die met de waarnemingen van gekende deeltjes proberen om beter te achterhalen hoe bepaalde processen in ons universum tot stand komen. Een voorbeeld hiervan is het IceCube neutrino observatorium dat gesitueerd is in het ijs centraal op de Zuidpool. Het voornaamste doel van dit experiment is om gebruik te maken van neutrino's, deeltjes die zelden met materie interageren en net daarom een grote bron aan informatie bevatten omdat ze veel vertellen over hun oorsprong. We weten tot op heden nog maar weinig over de precieze werking van de bronnen van deze neutrino's.

Om zoveel mogelijk gebruik te maken van bestaande infrastructuur worden bestaande detectoren zoals IceCube ook gebruikt in zoektochten naar nieuwe fysica. Het doel van dit werk is om met behulp van het IceCube experiment na te gaan of er deeltjes bestaan met een electromagnetische lading die het standaardmodel niet voorspelt.

Het IceCube experiment werkt met behulp van lichtgevoelige modules die per 60 aan een kabel bevestigd zijn. 86 van zo'n kabels zijn verspreid in een hexagonaal vlak in het ijs dat in het totaal ongeveer een kubieke kilometer van volume inneemt. Geladen deeltjes zoals electronen en muonen die uit een neutrino-interactie kunnen komen, produceren licht in het ijs dat door deze modules waargenomen kan worden. Dit fenomeen is gekend als het Cherenkov-effect en zegt dat de hoeveelheid licht dat geproduceerd wordt afhangt van de lading van het deeltje. Aangezien de enige vrije deeltjes die we kennen een lading hebben die een veelvoud is van de elementaire lading van een elektron e , is het in theorie mogelijk om een onderscheid te maken tussen de gekende deeltjes en deeltjes met een lading die lager is dan e . Deze laatste maken geen deel uit van het standaardmodel en hun observatie zou een nieuwe start kunnen geven naar een meer omvattende theorie die mogelijks andere onopgeloste vragen helpt te verklaren.

De voornaamste uitdaging om op zoek te gaan naar dergelijke deeltjes blijkt de beperking van de detector zelf te zijn. Gekende deeltjes met een hele lage energie blijken niet eenvoudig te onderscheiden van deeltjes met een lage lading. Dit komt voornamelijk omdat de modules van de detector minimaal 17 meter van elkaar liggen. Hierdoor gaat veel van het licht verloren omdat het de optische instrumenten niet kan bereiken. In dit werk wordt er beschreven hoe deze nieuwe deeltjes onderscheiden kunnen worden van muonen en elektronen. Deze laatste ontstaan uit botsingen van kosmische straling met onze atmosfeer waar ze veelvuldig worden geproduceerd in zogenoemde "air showers". Ze kunnen ook de detector betreden als secundaire deeltjes nadat neutrino's interageren met het ijs. Deze neutrino's kunnen geproduceerd worden in kosmische processen zoals gamma ray bursts of supernova's, maar zijn er vooral in grote getale aanwezig door de voorgenoemde air showers.

De analyse beschrijft hoe er vanuit de IceCube data een selectie gemaakt kan worden om deze nieuwe fysica - als ze er is - zo goed mogelijk zichtbaar te maken. Na een reeks selecties om de kwaliteit van de data te verhogen, werden meerdere variabelen gebruikt en ontwikkeld om nadien geïmplementeerd te worden in een "Boosted Decision Tree", i.e. een machine learning techniek die wordt gebruikt in datamining. Er werd tevens ook gebruik gemaakt van een resampling techniek genaamd "pull-validation" om de beperkte statistische mogelijkheden beter te handhaven. De enige mogelijke conclusie die getrokken kon worden was dat er geen indicatie was voor de aanwezigheid van deeltjes met een lage lading. Er werd een bovenlimiet opgesteld waarbij ook rekening gehouden werd met meerdere onzekerheden die deze limiet zouden kunnen beïnvloeden zoals de eigenschappen van het ijs waardoor het licht schijnt. Deze limieten zijn een verbetering van voorgaande experimenten en werden berekend volgens de techniek van Feldman en Cousins binnen een 90% betrouwbaarheidsinterval.

Dit werk was een eerste poging om gebruik te maken van het IceCube experiment om op zoek te gaan naar nieuwe fysica in de vorm van deeltjes met een lading die tot op heden nog nooit zijn geobserveerd. Dergelijke deeltjes werden niet waargenomen waardoor een bovenlimiet werd opgesteld in de mate van hun aanwezigheid mochten ze weldegelijk bestaan.



Scientists have become the bearers of the torch of discovery in our quest for knowledge ~ Stephen Hawking

Having a quest for knowledge seems to be a trait that belongs to human kind. The last couple of centuries there was a transition from providing simple explanations of physical phenomena to *really understanding* the problem and properly describing it. More and more, a critical mindset became important in having new insights; being convinced of having the final answer is no longer enough. Theories are tested and are only accepted if they can be reproduced in experiments. This approach is not the most easy one and more than often, scientists encounter many obstacles along their way. However, I believe that the feeling scientists get when they have solved a puzzle and see their theory confirmed in an experiment is to be the driving force behind new discoveries and pushing the limits of current theories. Wanting to know what is beyond our current understanding has made us discover our planet (and others) and never stops us to come up with new questions.

Experimental particle physics is a field that tries to find the smallest detectable particles that make up matter and radiation. These particles carry certain properties such as mass, charge, spin, etc. and allow them to interact with each other. There are only a handful of fundamental interactions known to date: gravity, the strong force, the weak force and the electromagnetic force. It appears that nature follows certain physical rules that can be expressed in a mathematical form. Mathematics made it possible to write down our findings and to expand our knowledge. The theory that describes the last three of the four forces and classifies all known fundamental particles is called the Standard Model (SM) of particle physics. In Chapter 1, an overview is given of the properties of particles and interactions and ends with why we think the SM in its current form cannot be the final answer.

There are many theories that try to expand the SM and are called “Beyond-the-Standard-Model theories” (BSM). They introduce new symmetries, new particles, new interactions, etc. Some of these theories also predict the existence of free particles with an electromagnetic charge that is lower than the electron charge, e . Quarks are known to have charges lower than e , but cannot exist freely. In Chapter 2 we motivate the possible existence of these particles and describe their assumed properties.

With the discovery of cosmic rays a new field of physics was born: astroparticle physics. Research could be done on particles that could not originate from our solar system. The energy of these particles also has a wide energy range and offers to examine particles with a very high energy that do not have to be accelerated by man-made objects. For example, positrons, muons, pions, and kaons were first discovered in cosmic ray interactions. Cosmic rays can also help us learn about distant objects in the universe together with electromagnetic radiation, gravitational waves and neutrinos. Neutrino astronomy is only feasible with gigaton detectors. Luckily, neutrino observatories can also be used for BSM experiments. In Chapter 3, we give an overview of the physical processes that are visible in the detector. We will describe the origin of cosmic rays and neutrinos and how showers of particles are produced from cosmic ray interactions. These phenomena have to be accounted for when searching for rare exotic particles.

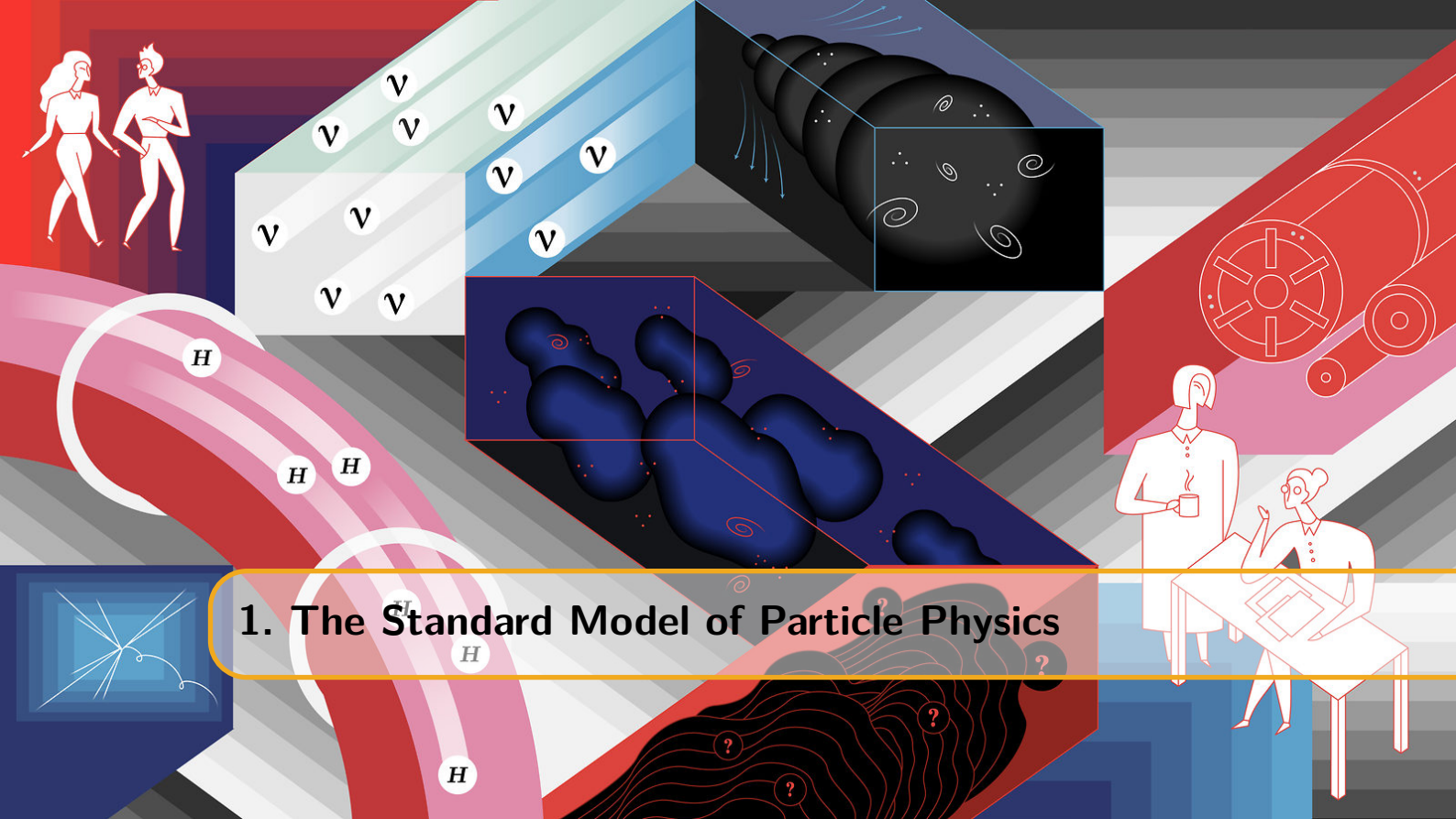
Charged particles can be detected by the production of Cherenkov radiation. These particles can be exotic particles, particles produced in cosmic air showers or secondaries that are created from neutrino interactions. The Cherenkov effect is explained in Chapter 4, together with how charged particles lose their energy when traveling through a medium. To be able to detect high energetic neutrinos it is crucial to make the instrumented volume of a detector as large as possible. In Chapter 5, we describe how the IceCube Neutrino Observatory is constructed in the South Pole ice. We describe the hardware components and how the ice is used and modeled for neutrino and charged particle detection.

The next part of this work has a larger focus on the technical details of the analysis. The simulation steps are discussed in Chapter ?? and several analysis techniques that were used in this work are explained in Chapter ?? . Finally, in Chapter ?? an overview of the analysis is given and how it was possible to discriminate background events from events that originate from particles with an anomalous charge.

Chapter ?? provides a summary and discussion of the work.

Theory and Experiment

1	The Standard Model of Particle Physics	11
1.1	What we call matter: fermions	
1.2	How particles communicate: interactions	
1.3	The Standard Model in theory	
1.4	A success story	
1.5	The need for physics beyond the Standard Model	
2	Motivation of the Analysis	31
2.1	Introduction	
2.2	Theory	
2.3	Previous searches	
2.4	Properties of the signal	
3	Cosmic Rays and Neutrinos	37
3.1	Cosmic rays	
3.2	Air showers	
3.3	Neutrinos	
4	Relativistic Particles in Matter	55
4.1	Cherenkov effect	
4.2	Neutrino interactions	
4.3	Propagation	
4.4	Energy loss formulae	
5	The IceCube Experiment	65
5.1	Geometry	
5.2	Hardware components	
5.3	Deployment	
5.4	Data taking	
5.5	Antarctic ice	
5.6	IceCube event topology	
5.7	Future upgrades	
5.8	Beyond the Standard Model searches	
5.9	Discussion	
	Bibliography	85



1. The Standard Model of Particle Physics

A physicist is an atom's way of knowing about atoms ~ George Wald

The aim of this chapter is to give a summary of the framework that is used in particle physics. This framework was developed in stages throughout the latter half of the 20th century and is known as the Standard Model of particle physics. This model is a quantum field theory that is able to describe most of what is seen in particle physics experiments, and proved to be successful in predicting later experimental discoveries. In this chapter, a brief historical overview of the development of this theory will be given together with a limited description in order to familiarize the reader with concepts that will be used throughout this work. For a more in-depth and exhaustive discussion I refer to Refs. [1, 2, 3, 4]. We start with an overview of the constituent particles of the Standard Model, linking them to our everyday life. Secondly, a general description is given of the nature of forces. Thirdly, we go to a more mathematical and in-depth description of the Standard Model. Lastly, we present the many successes of this model and finish with an argumentation of why there is a need for physics beyond this model.

1.1 What we call matter: fermions

Physics (from Ancient Greek: φυσική - *physikē*, “knowledge of nature”) is the natural science that studies matter. Matter is made up of *atoms* (from Greek: *atomos** , “indivisible”) that can bind together into molecules and account for what is around us in our everyday life. Atoms are made up of a positively charged *nucleus* that is surrounded by one or more *electrons*. The nucleus and electrons are bound to each other via the electromagnetic force. The nucleus is made up of one or more *protons* and, typically, an approximately equal amount of *neutrons*. Because of their similar characteristics, protons and neutrons are often referred to as *nucleons* and together they make up more than 99.9% of an atom’s mass. Nucleons are made up of smaller particles called *quarks*[†], which are, as far as we know, *fundamental particles*. This means that

*Coined by ancient Greek philosophers Leucippus and his pupil Democritus who believed matter was made up of discrete units.

[†]The word “quark” originally appeared in the novel *Finnegans Wake* written by the Irish author James Joyce (1882–1941). The protagonist of the book dreams that he is serving beer to a drunken seagull. Instead of asking for “three quarts for Mister Mark” the inebriated bird says “three quarks for Muster Mark”. Murray Gell-Man had the habit of using names like “squeak” and “squark” for peculiar objects and after encountering the sentence in the book the name struck him as appropriate since the (then hypothetical) particle came in threes.

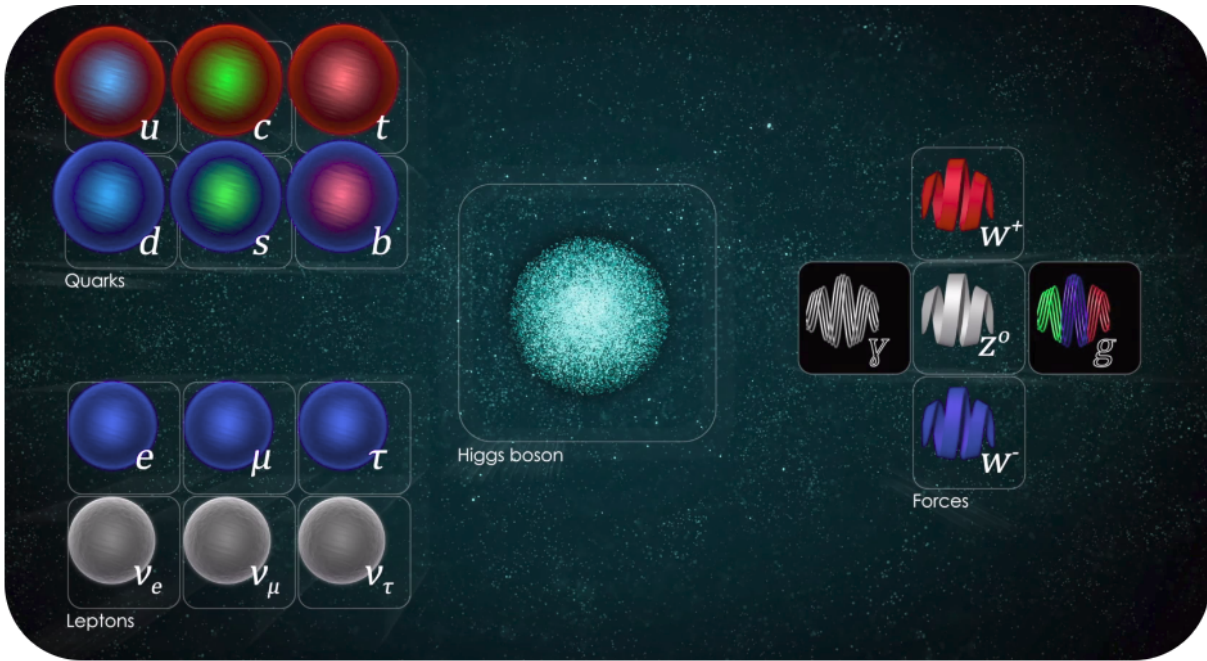


Figure 1.1: The Standard Model of particle physics distinguishes fermions (left) from bosons (right). The Brout-Englert-Higgs boson (middle) is more peculiar as it has no intrinsic spin and plays a special role in the theory. Charges for fermions are not explicitly written to account for antiparticles. Illustration from Ref. [5].

we believe that there are no smaller substructures making up these objects and they are in essence mathematically best described as infinitely small. Because of this, they are often referred to as pointlike. In the Standard Model (SM), these particles are found to be *fermions*, which have odd half-integer spins, obeying the laws of quantum mechanics. The spin of a particle is often illustrated with its classical counterpart in which an object is spinning and thus carries an intrinsic angular momentum. This analogy cannot be extrapolated to pointlike particles, but the property happens to hold the same units as the classical orbital momentum. The spin of a particle seems to be just another property particles have, like charge or mass. Fermions follow Fermi-Dirac statistics and therefore obey the Pauli exclusion principle. As a consequence, fermions cannot occupy the same place at the same time (more formally: no two fermions may be described by the same quantum numbers). This agrees with our macroscopic observations of matter in everyday life: matter interacts with matter; people cannot walk through walls!

In total, the SM distinguishes 24 different fermions that can be subdivided into two distinct classes: *quarks* and *leptons*. There are six quarks (up, down, charm, strange, top and bottom), and six leptons (electron, electron neutrino, muon, muon neutrino, tau and tau neutrino), along with the corresponding antiparticle for each of these fermions. A summary of all the particles in the Standard Model is given in Figure 1.1.

1.1.1 Leptons

Leptons* can be subdivided in two classes: electromagnetically charged particles (e^- , μ^- and τ^-) and the neutral neutrinos† (ν_e , ν_μ and ν_τ). Because of their charge, electrons are the well known particles that combine together with nucleons into atoms. Being the lightest of the three charged leptons, the electron is said to be part of the first *generation*, together with the electron

*λεπτός (leptos) meaning thin, delicate, lightweight, or small. Originally leptons were considered the “light” particles and hadrons the “heavy” particles, but the discovery of the tau lepton in 1975 broke that rule.

†The Italian word for neutron (neutrono) sounds like the word neutral (neutro) with an augmentative suffix (-one) tacked on the end, making the word a little wordplay. In Italian, it sounds something like “big neutral”. Replace the augmentative suffix -one with the diminutive suffix -ino and you have a “little neutral”, which is a good description of what a neutrino is — a diminutive neutral particle.

neutrino. Muons differ only from electrons in mass* and make up the second generation together with muon neutrinos. Similarly, tau particles and tau neutrinos define the third generation. All leptons have a corresponding antiparticle indicated by a positive charge (e.g. e^+) or a bar (e.g. $\bar{\nu}_e$). Neutrinos are proven to have a very small mass [6] and interact only via the weak force (Section 1.2.3), making them inherently very hard to detect.

1.1.2 Quarks

The six quarks are called up, down, charm, strange, top and bottom quarks ((u, d), (c, s), (t, b)). Each generation is made up of a particle with charge $+1/3$ and one with $-2/3$ (also visualized in Figure 1.1). These charges are multitudes of the absolute electron charge. The difference between generations is again essentially the bare mass of the particles. Because quarks also interact through the strong force (see Section 1.2.4), they combine into *hadrons*[†] (of which nucleons are the best known examples). Due to their color charge and the intrinsic behaviour of the strong force, quarks cannot be observed freely: they always combine into color neutral particles, a property called *confinement*. When a hadron, with its constituent quarks, is pulled apart, the attractive force between the quarks does not fall down rapidly since gluons carry color charge themselves. When these particles are pulled apart far enough, it becomes energetically more favorable to produce new quark-antiquark pairs, which again combine into color neutral particles[‡]. The energy requirement for the production of new particles is far below the one to separate the quarks far enough from each other to observe them separately. Antiquarks are again denoted with a bar (i.e. \bar{u}).

Because of their ability to interact via the strong force, particle accelerators in the 1960s led to the discovery of a plethora of possible quark combinations, something that is often referred to as the “particle zoo”.

1.2 How particles communicate: interactions

There are four fundamental interactions known to exist: gravity and electromagnetism, which produce significant long-range forces, and the strong and weak forces that only express themselves at (sub)atomic distances and govern nuclear interactions. These are explained in more detail below and an overview is given in Table 1.1.

Particles interact with each other through the exchange of *gauge bosons* or *force carriers*[§]. Gauge bosons are bundles of energy, *quanta*, and can be seen as excitations of one of the force fields.

Fields are a mathematical approach used by physicists to describe what we observe in experiments. Although the use of fields is very natural, the concept might feel a bit unfamiliar. In the following, the known forces are described in more detail. Gravity plays less of a role in subatomic physics, but is added for completeness and is mainly used to make the reader more familiar with the concept of a field.

1.2.1 Gravity

Gravity (from Latin/old French: *gravitas*/grave, “weighty, heavy”) is the phenomenon wherein massive objects are attracted to each other. Gravitation is famously described by the general theory of general relativity proposed by Einstein in 1915. Compared to the other forces, gravity is intrinsically very weak[¶] and is not described in the SM (see Section 1.3). This is why gravity

*This characteristic is often referred to as *lepton universality*.

[†]ἀδρός (adros) meaning thick, robust, massive, or large. This name alludes to the ability of the point-like quarks to bind together and form particles that are massive in a certain sense.

[‡]This process is called *hadronization* and results into the production of “jets” in particle accelerators [7].

[§]A classic and very simplistic way of looking at force carriers is to imagine two people standing on a boat. The force carrier is a heavy ball that can be thrown from one person to the other. Doing so, both persons will move in opposite direction.

[¶]Two magnets that fit in the palm of your hand can deliver a force which is of similar strength as the force that our entire planet exerts on a human body.

Table 1.1: Summary of the known forces and their properties. The relative strength is compared to the electromagnetic force, but also depends on the energy scale.

Interaction	Gravitational	Weak	Electromagnetic Electroweak	Strong
Acts on	mass/energy	weak flavor	electric charge	color charge
Couples to	all particles	all fermions	electrically charged particles	quarks, gluons
Mediation	not yet observed	W^+, W^-, Z	γ	gluons
Rel. strength	10^{-35}	10^{-11}	1	10^2

is often left out in discussions of particle physics experiments, but is crucial for understanding astronomical objects and how they influence each other. It can, however, be used to explain the concept of a field in a very natural way.

A very good description of gravitation was already provided centuries ago. First published on July 5th, 1686 was Newton's work *Philosophiae Naturalis Principia Mathematica* ("the Principia") that first introduced formula that are still widely used today. The equation of the force exerted by two massive bodies takes the following form,

$$F = G \frac{m_1 m_2}{r^2}, \quad (1.1)$$

where F is the gravitational force acting between two objects, m_1 and m_2 are the masses of the objects, r is the distance between their center of mass, and G is the gravitational constant.

Newton's law states that two massive bodies will exert a force on one another which is proportional to their masses, but inversely proportional to the square of the distance between them. Newton realized this would mean that at any given instant in time all massive objects in the universe would know from every other object in the universe where it is located and how massive it is*. Because of this, Newton himself believed his explanation could not be the final answer. The answer is fully described in Einstein's work of general relativity, but the first idea in the right direction was introduced by Laplace in 1783. Laplace explained that massive objects do not "feel" each other but distort space and time in such a way that objects that are attracted, "fall" towards each other. Field theory makes it possible to treat the laws of physics as a local property instead of an action from a distance.

To date, it has not been possible to describe gravity in the framework of quantum field theory like the other fundamental forces, although, there is still much ongoing work. The gauge bosons from such a quantum field theory for gravity are mostly referred to as *gravitons*.

1.2.2 Electromagnetism

The electromagnetic field (from Ancient Greek: ἥλεκτρον *ēlektron*, "amber", and μαγνῆτις λίθος, *magnetis lithos*, which means "Magnesian stone"[†]) presents itself in the electrical and magnetical forces. In the late 1870s, the publication of Maxwell's *A Treatise on Electricity and Magnetism* showed that the electric and magnetic interactions of negative and positive charges are mediated by one force: electromagnetism. Particles carrying a charge of one of these forces can attract or repel each other.

Similar to the gravitational field, the electromagnetic field pervades all around us, providing the necessary description of how charged particles interact with each other. The interaction of nuclei, which have a positive electric charge, and electrons makes up most of what is described in chemistry.

The force carrier of electromagnetism is called a *photon*, or in other words: light.

*Imagine the attraction of the Moon to the Earth: how are both "communicating"?

[†]In 1641, Kircher described the magnetic properties of the Magnesian stone in his book *Magne sive de arte magnetica opus tripartitum* [8].

1.2.3 Weak force

The weak force is one aspect of the overarching electroweak theory that combines electromagnetism and the weak force. As opposed to gravity and electromagnetism, it only takes place at very small subatomic distances*. One well known phenomenon that is governed by the weak force is *beta decay* in which free neutrons decay into protons and produce an extra electron and antielectron neutrino. Another beautiful example of the weak force is the driving mechanism in the Sun's thermonuclear process that makes it shine. This process cannot be explained by chemical processes but with the fusion of hydrogen cores into helium where two out of four protons are converted to neutrons. This conversion of the proton into a neutron is explained by the weak force.

The force carriers of the weak force are the W^+ , W^- and Z bosons. Quantum field theory tells us that the interaction strength of particles depends on the coupling constants and the properties of the mediator particles. The coupling constants of the weak force are of similar magnitude than those in electromagnetism. However, because of the mass of the weak force carriers, the interaction strength at low energies, such as radioactive decay, becomes much smaller[†]. This makes the force seem weak, hence the name[‡].

The weak force also has some peculiar properties that are unique in a number of respects:

- it is the only interaction that violates parity symmetry and even does so maximally (V-A interaction),
- its force carriers are massive as opposed to all other force carriers,
- it is the only force capable of changing quarks from one family into a quark of another family.

1.2.4 Strong force

As indicated in Section 1.1, nuclei are made up of protons and neutrons. However, up to now the forces described in this section cannot explain how they can make up a stable combination. The positive/neutral electromagnetic charge of the protons/neutrons would even suggest the opposite. Protons and neutrons are made up by quarks that carry a quantity called *color charge*. Particles carrying a color charge participate in interactions of the strong force. Due to the principle of *self interaction*, the strong force only manifests itself on very small scales[§].

The force carriers of the strong force are called *gluons*. These gluons carry a color charge themselves and are massless.

Aside from holding nucleons together, the strong force is also responsible for around 99% of the mass of the nucleon's mass. The massless gluons have a *quantum chromodynamics binding energy* so large that it makes up the bulk of the mass via Einstein's $E = mc^2$ relation. Only a small percentage of the total nucleon mass comes from the bare quark masses.

1.2.5 A note about bosons

As opposed to fermions, which obey Fermi-Dirac statistics and cannot occupy the same quantum state, bosons follow Bose-Einstein statistics[¶]. Bosons carry integer spins ($s = 0, 1, 2$, etc.) while fermions carry half-integer spins ($s = 1/2, 3/2$, etc.). As a result, bosons have no problem occupying the same place at the same time (more formally: two or more bosons may be described

*The reason being is that the force carriers are massive; more info in Section 1.3.

[†]The mediator term for photons scales with $\frac{1}{q^2}$ with q the momentum of the mediator. W and Z boson mediator terms scale with $\frac{1}{q^2 - M^2}$ with M the mass of the particle. When q is low, for example in radioactive decays, this term becomes very small due to the mass of the bosons. On the other hand, if q and M are of similar magnitude, the weak force is strong. For example, the top quark decay will most likely happen via the weak force.

[‡]It was Fermi who first came up with a proper description of the beta decay in 1933. However, he described the interaction as a 4-point interaction, making it only valid up to energies below 100 GeV.

[§]As opposed to the weak force where the short distance behaviour is explained due to the mass of the force carriers.

[¶]The name "boson" originates from Dirac who wanted to commemorate the contributions of Indian physicist S.N. Bose who, together with Einstein, theorized the characteristics of elementary particles that follow Bose-Einstein statistics [9].

by the same quantum numbers). As an example, lasers are very powerful tools that make large numbers of photons to have almost exactly the same energy (which is expressed in having the same color) and direction. Fermions, on the other hand, cannot share the same quantum number, e.g. electrons cannot have the same orbit in an atom. If electrons were bosons, chemistry and matter all around us would be nothing like we see today.

1.3 The Standard Model in theory

Most of the text below is based on the very elaborate book from Franz Mandl and Graham Shaw, *Quantum Field Theory* [10].

The Standard Model is a *quantum field theory*, meaning its fundamental objects are fields of a quantum nature that are defined at all points in spacetime. These fields are

- fermion fields, ψ , which describe “matter particles”;
- electroweak boson fields, W^1, W^2, W^3 and B ;
- gluon fields, G^a ; and
- the Higgs field, ϕ .

Quantum field theory treats particles as excited states of one of these underlying fields, so called *field quanta*. The difference between classical and quantum fields is that they are operator-valued. Classical fields can in principle take on distinct values at each point in space whereas a quantum field accommodates observations of quantum mechanics such as

- objects have characteristics of both particles and waves (called “wave-particle duality”);
- the quantization of energy, meaning that only discrete energy values are possible;
- the lowest achievable energy is not equal to absolute zero, but has a zero-point energy*.

The dynamics of the quantum state and the fundamental fields are determined by the Lagrangian density \mathcal{L} . Writing the time and space coordinates in the form $(t, \mathbf{x}) = (x^0, x^1, x^2, x^3) = x^\mu$, the equations of motion of these fields can be written as:

$$\frac{\partial}{\partial x_\mu} \left[\frac{\partial \mathcal{L}}{\partial (\partial \phi / \partial x^\mu)} \right] - \frac{\partial \mathcal{L}}{\partial \phi} = 0, \quad (1.2)$$

which follow from the principle of least action. The Lagrangian function depends on the fields and how these fields change in spacetime: $\mathcal{L}(\phi, \nabla \phi)$. Quantization of these fields can be obtained by interpreting the coordinates and momenta as Heisenberg operators, and subjecting these to canonical commutation relations.

Furthermore, the Standard Model is a gauge theory in which the Lagrangian is invariant under certain Lie groups (referred to as the symmetry group or the gauge group of the theory) of local transformations. For quantized gauge groups, the quanta of the gauge fields are referred to as *gauge bosons*. A gauge theory is a mathematical model that has a gauge freedom; there are mathematical degrees of freedom that are redundant. In other words: different mathematical expressions describe the exact same physical system and are in that sense not physical. An experiment could never uniquely determine their values, even in principle[†]. If the phase of the wavefunction is changed by a different amount at each point in spacetime and the physics remains unchanged, the Lagrangian is said to follow a *local phase symmetry*[‡].

The Standard Model is defined by the local $SU(3) \times SU(2) \times U(1)$ gauge symmetry. Each element gives rise to one of the three fundamental forces.

*The zero-point energy follows from the Heisenberg uncertainty principle that states that the position and momentum of a particle are not fixed but have a small range of variance: $\sigma_x \sigma_p \geq \frac{\hbar}{2}$. A system having zero energy would imply a motionless system at a fixed location, violating the uncertainty principle and is therefore forbidden.

[†]Imagine a perfect cylinder that can be twisted without deforming. It is not possible to distinguish a cylinder that has been twisted or not. To be able to determine it, an initial gauge has to be present. A horizontal line drawn on the cylinder can determine if the cylinder has been deformed or not.

[‡]See Ref. [10].

1.3.1 SU(3): quantum chromodynamics

The quantum chromodynamics (QCD) sector defines the interactions between quarks and gluons. Since leptons do not carry color charge, they do not participate in this interaction. The Dirac Lagrangian of the quarks coupled to the gluon fields is given by

$$\mathcal{L}_{QCD} = \sum_{\psi} \bar{\psi}_i \left(i\gamma^\mu \left(\partial_\mu \delta_{ij} - ig_s G_\mu^a T_{ij}^a \right) - m_\psi \delta_{ij} \right) \psi_j - \frac{1}{4} G_{\mu\nu}^a G_a^{\mu\nu}, \quad (1.3)$$

where we sum over the fields of the strong charge and

ψ_i is the Dirac spinor of the quark field (the subscript $i = r, g, b$ represents the color charges);

γ^μ are the Dirac matrices;

G_μ^a is the 8-component ($a = 1, 2, \dots, 8$) SU(3) gauge field;

T_{ij}^a are the 3×3 Gell-Mann matrices (generators of the SU(3) color group);

$G_{\mu\nu}^a$ are the field strength tensors for the gluons;

g_s is the strong coupling constant;

m_ψ corresponds to the quark masses.

1.3.2 SU(2) \times U(1): electroweak

The electroweak (EW) sector is a Yang-Mills gauge theory with the symmetry group $SU(2)_L \times U(1)$. The Lagrangian is given by

$$\begin{aligned} \mathcal{L}_{EW} &= \sum_{\psi} \bar{\psi} \gamma^\mu \left(i\partial_\mu - \frac{g'}{2} Y_W B_\mu - \frac{g}{2} \vec{\tau}_L \vec{W}_\mu \right) \psi - \frac{1}{4} W_a^{\mu\nu} W_{a\mu\nu} - \frac{1}{4} B^{\mu\nu} B_{\mu\nu} \\ &= \bar{Q}_i i D_\mu \gamma^\mu Q_i + \bar{u}_i i D_\mu \gamma^\mu u_i + \bar{d}_i i D_\mu \gamma^\mu d_i + \bar{L}_i (i D_\mu \gamma^\mu) L_i + \bar{e}_{R,i} (i D_\mu \gamma^\mu) e_{R,i} \\ &\quad - \frac{1}{4} W_a^{\mu\nu} W_{a\mu\nu} - \frac{1}{4} B^{\mu\nu} B_{\mu\nu}, \end{aligned} \quad (1.4)$$

where

B_μ is the U(1) gauge field;

Y_W is the weak hypercharge* (the generator of the U(1) group);

\vec{W}_μ is the 3-component SU(2) gauge field;

$\vec{\tau}_L$ are the Pauli matrices (infinitesimal generators of the SU(2) group with subscript L to indicate that they only act on left-chiral fermions);

g' (weak hypercharge) and g (weak isospin) are the U(1) and SU(2) coupling constants respectively;

$W^{a\mu\nu}$ ($a = 1, 2, 3$) and $B^{\mu\nu}$ are the field strength tensors for the weak isospin and weak hypercharge fields;

Q, u and d are the left-handed doublet, right-handed singlet up and right-handed singlet down quark fields;

L and e are the left-handed doublet and right-handed singlet electron fields.

The field strengths are given by

$$\begin{aligned} W_{\mu\nu}^a &= \partial_\mu W_\nu^a - \partial_\nu W_\mu^a + g \epsilon^{abc} W_\mu^b W_\nu^c, \\ B_{\mu\nu} &= \partial_\mu B_\nu - \partial_\nu B_\mu, \end{aligned}$$

and the covariant derivative for the left- and right-handed fermions by,

$$\begin{aligned} D_\mu \psi_L &= \left(\partial_\mu - i \frac{g}{2} \tau_a W_\mu^a - i \frac{g'}{2} Y_W B_\mu \right) \psi_L, \\ D_\mu \psi_R &= \left(\partial_\mu - i \frac{g'}{2} Y_W B_\mu \right) \psi_R, \end{aligned}$$

*The weak hypercharge follows the relation $Y_W = 2(Q - T_3)$ where Q is the electric charge and T_W the third component of the weak isospin.

where one simply has to fill in the appropriate weak hypercharge for the corresponding quark and lepton fields.

It is worth noting that no terms are included for fermion masses. These would have the form of $m\bar{\psi}\psi$ but are forbidden as they would break the $SU(2)_L \times U(1)$ gauge invariance. Neither is it possible to add explicit mass terms for the $U(1)$ and $SU(2)$ gauge fields.

1.3.3 Brout-Englert-Higgs mechanism

To come to a viable description of the elementary particles one is required to introduce masses into a chiral theory. The masses of the W and Z bosons are explained by use of the Brout-Englert-Higgs (BEH) mechanism formulation. Introducing one or more scalar fields, the Higgs fields, which can acquire a vacuum expectation value (vev), make it is possible to spontaneously break a symmetry in the Lagrangian. We say that electroweak symmetry is broken down to a weak symmetry and electromagnetism.

Since the electroweak theory after symmetry breaking should contain three massive gauge bosons (W^+ , W^- and Z), the scalar fields of the Higgs fields should contain at least three degrees of freedom. The simplest approach to do this is by introducing a complex, scalar $SU(2)$ doublet Φ with positive hypercharge ($Y_W = 1$),

$$\Phi = \begin{pmatrix} \phi^+ \\ \phi^0 \end{pmatrix} = \frac{1}{\sqrt{2}} \begin{pmatrix} \phi_1 + i\phi_2 \\ \phi_3 + i\phi_4 \end{pmatrix}, \quad (1.5)$$

Similar to the $SU(2)$ symmetry of the EW theory, four new gauge particles are introduced: H^+ , H^- , H^0 and H .

Massive bosons

Having introduced this scalar doublet, one needs to add the corresponding Lagrangian term to the electroweak Lagrangian from Eq. 1.4,

$$\mathcal{L}_S = (D^\mu \Phi)^\dagger (D_\mu \Phi) - V(\Phi), \quad \text{with } V(\Phi) = \mu^2 \Phi^\dagger \Phi + \lambda (\Phi^\dagger \Phi)^2. \quad (1.6)$$

The first term is the kinetic term while the second corresponds to the potential of the scalar field*. The linear term in the potential needs to be positive to ensure an absolute minimum in the Lagrangian. The quadratic term can either be positive or negative, depending on whether $\mu^2 > 0$ or $\mu^2 < 0$. This is illustrated in Figure 1.2. In the former case the scalar potential has an absolute minimum at the origin:

$$\langle 0 | \Phi | 0 \rangle \equiv \Phi_0 = \begin{pmatrix} 0 \\ 0 \end{pmatrix}. \quad (1.7)$$

From Eq. 1.6 and 1.7, one can see that the kinetic term does not give rise to massive particles in this scenario†. In the case of $\mu^2 < 0$, the minimum is no longer located at the origin of the fields: $\partial_{|\Phi|} V(|\Phi|) = 0$ for $|\Phi| = \sqrt{-\frac{\mu^2}{2\lambda}}$, hence one possible solution is‡

$$\langle 0 | \Phi | 0 \rangle \equiv \Phi_0 = \begin{pmatrix} 0 \\ \frac{v}{\sqrt{2}} \end{pmatrix}, \quad \text{with } v = \sqrt{-\frac{\mu^2}{\lambda}}. \quad (1.8)$$

v is referred to as the *vacuum expectation value* to reflect that the Higgs field is always “on”. To investigate the terms, we can expand the field around the minimum:

$$\Phi(x) = \begin{pmatrix} \theta_2(x) + i\theta_1(x) \\ \frac{v+H(x)}{\sqrt{2}} - i\theta_3(x) \end{pmatrix} = e^{i\theta_a \tau_a} \begin{pmatrix} 0 \\ \frac{v+H(x)}{\sqrt{2}} \end{pmatrix}. \quad (1.9)$$

*The form of the potential is not known from first principles, but is the simplest form that can explain the spontaneous symmetry breaking mechanism.

†Easy to see when substituting $v = 0$ in Eq. 1.13.

‡It is not possible for the charged part of the fields to have a vacuum expectation value as this would not be in agreement with electromagnetism. The upper part in Eq. 1.8 is therefore set to zero.

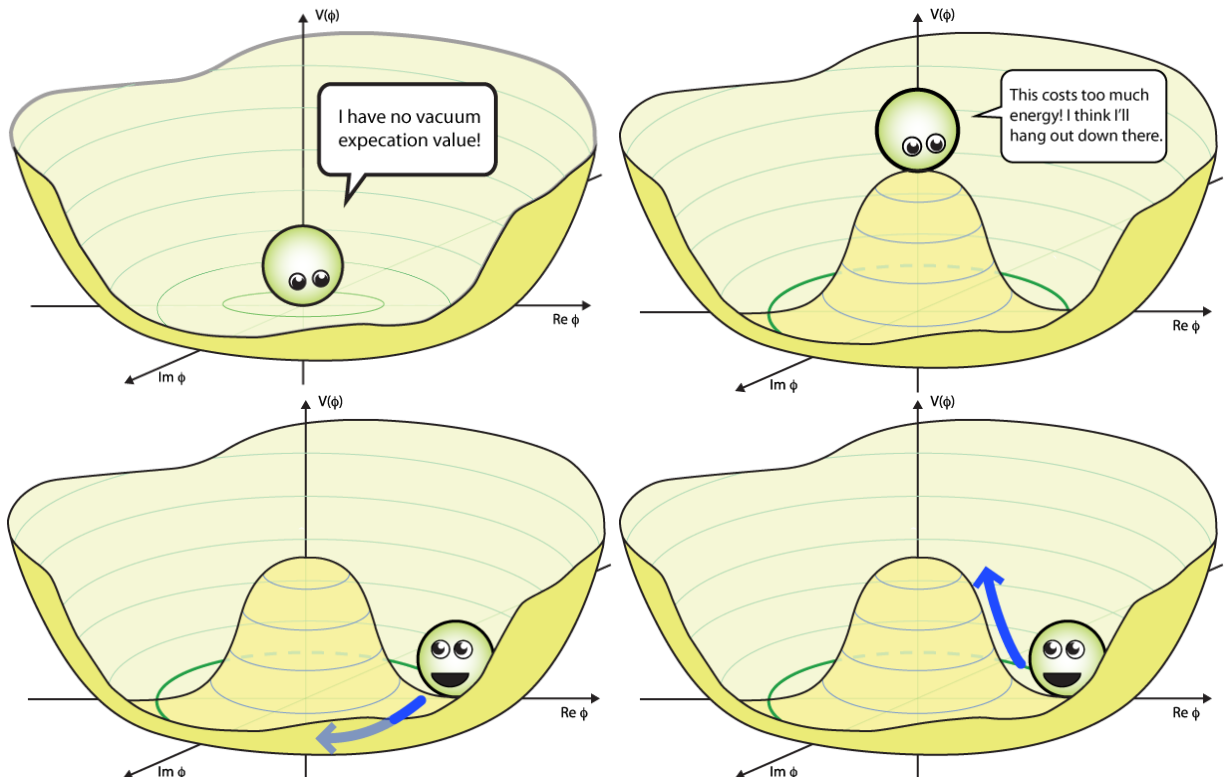


Figure 1.2: In this example the Higgs potential is illustrated in function of a complex scalar field (2D). The principle is the same for a complex scalar doublet but a lot harder to visualize. *Top left:* the Higgs potential with $\mu^2 > 0$, there is no vacuum expectation value. *Top right:* $\mu^2 < 0$, the origin is now a maximum and not stable; the scalar field will move to the lowest possible energy state. *Bottom left:* a flat direction in the potential corresponds to a massless Goldstone mode (remember there are two extra scalar fields in the full theory, meaning there are a total of three). *Bottom right:* the concave shape of the potential near the minimum defines the Higgs boson mass. Illustrations from Ref. [11].

Implementing this into Eq. 1.6 would yield the existence of unphysical fields $\phi_{1,2,3}$ that give rise to three extra degrees of freedom that were not present in the original Lagrangian*. Since a change of variables cannot alter the number of d.o.f. of a system, one can conclude that three fields do not represent physical fields. They can be removed by fixing a gauge, the unitary gauge, that breaks the original symmetry of the system.

$$\Phi(x) \rightarrow e^{-i\theta_a \tau_a} \Phi(x) = \begin{pmatrix} 0 \\ \frac{v+H(x)}{\sqrt{2}} \end{pmatrix}, \quad (1.10)$$

where we have introduced a new scalar field $H(x)$. After inserting this in the kinetic part of the scalar Lagrangian (Eq. 1.6) and redefining the gauge fields as

$$\begin{aligned} W_\mu^\pm &= \frac{1}{\sqrt{2}} (W_\mu^1 \mp iW_\mu^2), \\ Z_\mu &= \frac{1}{\sqrt{g^2 + g'^2}} (gW_\mu^3 - g'B_\mu), \\ A_\mu &= \frac{1}{\sqrt{g^2 + g'^2}} (gW_\mu^3 + g'B_\mu), \end{aligned} \quad (1.11)$$

we find for the kinetic part of the scalar Lagrangian:

$$|D_\mu \Phi|^2 = \frac{1}{2} (\partial_\mu H)^2 + \frac{1}{2} g^2 (v + H)^2 W_\mu^+ W^{-\mu} + \frac{1}{8} (v + H)^2 (g^2 + g'^2) Z_\mu Z^\mu. \quad (1.12)$$

Since mass terms enter this equation in the general form of $M_W^2 W_\mu W^\mu$ for the W bosons and $\frac{1}{2} M_Z^2 Z_\mu Z^\mu$ for the Z boson, the mass terms of the gauge bosons after spontaneous symmetry breaking can be written down as:

$$\begin{aligned} M_W &= \frac{1}{2} v g, \\ M_Z &= \frac{1}{2} v \sqrt{g^2 + g'^2}, \\ M_A &= 0, \end{aligned} \quad (1.13)$$

where it is clear that the photon remains massless†.

Using the potential term in Eq. 1.6 together with the vev in Eq. 1.10, we find for the Lagrangian of the Higgs boson

$$\mathcal{L}_H = \frac{1}{2} (\partial_\mu H) (\partial^\mu H) - \lambda v^2 H^2 - \lambda v H^3 - \frac{\lambda}{4} H^4. \quad (1.14)$$

The first term again corresponds to the kinetic term, whereas the third and forth refer to the three- and four-point self-interactions of the Higgs, respectively. Scalar masses have the general form $\frac{1}{2} m \phi^2$; the Higgs boson mass is thus equal to

$$m_H = 2\lambda v^2 = -2\mu^2, \quad (1.15)$$

and needs to be determined experimentally.

Working through the interaction terms of the Lagrangian, one can show that the electric charge e is related to the couplings of the weak isospin g and hypercharge g' .

$$e = g \sin \theta_W = g' \cos \theta_W, \quad (1.16)$$

*In Eq. 1.6, the vector fields are massless and each give rise to 2 d.o.f. The vev makes the three vector fields massive, thus adding 3 d.o.f. and introduce three unphysical fields.

†Because the W and Z bosons are massive, it costs energy to produce them and so the weak force is only really effective over a short distance. This is in contrast to the massless photons that result into a long range electromagnetic force. Thus, the Higgs field is responsible for the “weakness” of the weak force.

where the Weinberg angle is denoted as θ_W and indicates the magnitude of rotation of the boson fields after spontaneous symmetry breaking:

$$\begin{pmatrix} \gamma \\ Z \end{pmatrix} = \begin{pmatrix} \cos \theta_W & \sin \theta_W \\ -\sin \theta_W & \cos \theta_W \end{pmatrix} \begin{pmatrix} B^0 \\ W^0 \end{pmatrix}, \quad (1.17)$$

and is related to the weak isospin and hypercharge:

$$\cos \theta_W = \frac{g}{\sqrt{g^2 + g'^2}} \quad \text{and} \quad \sin \theta_W = \frac{g'}{\sqrt{g^2 + g'^2}}. \quad (1.18)$$

Massive fermions

A term like $-m\bar{\psi}\psi = -m[\bar{\psi}_L\psi_R + \bar{\psi}_R\psi_L]$, where we have decomposed the equation into the left- and right-handed chiral states* is not gauge invariant in the Lagrangian. The left-handed fermions form an isospin *doublet* and the right-handed fermions form isospin *singlets*. They transform differently under $SU(2)_L \times U(1)_Y$:

$$\begin{aligned} \chi_L &\rightarrow \chi'_L = \chi_L e^{i\tau_L^3 \vec{W} + i\alpha Y_W}, \\ \psi_R &\rightarrow \psi'_R = \psi_R e^{i\alpha Y_W}. \end{aligned} \quad (1.19)$$

It is possible for the fields to couple to the complex Higgs doublet, defined in Eq. 1.5, by adding Yukawa couplings. This results into terms that are singlets under $SU(2)_L$ and $U(1)_Y$:

$$\mathcal{L}_{Yuk} = \lambda_e \overline{L_L} \Phi e_R - \lambda_d \overline{Q_L} \Phi d_R - \lambda_u \overline{Q_L} \tilde{\Phi} u_R + h.c., \quad (1.20)$$

where we have introduced the conjugate of $\Phi, \tilde{\Phi} = i\tau_2 \Phi^*$, which has a negative hypercharge. After spontaneous symmetry breaking (Eq. 1.10), we find:

$$\begin{aligned} L_{Yuk} &= -\frac{1}{\sqrt{2}} \lambda_e (\bar{\nu}_e, \bar{e}_L) \begin{pmatrix} 0 \\ v + H(x) \end{pmatrix} e_R + \dots \\ &= -\frac{1}{\sqrt{2}} \lambda_e (v + H(x)) \bar{e}_L e_R + \dots, \end{aligned} \quad (1.21)$$

where we highlighted only the electron part. Fermion mass terms have the general form $m_f \bar{f}_L f_R + h.c.$. Therefore, one finds:

$$m_e = \frac{\lambda_e v}{\sqrt{2}}, \quad m_u = \frac{\lambda_u v}{\sqrt{2}}, \quad m_d = \frac{\lambda_d v}{\sqrt{2}}. \quad (1.22)$$

The mass of the fermions is again not predicted since the Yukawa coupling parameters are free parameters.

1.3.4 Particle mixing

In Eq. 1.20, we introduced Yukawa coupling constants to explain the mass of fermions. In its most general realizations, these couplings are not constants but matrices. This will introduce possible mixing of *flavor eigenstates* into different *mass eigenstates*. Let us write out the second term in Eq. 1.20:

* $\psi_L = P_L \psi = \frac{1-\gamma^5}{2} \psi$ and $\psi_R = P_R \psi = \frac{1+\gamma^5}{2} \psi$.

$$\begin{aligned} \lambda_d \overline{Q_L} \Phi d_R &= \Lambda_{ij}^d \overline{Q_{Li}^I} \Phi d_{Rj}^I = \Lambda_{ij}^d (\text{up-type down-type})_{Li}^I \begin{pmatrix} \phi^+ \\ \phi^0 \end{pmatrix} (\text{down-type})_{Rj}^I \\ &= \begin{pmatrix} \Lambda_{11} \overline{(u\ d)_L^I} \begin{pmatrix} \phi^+ \\ \phi^0 \end{pmatrix} & \Lambda_{12} \overline{(u\ d)_L^I} \begin{pmatrix} \phi^+ \\ \phi^0 \end{pmatrix} & \Lambda_{13} \overline{(u\ d)_L^I} \begin{pmatrix} \phi^+ \\ \phi^0 \end{pmatrix} \\ \Lambda_{21} \overline{(c\ s)_L^I} \begin{pmatrix} \phi^+ \\ \phi^0 \end{pmatrix} & \Lambda_{22} \overline{(c\ s)_L^I} \begin{pmatrix} \phi^+ \\ \phi^0 \end{pmatrix} & \Lambda_{23} \overline{(c\ s)_L^I} \begin{pmatrix} \phi^+ \\ \phi^0 \end{pmatrix} \\ \Lambda_{31} \overline{(t\ b)_L^I} \begin{pmatrix} \phi^+ \\ \phi^0 \end{pmatrix} & \Lambda_{32} \overline{(t\ b)_L^I} \begin{pmatrix} \phi^+ \\ \phi^0 \end{pmatrix} & \Lambda_{33} \overline{(t\ b)_L^I} \begin{pmatrix} \phi^+ \\ \phi^0 \end{pmatrix} \end{pmatrix} \cdot \begin{pmatrix} d_R^I \\ s_R^I \\ b_R^I \end{pmatrix}, \end{aligned} \quad (1.23)$$

where the superscript I implies that the fermion fields are expressed in the *interaction (flavor)* basis. The subscript i stands for the three generations. This means that after symmetry breaking the quark mass terms break down into

$$\begin{aligned} -\mathcal{L}_{Yuk}^{\text{quarks}} &= \Lambda_{ij}^d \overline{d_{Li}^I} \frac{v}{\sqrt{2}} d_{Rj}^I + \Lambda_{ij}^u \overline{u_{Li}^I} \frac{v}{\sqrt{2}} u_{Rj}^I + \dots \\ &= M_{ij}^d \overline{d_{Li}^I} d_{Rj}^I + M_{ij}^u \overline{u_{Li}^I} u_{Rj}^I + \dots \end{aligned} \quad (1.24)$$

where we have omitted the hermitian conjugate terms and the Higgs field interaction terms. Note that the u - and d -terms in the equation still each represent the three up- and down-type quarks respectively. There is mixing between the flavor fields as there is no reason why the matrix M should be diagonal*.

To obtain proper mass terms, one has to diagonalize the mass matrices M^u and M^d and find proper eigenstates. We introduce unitary matrices V as follows

$$\begin{aligned} M_{diag}^d &= V_L^d M^d V_R^{d\dagger}, \\ M_{diag}^u &= V_L^u M^u V_R^{u\dagger}, \end{aligned} \quad (1.25)$$

which can be done when the matrices V are unitary ($V_L^{d,u\dagger} V_L^{d,u} = \mathbb{1}$). Eq. 1.24 can now be expressed as follows:

$$\begin{aligned} -\mathcal{L}_{Yuk}^{\text{quarks}} &= \overline{d_{Li}^I} M_{ij}^d d_{Rj}^I + \overline{u_{Li}^I} M_{ij}^u u_{Rj}^I + \dots \\ &= \overline{d_{Li}^I} V_L^{d\dagger} V_L^d M_{ij}^d V_R^d V_R^d d_{Rj}^I + \overline{u_{Li}^I} V_L^{u\dagger} V_L^u M_{ij}^u V_R^u V_R^u u_{Rj}^I + \dots \\ &= \overline{d_{Li}^I} (M_{ij}^d)_{diag} d_{Rj}^I + \overline{u_{Li}^I} (M_{ij}^u)_{diag} u_{Rj}^I + \dots \\ &\quad , \end{aligned} \quad (1.26)$$

where the V matrices have been absorbed in the quark flavor eigenstates and have formed mass eigenstates. These mass eigenstates couple differently to the gauge fields of the weak interaction. Working out one term from Eq. 1.4, the mixing of the flavor eigenstates is clearly visible

$$\begin{aligned} \mathcal{L}_{kinetic}(Q_L) &= i \overline{Q_{Li}^I} \gamma_\mu D^\mu Q_{Li}^I \\ &= \frac{g}{\sqrt{2}} \overline{u_{Li}^I} \gamma_\mu W^{-\mu} d_{Li}^I + \frac{g}{\sqrt{2}} \overline{d_{Li}^I} \gamma_\mu W^{+\mu} u_{Li}^I + \dots \\ &= \frac{g}{\sqrt{2}} \overline{u_{Li}^I} (V_L^u V_L^{d\dagger})_{ij} \gamma_\mu W^{-\mu} d_{Lj}^I + \frac{g}{\sqrt{2}} \overline{d_{Li}^I} (V^d V^{u\dagger})_{ij} \gamma_\mu W^{+\mu} u_{Lj}^I + \dots \end{aligned} \quad (1.27)$$

*The question and answer of flavor/mass mixing can be put as: Q: “Why is there mixing?”; A: “Because it can.”

The combination of matrices $\left(V_L^d V_L^{u^\dagger}\right)_{ij}$, a unitary 3×3 matrix is known as the *Cabibbo-Kobayashi-Maskawa (CKM)* mixing matrix. By convention, the interaction and flavor eigenstates of the up-type quarks are chosen to be equal. The down-type quarks are therefore chosen to be rotated:

$$\begin{aligned} u_i^I &= u_i, \\ d_i^I &= V_{CKM} d_i, \end{aligned} \quad (1.28)$$

or explicitly:

$$\begin{pmatrix} d^I \\ s^I \\ b^I \end{pmatrix} = \begin{pmatrix} V_{ud} & V_{us} & V_{ub} \\ V_{cd} & V_{cs} & V_{cb} \\ V_{td} & V_{ts} & V_{tb} \end{pmatrix} \begin{pmatrix} d \\ s \\ b \end{pmatrix}. \quad (1.29)$$

Because the choice of the global phases of the quark fields is arbitrary and the matrix is unitary, the nine unknown complex elements can be reduced to three real numbers and one phase*. The matrix is most often written as:

$$V_{CKM} = \begin{pmatrix} c_{12}c_{13} & s_{12}c_{13} & s_{13}e^{-i\delta} \\ -s_{12}c_{23} - c_{12}s_{23}s_{13}e^{i\delta} & c_{12}c_{23} - s_{12}s_{23}s_{13}e^{i\delta} & s_{23}c_{13} \\ s_{12}s_{23} - c_{12}c_{23}s_{13}e^{i\delta} & -c_{12}s_{23} - s_{12}c_{23}s_{13}e^{i\delta} & c_{23}c_{13} \end{pmatrix}, \quad (1.30)$$

where $c_{ij} = \cos(\theta_{ij})$ and $s_{ij} = \sin(\theta_{ij})$ for $i < j = 1, 2, 3$ and δ is the *CP*-violating phase.

The mixing of the flavor quantum states is necessary to explain charged current interactions changing the strangeness with 1 [12] and *CP*-violating processes [13].

Without going into detail, it is worth noting that a similar matrix exists that connects the lepton flavor and mass eigenstates. In contrast to the quarks, the down-type interaction doublet states are chosen to be the same as the mass eigenstates. Therefore, the mixing of the mass and interaction eigenstates is in the neutrino sector. The three eigenstates of the weak interaction form an orthonormal basis. Left-handed neutrinos and leptons form doublets L as can be seen in Eq. 1.20: $\begin{pmatrix} \nu_e \\ e \end{pmatrix}$, $\begin{pmatrix} \nu_\mu \\ \mu \end{pmatrix}$ and $\begin{pmatrix} \nu_\tau \\ \tau \end{pmatrix}$. One can also construct an eigenbasis out of three neutrino states with definite mass, ν_1, ν_2 and ν_3 that diagonalize the neutrino's free-particle Hamiltonian. Similar to quarks, this mass-eigenbasis is rotated relative to the flavor-eigenbasis:

$$\begin{pmatrix} \nu_e \\ \nu_\mu \\ \nu_\tau \end{pmatrix} = \begin{pmatrix} U_{e1} & U_{e2} & U_{e3} \\ U_{\mu 1} & U_{\mu 2} & U_{\mu 3} \\ U_{\tau 1} & U_{\tau 2} & U_{\tau 3} \end{pmatrix} \begin{pmatrix} \nu_1 \\ \nu_2 \\ \nu_3 \end{pmatrix} \quad (1.31)$$

This matrix is known as the Pontecorvo-Maki-Nakagawa-Sakata (PMNS) matrix [14],

$$\mathcal{U} = \begin{pmatrix} 1 & 0 & 0 \\ 0 & c_{23} & s_{23} \\ 0 & -s_{23} & c_{23} \end{pmatrix} \begin{pmatrix} c_{13} & 0 & s_{13}e^{-i\delta} \\ 0 & 1 & 0 \\ s_{13}e^{-i\delta} & 0 & c_{13} \end{pmatrix} \begin{pmatrix} c_{12} & s_{12} & 0 \\ -s_{12} & c_{12} & 0 \\ 0 & 0 & 1 \end{pmatrix} \quad (1.32)$$

The matrix is again parameterized by three mixing angles θ_{12}, θ_{13} and θ_{23} where s_{ij} and c_{ij} are used to denote $\sin(\theta_{ij})$ and $\cos(\theta_{ij})$. The phase δ relates to charge-parity violations. It is possible to add additional "Majorana" phases, but this will not be discussed in this work [15].

1.4 A success story

Over the course of multiple decades, the Standard Model was built up into an extremely comprehensive theory. The first building blocks necessary for its construction came from

*This phase is responsible for *CP-violation*.

experiments in the early 20th century when its quantum characteristics became more apparent. The theory was formulated as a gauge theory in the 1960s and 1970s and for decades it has been rigorously tested and checked, leading to extremely accurate experimental precision measurements that agree with the theory. Apart from precision measurements, it has led to predictions of particles and their interactions, which could only be tested years or decades after they were first proposed. In the following, we give a brief overview of some experimental results.

1.4.1 Predictions

By 1932, scientists knew that atoms were made up by protons, neutrons and electrons. Together with the photon, a total number of four particles were known. Four grew to five when Anderson discovered the existence of positrons [16] (predicted by Dirac [17]). Then came the muon [18] and pion [19]. By the 1960s, there were “fundamental particles” with no good guiding principles to link them together. They were often referred to as the “particle zoo”.

By a series of insights by several individuals, the Standard Model as a quantum field theory became more widely accepted. Since then, the model has predicted the results of experiment after experiment. Some of them are:

- Neutral weak currents. Postulated by Salam, Weinberg and Glashow, the theory of electroweak interactions predicted the existence of a new type of weak interaction, in which the reacting particles do not change their charges. The first observation was made in 1973 in the Gargamelle experiment at the European nuclear research laboratory, CERN [20].
- Weak gauge bosons. Again postulated by the abovementioned people. These particles were discovered in the UA1 and UA2 experiments in CERN, 1983 [21, 22].
- Heavy quarks. To explain the CP -violations in kaon decays, M. Kobayashi and T. Maskawa predicted the existence of a third generation of quarks: the *top* and *bottom* quarks. The bottom quark was discovered in 1977 at Fermilab [23]. It took another 18 years for the top quark to be found in the same institute [24].
- Gluons. The gauge bosons of quantum chromodynamics were discovered in 1978 and 1979 [25].
- Higgs boson. On July 4, 2012, physicists at CERN announced the discovery of the only fundamental particle predicted by the Standard Model that was not yet discovered.

1.4.2 Precision tests

Inconsistencies between experiment and theory can be signs of wrong or incomplete theories. For this reason, experimentalists are continuously testing parameters of the SM. These precision tests are most often done by testing the theory of quantum electrodynamics (QED). With the use of *renormalization theory*, many parameters of the theory can be calculated with high precision. High-precision measurements of various observables have been performed at LEP 1 and SLC [26, 27, 28, 29, 30, 31] for physics at the Z -boson mass ($\sqrt{s} \approx M_Z$) and other observables at Tevatron [32, 33], LEP 2 [33], ATLAS [34, 35] and CMS [36, 37]. Some of them are listed in Table 1.2. The parameters in the table show that the SM best fit predictions are very consistent with what we see in experiments.

The SM predicts kaons to decay into charged pions and a neutrino-antineutrino pair to happen once every ten billion kaon decays. The SM fit to this decay has a small uncertainty, making the search interesting for possible anomalies. A candidate event of this very rare decay has been reported by the NA62 collaboration in 2018 and is in accordance with the SM predictions [38].

Another example is the measurement of the *Lamb shift*, a difference in energy between two energy levels of the hydrogen atom that was not predicted by the Dirac equation and currently provides a measurement of the fine-structure constant α to better than one part in a million, allowing a precision test of QED.

Electrons have a magnetic dipole moment as a result from their intrinsic spin. A charge distribution in these particles, which we do not expect to happen for fundamental particles, would make the electron charge not seem perfectly spherical. This electron electric dipole moment (EDM) is expected from the SM only with an extremely small value from radiative corrections

Table 1.2: Observables compared with the SM best fit. Errors are the total (experimental plus theoretical) uncertainties. Results are taken from Tables 10.4 and 10.5 in [42].

Parameter	Experimental value	Theoretical value	Standard deviation
m_t [GeV]	172.74 ± 0.46	172.96 ± 0.45	-0.5
m_W [GeV]	80.387 ± 0.016	80.358 ± 0.004	1.8
	80.376 ± 0.033		0.6
	80.370 ± 0.019		0.6
	2.046 ± 0.049		-0.9
Γ_W [GeV]	2.195 ± 0.083	2.089 ± 0.001	1.3
	125.14 ± 0.15		0.0
$g_V^{\nu e}$	-0.040 ± 0.015	-0.0398 ± 0.0001	0.0
$g_A^{\nu e}$	-0.507 ± 0.014	-0.5063	0.0
τ_τ [fs]	290.75 ± 0.36	290.39 ± 2.17	0.1
$\frac{1}{2}(g_\mu - 2 - \frac{\alpha}{\pi})$	$(4511.18 \pm 0.77) \times 10^{-9}$	$(4508.63 \pm 0.03) \times 10^{-9}$	3.3
M_Z [GeV]	91.1876 ± 0.0021	91.1884 ± 0.0020	-0.4
Γ_Z [GeV]	2.4952 ± 0.0023	2.4942 ± 0.0008	0.4
$\Gamma_Z(\text{had})$ [GeV]	1.7444 ± 0.0020	1.7411 ± 0.0008	-
$\Gamma_Z(\text{inv})$ [MeV]	499.0 ± 1.5	501.44 ± 0.04	-
$\Gamma_Z(l^+l^-)$ [MeV]	83.984 ± 0.086	83.959 ± 0.008	-

with CP -violating interactions, at most $10^{-38} e \cdot \text{cm}$. Recent measurements from the ACME experiment set the current upper limit at a value of $1.110^{-29} e \cdot \text{cm}$ [39].

There have been other, more challenging precision test, such as neutrino cross-section measurements [40] and measurements of the top quark mass in the CMS experiment [41]. Both are again in agreement with the SM.

1.5 The need for physics beyond the Standard Model

Despite its incredible success, many physicists believe the Standard Model is certainly not the full story. There are a number of features that seem arbitrary, but also some that cannot be explained by the theory alone. Below, I give a list of open questions:

- Why are there **three families** for both leptons and quarks? Why not two? Or four? Or even a thousand?
- What is the **cause of the symmetries** we see in the Standard Model? Why is, for example, QCD not an SU(4) gauge theory?
- There are a number of **parameters** in the SM that cannot be explained by first principles. We have no good explanation for why the top quark is 75 000 times heavier than the up quark. Why is the vev of the Higgs potential 246 GeV? Why is the Higgs mass 125 GeV? There are in total 26 parameters in the SM that are determined by experiments and can be found in Table 1.3.
- Why does the Higgs potential have this **Mexican hat shape**? In other words, why is μ^2 in $\lambda (\Phi^\dagger \Phi)^2 + \mu^2 (\Phi^\dagger \Phi)$ negative? Also, the vev, the mass of the Higgs boson and the mass of the fermions due to the Yukawa couplings all appear in Table 1.3. This makes us believe there is something we do not fully understand about the BEH mechanism.
- Right-handed neutrinos can be introduced into the SM. They are singlets with respect to the strong and weak interaction and would therefore not carry an electric charge, weak hypercharge or weak isospin. Due to this lack of charge, right-handed neutrinos would be extremely difficult to detect. They have Yukawa interactions with other leptons and the Higgs boson, but its coupling would be extremely small. Neutrinos can become massive with Dirac mass terms in the same way charged leptons become massive in the BEH mechanism. Their **extremely small masses** suggest another mechanism in which the very light left-

handed neutrinos are accompanied with extremely heavy right-handed neutrinos. This mechanism is called the *Seesaw mechanism* and requires the addition of Majorana mass terms.

Aside from these, there are a number of unexplained phenomena that probably cannot be explained in a simple extension of the Standard Model but need a non-trivial approach. For example:

- It is a natural assumption that the universe is neutral with all conserved charges. Both the SM and general relativity give no explanation for the **matter-antimatter imbalance** we see in the universe. The Big Bang was expected to produce equal amounts of matter and anti-matter, yet we see that the observable universe consists almost exclusively out of baryonic matter*. The most likely explanation is that in the early universe physical laws we know today were absent or have acted differently. The observed *CP*-violation is insufficient to account for the observed baryon asymmetry of the universe given the limits on baryon number violation.
- The stars, planets, interstellar clouds, etc. we see in space consist of baryonic matter. Assuming general relativity is the correct theory to describe gravity on cosmological scales, the Lambda-CDM model predicts that the matter we see is only around 15% of the total matter present in our visible universe [43]. To explain the galaxy rotation curves [44], galaxy velocity dispersions [45], galaxy cluster masses [46], gravitational lensing [47], and many more, it is predicted that around 85% of the mass is not yet observed. This matter is referred to as **dark matter** as it cannot interact electromagnetically because it would have already been observed otherwise. No known particles in the SM can explain this phenomenon.
- Similar to dark matter, the Lambda-CDM model predicts that the total energy in the visible universe should consist mostly out of a constant energy density for the vacuum called **dark energy**. 5% of the total energy consists of baryonic matter, 26% should be dark matter and the remaining 69% of dark energy is necessary to explain the expansion of the universe[†].
- General relativity is generally accepted to describe gravity on cosmological scales. Thusfar, it has not been possible to describe **gravity** on a quantum scale, as is the case for the Standard Model, and still be valid on very large scales. The inclusion of the graviton would for example not recreate what is observed experimentally without other modifications to the SM, which have not been observed. There is a need for a more complete theory beyond the range of their combined applicability [48].
- Why is the *CP*-violation in the strong interaction extremely small or even zero?
- Often referred to as the muon g-2 anomaly, there are possible hints of new physics as the theoretical prediction of magnetic moment of the muon and experimental values have a small but significant offset (see Table 1.2).
- Why is there much more mixing in the lepton sector (PMNS) compared to the quark sector (CKM)?
- To explain the apparent quantum fluctuations on cosmological scales together with the horizon, flatness and magnetic monopole [49] problems, we have a theory of exponential expansion of space in the early universe: **cosmic inflation**. The theory states that between 10^{-36} and 10^{-32} seconds after the Big Bang, a rapid exponential expansion happened. This could explain the apparent thermal equilibrium between parts of the visible universe that are not in causal contact with each other and the even distribution of the cosmic microwave background. The hypothetical field that is thought to be responsible for inflation, the inflaton field, is not observed and would be an extension of the Standard Model.

*Why are there protons, neutrons and electrons everywhere while it is perfectly possible for antiprotons and antineutrons to form atomic nuclei with positrons?

[†]If there is only matter and the Big Bang acceleration only happened in the beginning of the creation of the universe, then one would expect the expansion to diminish due to the gravitational pull of matter. Measurements say the opposite is true: the universe is expanding and in an accelerating rate.

Table 1.3: The 26 free parameters in the Standard Model that have to be measured experimentally.

Parameter	Description	Value	Uncertainty	Reference
m_e	Electron mass	511 keV	$\pm 3.1 \cdot 10^{-6}$ keV	[42]
m_μ	Muon mass	105.7 MeV	$\pm 2.4 \cdot 10^{-6}$ MeV	[42]
m_τ	Tau mass	1.78 GeV	$\pm 1.2 \cdot 10^{-4}$ GeV	[42]
m_u	Up quark mass	2.2 MeV	$[-0.4, +0.5]$ MeV	[42]
m_d	Down quark mass	4.7 MeV	$[-0.3, +0.5]$ MeV	[42]
m_c	Charm quark mass	1.275 GeV	$[-0.035, +0.025]$ GeV	[42]
m_s	Strange quark mass	95 MeV	$[-3, +9]$ MeV	[42]
m_t	Top quark mass	173.0 GeV	± 0.4 GeV	[42]
m_b	Bottom quark mass	4.18 GeV	$[-0.03, +0.04]$ GeV	[42]
$\theta_{12,\text{CKM}}$	CKM 12-mixing angle	13.04°	$\pm 0.05^\circ$	[42]
$\theta_{23,\text{CKM}}$	CKM 23-mixing angle	2.38°	$\pm 0.06^\circ$	[42]
$\theta_{13,\text{CKM}}$	CKM 13-mixing angle	0.201°	$\pm 0.011^\circ$	[42]
$\delta_{CP,\text{CKM}}$	CKM CP violation phase	1.20 rad	± 0.08 rad	[42]
$\alpha^{-1}(M_Z)$	Electromagnetic coupling constant *	127.955	± 0.010	[42]
$\sin^2 \theta_W(M_Z)$	Weinberg angle *	0.23122	$\pm 3 \cdot 10^{-5}$	[42]
$\alpha_s(M_Z)$	Strong coupling constant *	0.1187	0.0016	[42]
θ_{QCD}	QCD vacuum angle	$< 10^{-9}$	/	[50]
v	Higgs vacuum expectation value	246 GeV	/	[51]
m_H	Higgs mass	125.09 GeV	$\pm 0.21(\text{stat}), \pm 0.11(\text{syst})$ GeV	[52]
$m_{\nu 1}$	Neutrino mass parameter	$\sum_i m_{\nu i} < 120$ meV	95% C.L.	[53]
$m_{\nu 2}$	Neutrino mass parameter	$\frac{\Delta m_{21}^2}{10^{-5}\text{eV}^2} = 7.39$	$[-0.20, +0.21]$	[54, 55]
$m_{\nu 3}$	Neutrino mass parameter	$\frac{\Delta m_{31}^2}{10^{-3}\text{eV}^2} = 2.525$	$[-0.032, +0.033]$	[54, 55]
$\theta_{12,\text{PMNS}}$	PMNS 12-mixing angle†	33.82°	$[-0.76^\circ, +0.78^\circ]$	[54, 55]
$\theta_{23,\text{PMNS}}$	PMNS 23-mixing angle†	49.6°	$[-1.2^\circ, +1.0^\circ]$	[54, 55]
$\theta_{13,\text{PMNS}}$	PMNS 13-mixing angle†	8.61°	$[-0.13, +0.13^\circ]$	[54, 55]
$\theta_{CP,\text{PMNS}}$	PMNS CP violation phase†	215°	$[-29^\circ, +40^\circ]$	[54, 55]

* The coupling constants depend on the energy scale: “running of the coupling constants”.

† Assuming normal mass ordering, for inverted ordering see reference.

- With the use of renormalization theory, it is possible to show that bare parameters should not be the same as parameters measured in experiments. These parameters, such as the mass of particles, depend on the energy scale at which they are probed and physics far beyond the scope of the probed energy scale can influence these parameters. An example are the screening and anti-screening effects. If one believes that all forces can be described by one theory at higher energies, these constants can converge at higher energy scales which is not the case when extrapolating these parameters as can be seen in Figure 1.3. Similarly, one-loop corrections to the Higgs boson mass* will have radiative corrections with a quadratic dependence on the cutoff scale. Virtual particles in one-loop corrections can have infinite momenta that should contribute to the total mass of the Higgs boson. Since we expect new physics to be present at energies close to the Planck mass ($\approx 10^{18}$ GeV), these loop corrections should push the Higgs mass to similar energy ranges. But, we see that the Higgs mass is around 125 GeV. This would mean that there are other parameters which should almost *exactly* cancel these absurdly large numbers. This is called *fine-tuning*, and it’s the intuition of most physicists that this incredible fine-tuning has a deeper, yet unknown, meaning. This problem is often referred to as the **hierarchy problem**.

Many of these problems can be seen as unwarranted. Why there are three families and why so many parameters in the Standard Model have no fundamental explanation could just be because it’s just the way it is. Maybe there is a multiverse, a plethora of universes with similar Standard Models, which have slightly or vastly different parameters. Some questions might even be impossible to answer because of a lack of statistics: we only have one universe and mankind has not been around very long in the timescale of the universe. This consideration might be

* Fermions and bosons are not affected by higher energy physics in the same way as a scalar particle is.

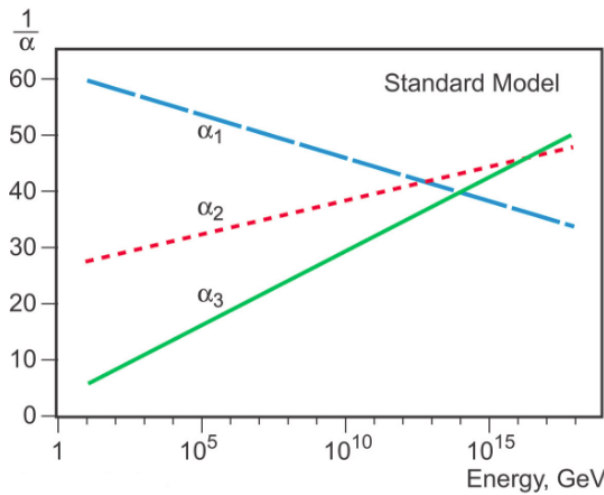


Figure 1.3: Running of the coupling constants in the Standard Model. Figure from [56].

valid but again not answers all our questions, it does not solve the question of dark matter for example.

This argument should not prevent us to try and find a more general theory for the Standard Model and general relativity. A better explanation could be fairly simple, but infinitely hard as well. There is only one way in trying to find a better understanding: experiments.

Unification is the most popular approach in describing physics beyond the Standard Model. Unification would mean that well-established theories are low-energy approximations of a more grand unified theory. Historically, this has worked very well: the unification of celestial gravitation of Kepler with terrestrial gravitation of Galileo into universal gravitation and the unification of electricity, magnetism, and later optics into electromagnetism. Gravity was overhauled by the much broader theory of general relativity. Lastly, the birth of gauge theories have combined QED and the weak interaction into the combined electroweak theory. The similarities in QCD and the electroweak theory, both being gauge theories, has led people to believe a unification is possible. This would unify the forces and particles known from the Standard Model into a *Grand Unified Theory* or GUT. A theory that would add gravity is called a *Theory Of Everything* or TOE.

1.5.1 Unifying theories

Linking the seemingly arbitrary parameters in the Standard Model has been ongoing for the last couple of decades. Combining these theories is not straightforward since they exhibit very different behaviors. Electromagnetism is long-ranged, the weak force is short-ranged and the strong force is weak in high-energy environments such as the early universe and strong where the probing energy is low. Many GUTs predict that quarks and leptons are part of a single representation of a gauge group with one single hypercharge and would explain why the electric charge of electrons and protons seem to be exactly the same [57].

The simplest GUT is SU(5), which would break down into the Standard Model at lower energies due to spontaneous symmetry breaking. Other possible extensions are, for example, SO(10) [58], SU(8) [59] and O(16) Lie groups. Another example is string theory, a theoretical framework that starts with the idea that point-like particles of particle physics can be replaced by one-dimensional objects called strings. These strings can propagate through space and interact with each other. Properties that we are more familiar with, such as charge, mass, etc. are determined by the vibrational state of the strings.

Unfortunately, the full theory does not have a definition in all circumstances and describes an enormous landscape of possible universes and is mainly used to describe quantum gravity. However, charge quantization is often not assumed in string theory, making particles with an anomalous charge plausible [60, 61].

Without experimental results there is still much ongoing debate into which theory is the correct

one. There are many more theories aside from the possible extentionst that are listed here such as Supersymmetry, Little Higgs, Technicolor... but go beyond the scope of this work.

1.5.2 How to look for new physics

In general one could say there are two possible ways to look for new physics. Essentially all of the physics in our solar system can be explained with what we know from the Standard Model. Interactions in controlled laboratory environments are currently on the order of ~ 10 TeV center of mass energy in the experiments at the LHC. This could still be well below the energy levels to produce new, exotic, particles. In the energy frontier it is the goal to reach the highest energies possible in order to get as close to the energy requirements where new physics becomes more prominent. As a consequence, more and more cosmic ray experiments have found an interest in searches for physics beyond the Standard Model. This is sometimes called the *cosmic frontier*. This analysis tries to explore this possibility in more detail for the IceCube experiment. Cosmic ray experiments have the disadvantage that they are not fully contained experiments and information is lost as the primary interaction is unknown and important parameters such as energy, direction, type,... of the particle have to be reconstructed.

The other approach tries to extract information from precision experiments and is therefore reliant on lowering the statistical and systematical uncertainties. In these experiments, the intensity of the beam of particle accelerators is pushed to its highest value and this is therefore referred to as the intensity frontier. This strategy tries to generate huge numbers of particles needed to study rare or exotic subatomic processes. Rare processes could give us a lot of information on unknown physics. Some parameters which can be calculated in the SM have a small offset with respect to what is measured in experiments.

The difference between the two methods can be summarized by saying that new physics at higher energies can produce new particles at high-energy collisions that are sought for in the energy frontier. The higher the scale where new physics enters, the more energy is needed in particle collisions. Parameters from our current theories that not include new physics could have a small but measurable offset at lower energies (the ones we are able to probe currently), which is what is measured in the intensity frontier.

I'd like to finish this chapter with quotes from Steven Weinberg in an interview with Nova about his vision on string theory. It shows the apparent stalemate physicists seem to find themselves into: there are no theoretical breakthroughs regarding long standing problems.

"I believe that there is a simple theory that governs everything—the four forces we know about, perhaps other forces as well. I'm not sure that's true. It may be that nature is irreducibly messy. I'm sure that we should assume it's not, because otherwise we're never going to find a fundamental theory. But even so, we're not guaranteed that we'll find it. We may not be smart enough. Dogs are not smart enough to understand quantum mechanics. I'm not sure that people are smart enough to understand the whatever-it-is that unifies everything. I think we probably are, because of our ability to link our minds through language, but I'm not certain."

"There was a marvelous period from, I'd say, the mid-'60s until the late '70s when theoretical physicists actually had something to say that experimentalists were interested in. Experimentalists made discoveries that theoretical physicists were interested in. Everything was converging toward a simple picture of the known particles and forces, a picture that eventually became known as the Standard Model. I think I gave it that name. And it was a time when graduate students would run through the halls of a physics building saying they had discovered another particle and it fit the theories, and it was all so exciting."

“Since the late ’70s, I’d say, particle physics has been in somewhat of a doldrums. Partly it’s just the price we’re paying for the great success we had in that wonderful time then. I think cosmology now, for example, is much more exciting than particle physics. The string theorists are trying to push ahead without much support from relevant experiments, because there aren’t any relevant experiments that can be done at the kind of scales that the string theorists are interested in.”

Even though it might take us a long time to find the answers we are looking for this current stalemate should not prevent us doing more fundamental research. We still do not know everything and probably even foolish in thinking we almost do. Finding some answers might be difficult but probably all the more fulfilling once we have them.



2. Motivation of the Analysis

The world is divided into people who think they are right ~ Anonymous

As seen in Chapter 1, there is an ongoing debate which beyond-the-Standard-Model physics models could help explain questions we do not have answers for. Over the last decades, this quest has proven to be non-trivial since many accelerator experiments have not given any clear hints towards physics that cannot be explained by the Standard Model. A big part of the physics community is trying its best to help answer these riddles and dedicated experiments have been constructed in the search for new physics. Other collaborations try to make use of their detector in the most efficient way possible. These experiments most often try to look for BSM physics by searching for signals in their detector that could not be explained by the particles we know today. One example, and also the subject of this work, is to try to look for particles that have a lower electromagnetic, but non-zero, charge than the charged particles of the Standard Model.

2.1 Introduction

As seen in Chapter 1, all free particles have an electromagnetic charge that is a multiple of the absolute electron charge, e , equal to 1.602×10^{-19} C. Elementary particles such as (anti)quarks have fractional charges equal to $\pm \frac{1}{3}e$ and $\pm \frac{2}{3}e$, but have never been seen as isolated particles due to *confinement* as explained in Section 1.1.2. No other particles are expected to have a charge lower than e and are therefore perfect candidates for searches beyond the Standard Model. Different experiments have sought these anomalously charged particles, which are referred to as *Lightly Ionizing Particles (LIPs)* or *Stable Massive Particles (SMPs)*. Throughout this work the latter denomination is used, indicating they do not rapidly decay and have masses significantly higher than the lightest leptons.

2.2 Theory

In Section 1.5.1, possible extensions of the Standard Model were already introduced. One of the simplest possible extensions of the $SU(3) \times SU(2) \times U(1)$ groups is the $SU(5)$ gauge group. It is the smallest Lie group that can contain the group of the Standard Model without introducing any new fermions. It could explain charge quantization [57], has complex representations and can accommodate fractional charges. In this scheme, new vector bosons, usually called X and

Y bosons, occur with charges $\frac{4}{3}$ and $\frac{1}{3}$. Extensions of the SU(5) models allow for color singlet particles with charges $\frac{1}{3}$ and $\frac{2}{3}$ [62]. Other possible extensions are based on the SU(7) [63], SU(8) [59], SO(14) [64], SO(18) [65], SO(10) \times SO(8) groups [66].

It should be noted that the simplest form of an SU(5) gauge group is already highly constrained as proton decay is allowed in this model and estimated to be around $10^{30} - 10^{31}$ years. However, experimental results have shown the lifetime to be $> 1.6 \times 10^{34}$ years ($\tau(p \rightarrow \pi^0 e^+)$) and $> 7.7 \times 10^{33}$ years ($\tau(p \rightarrow \pi^0 \mu^+)$) [67].

There are also some string theories where massive particles with a fractional charge are predicted [60, 68]. This was later confirmed to occur very often in certain compactifications [61].

More recently, there has been an increasing interest in searches for millicharged particles. New particles could couple to the Standard Model via a “kinetic mixing” or “hypercharge portal” [69, 70]. And in recent years, they were studied as possible candidates for dark matter [71, 72, 73, 74]. However, the charges of these particles are often $< 10^{-3}e$ and therefore no ideal candidates in neutrino Cherenkov experiments. It is possible to look for them in neutrino experiments [75], but more targeted toward future experiments such as DUNE [76] and SHiP [77]. A more detailed explanation of these particles can be found in Ref. [78]. The most stringent upper limit in millicharged particles known to the author is given in Ref. [79].

There are many other possible extensions, but these go beyond the scope of this work. One should just keep in mind that no free particles with an anomalous charge less than e are expected in the SM and that, if seen, they give clear hints of beyond-the-Standard-Model physics and would help in finding a more clear picture of what is possibly hidden beyond the realms of our understanding.

2.3 Previous searches

There are several ways one can assume to produce fractional charge particles. Different assumptions lead to different possible searches with previous and current detectors. In the following, the results of several experiments are shown. Accelerator and fixed target experiments look for particles that might be created in particle collisions, resulting in upper limits for production cross sections if no candidate events are found. Telescope experiments, on the other hand, often assume a flux of incoming particles that is bound to an upper limit if no candidate events are found.

2.3.1 Searches with accelerators and fixed targets

The total energy of the interaction should be large enough to produce particles of a certain mass. The square of the centre of mass energy is given by:

$$\begin{aligned} s &= (p_1 + p_2)^2 \\ &= m_1^2 + m_2^2 + 2E_1 E_2 - 2\vec{p}_1 \cdot \vec{p}_2, \end{aligned} \tag{2.1}$$

where $p_{1,2}$ are the four-momenta of the two particles and c , the speed of light, is set to 1 in natural units. Assuming E is the energy of the incoming particle with mass m_i and m_t the mass of a target particle in rest and $E \gg m_t, m_i$, the maximal mass reach of a search is given by:

$$m_{max} \approx \sqrt{2m_t E}. \tag{2.2}$$

If I is the incoming particle from the input beam and N a nucleus, the production of exotic particles can then be denoted as

$$I + N \rightarrow F + X, \tag{2.3}$$

Table 2.1: Highest-energy fractional charge particle searches in electron-positron colliders. No evidence for fractionally charged particles was found.

\sqrt{s} (GeV)	Charges sought	Collider	Reference
1-1.4	$\frac{2}{3}$	VEPP-2M	[82]
29	$\frac{1}{3}, \frac{2}{3}$	PEP	[83]
130-209	$\frac{2}{3}, \frac{4}{3}, \frac{5}{3}$	LEP	[84]
130-136, 161 and 172	$\frac{2}{3}$	LEP	[85]
91.2 (m_Z)	$\frac{2}{3}, \frac{4}{3}$	LEP	[86]
91.2 (m_Z)	$\frac{4}{3}$	LEP	[87]

Table 2.2: Highest-energy fractional charge particle searches in proton-(anti)proton colliders. No evidence for fractionally charged particles was found.

\sqrt{s} (GeV)	Type	Charges sought	Collider	Reference
540	$p\bar{p}$	$\frac{1}{3}, \frac{2}{3}$	SPS	[88]
1800	$p\bar{p}$	$\frac{2}{3}, \frac{4}{3}$	Tevatron	[89]
1800	$p\bar{p}$	$\frac{1}{3}, \frac{2}{3}$	Tevatron	[90]
7000	$p p$	$\frac{1}{3}, \frac{2}{3}$	LHC	[91]

where F stands for the fractional charged particle and X for the other particles that are produced in the interaction. No experiments that used accelerators and fixed targets found evidence for the existence of fractional charge particles [80]. The highest-energy search used muons with a beam energy of 200 GeV, resulting in an m_{max} of 19 GeV [81].

2.3.2 Colliders

Particle colliders can reach much higher energies than most fixed-target experiments. We see from Eq. 2.1 that the maximal mass of new particles in a storage ring that is colliding particles of energy E with $E \gg m_1, m_2$ scales with the energy:

$$s = 4E^2, \\ \rightarrow m_{max} = 2E \quad (2.4)$$

There is a big difference in lepton and hadron accelerator experiments since much less particles are being produced in the former due to the absence of strong interactions. The production is “cleaner” and the particles sought are easier to distinguish from other productions. But, it is more difficult to reach higher energies for lepton accelerators*. An overview of electron-positron colliders is given in Table 2.1. No evidence for fractionally charged particles was found.

Experiments that use proton-antiproton colliders have reached larger masses but have also found no evidence of fractionally charged particles. An overview is given in Table 2.2.

A more recent search was performed at the LHC, a proton-proton collider, when operating at a center of mass energy of 7 TeV. No evidence of particles with fractional charge was found. An upper limit of 95% confidence level was set for particles with electric charge $\frac{2}{3}$ up to a mass of 310 GeV and 140 GeV for those with charge $\frac{1}{3}$ [91].

2.3.3 Searches for particles with telescopes

There are several ways that particles with a fractional charge could be produced in cosmological events;

- the particles were produced early on in the Universe and are a stable component of the present matter;

*The radiative power of synchrotron radiation scales with a factor of m^{-4} : particles with low mass lose much more energy in circular accelerators with a fixed radius.

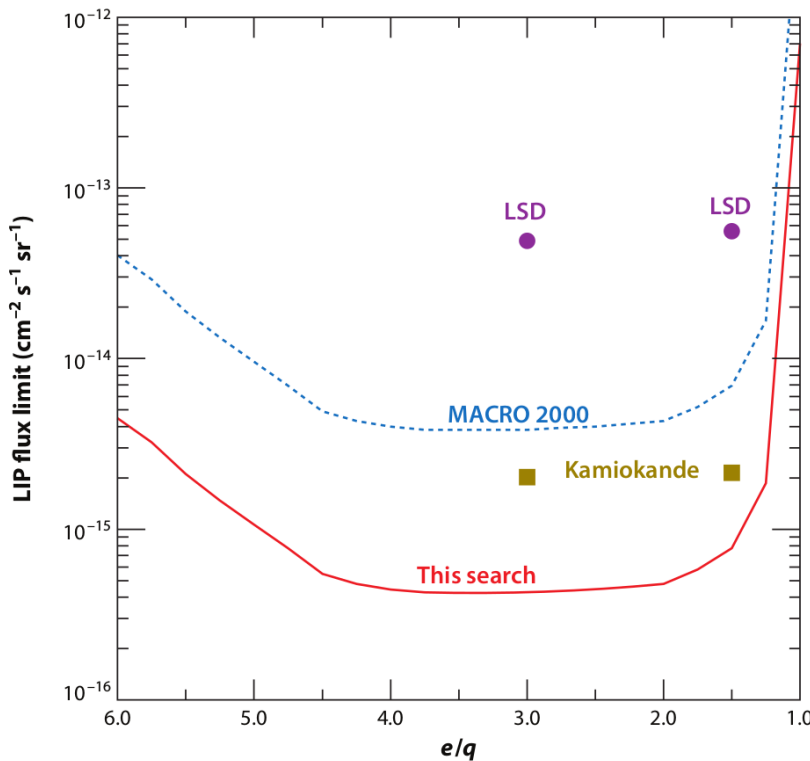


Figure 2.1: Upper limits on fluxes of particles close to the respective detectors. LIP stands for *Lightly Ionizing Particles*. “This search” refers to an unpublished result from the MACRO experiment that compares the published results from other experiments. Figure taken from Ref. [92], where I have changed the Kamiokande results which are wrong in the original figure.

- the particles are rare but can be continuously produced in high-energy astrophysical events; or
- the particles are produced in cosmic ray processes near Earth.

Because there is no clear preference for one of these possibilities, most telescope experiments express their search sensitivity as an incoming flux close to the detector in units of $\text{cm}^{-2} \text{s}^{-1} \text{sr}^{-1}$. This analysis has adopted the same search strategy and aims to improve on previous results. The most stringent upper limit was realized by the MACRO experiment found on the arXiv (not published, Ref. [92]) that compares results from older searches and can be seen in Figure 2.1. The best published result is set by Kamiokande II with upper limits of $2.1 \times 10^{-15} \text{ cm}^{-2} \text{s}^{-1} \text{sr}^{-1}$ and $2.3 \times 10^{-15} \text{ cm}^{-2} \text{s}^{-1} \text{sr}^{-1}$ for particles with charges $\frac{1}{3}$ and $\frac{2}{3}$ respectively [93].

2.4 Properties of the signal

Because there are many possible scenarios what these particles are, where they originate from, or how they are produced, one has to make certain assumptions about the properties of the signal. A particle traveling at the speed of light with a lifetime < 0.1 seconds traversing a detector will not give the same signal properties as one that has a very long lifetime. Therefore, I have assumed that the particles I am looking for

- behave leptonically, similar to muons. The particles will therefore produce long tracks instead of cascades in the IceCube detector (more info in Chapter 4);
- have a long lifetime and will not rapidly decay within the IceCube detector, or at least have a very low probability to do so;
- follow an energy spectrum with a spectral index of -2*;
- are assumed to produce an isotropic flux close to the detector.

*More information about spectra can be found in Section 3.1.2.

These assumptions are consistent with previous searches that are mentioned in Section 2.3. The behavior of such particles in the detector will depend on the charge (see Section 4.3.2.1) and, to a lesser extent, the mass. In this work the particles are assumed to have a

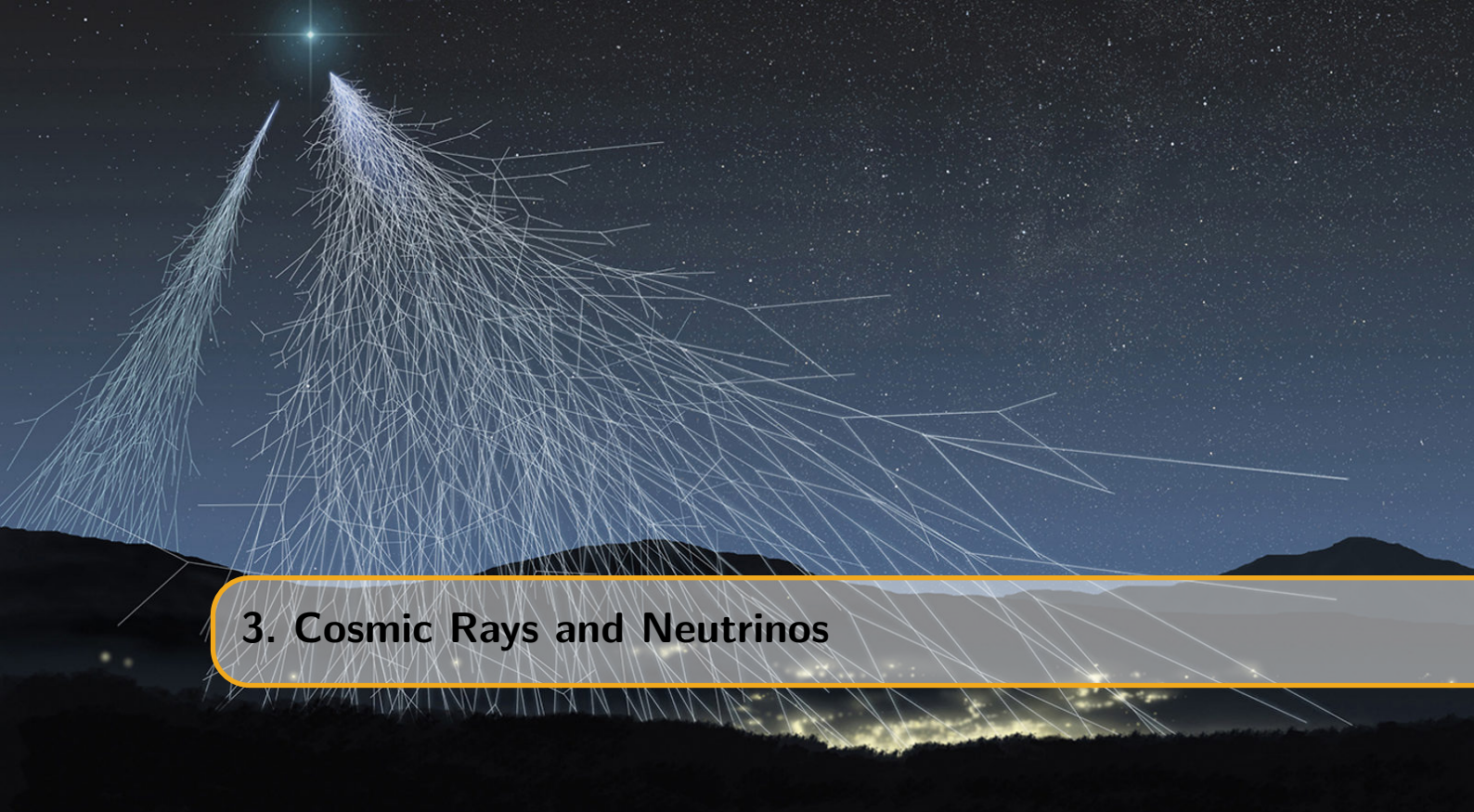
- charge of 1/3, 1/2 or 2/3;
- mass of 10 GeV, 100 GeV, 1 TeV, 10 TeV or 100 TeV,

where I have referred to the charge of the particles as relative to the absolute electron charge, e^* . The possible combinations result into a total of 15 unique signal samples that will be searched for.

The detector used in this analysis, the IceCube detector, is a neutrino telescope. The properties of the signal were defined to be able to compare this work to the results seen in Figure 2.1. The best limits were set by the MACRO and Kamiokande experiments. The former was a multipurpose underground detector located at Gran Sasso, Italy and designed to search for magnetic monopoles with the use of liquid scintillators and streamer tubes [94]. This design also made it possible to operate as a neutrino detector and cosmic ray observatory and allowed for BSM searches such as particles with a fractional charge.

The Kamiokande observatory, a water Cherenkov detector (see Chapter 4) was designed to search for proton decay and located deep underground to shield the detector from cosmic ray muons (see Chapter 3). Because of its design and very efficient shielding from cosmic rays, the detector also operates as a neutrino observatory and can also be used to search for particles with a fractional charge. The experiment was later extended to Kamiokande II, III and Super-Kamiokande.

*This will be done throughout this work from this point on.



3. Cosmic Rays and Neutrinos

We sit in the mud, my friend, and reach for the stars ~ Ivan Turgenev

Cosmic rays, contrary to their name, almost exclusively exist of particles with a finite rest mass. The term *rays* was historically attributed to these particles as they were thought to be mostly electromagnetic radiation. They are particles coming from outer space, impinging on our atmosphere and producing particles and large showers of electromagnetic radiation. The interest in cosmic rays within the field of modern particle physics is clear: many new particles were discovered from the interactions at energies that were higher than most experiments could reach. Positrons, muons, pions, and kaons were first discovered in cosmic ray experiments in the 1930s and 1940s. Today, high-energy cosmic ray interactions are still of interest as the highest energies of these particles go beyond what is feasible even at the most powerful accelerators such as the LHC.

Complementary to cosmic ray experiments is the field of neutrino astronomy as neutrinos are expected to be produced together with cosmic rays, near the source or close to Earth. This makes neutrino astronomy an interesting and possible powerful part of modern day astronomy. This chapter serves as an overview of the origin of cosmic rays and neutrinos with their properties. Both produce particles that are visible in neutrino telescopes such as the IceCube experiment and are important backgrounds in this analysis. For a more exhaustive description of cosmic rays I refer the reader to Ref. [95].

3.1 Cosmic rays

3.1.1 Discovery of cosmic rays

With the use of electrometers, the Austrian physicist Victor Hess performed several groundbreaking balloon flight experiments in 1912 to prove that the amount of ionizing radiation increases with altitude [96]. This was in strong contradiction with the widespread belief that ionizing radiation on Earth's surface mostly originates from radioactive substances in its crust. Hess concluded that extremely penetrating radiation existed. He described this radiation to be coming from space that enters Earth's atmosphere. Hess later ruled out the possibility that cosmic rays originate from the Sun as his observations showed no particular difference in night and day and during solar eclipses. In the late 1920s, first evidence was found that cosmic rays

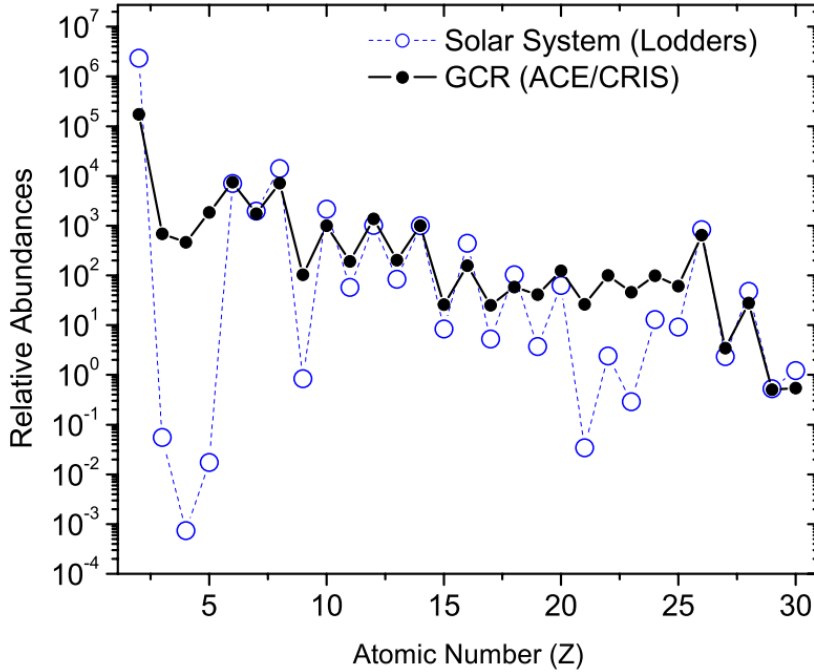


Figure 3.1: The cosmic ray elemental abundances measured on Earth compared to the solar system abundances, all relative to $^{14}\text{Si} = 10^3$. Figure from ACE news archive [99].

were charged due to a variation of their intensity with latitude, which indicated that they were deflected by the geomagnetic field [97].

Hess's ideas proved to be correct, but it was wrongfully attributed to electromagnetic radiation by Robert Millikan in the 1920s [98].

3.1.2 What are cosmic rays?

Cosmic rays are, almost exclusively, nuclei that are stripped of their electrons, making them electrically charged, heavy particles. Around 90% of the particles are ionized hydrogen atoms, or protons; 9% are alpha particles and 1% are nuclei of heavier elements. There is a striking resemblance between the relative abundance of cosmic rays and elements in the solar system as seen in Figure 3.1. A much smaller fraction of incoming particles are electrons, positrons and antiprotons.

There are, however, two important differences between cosmic rays and elements from our solar system. Firstly, the two groups of elements Li, Be, B and Sc, Ti, V, Cr, Mn are many orders of magnitude more abundant in cosmic rays than in the solar system. More massive cosmic rays (mainly C, O and Fe) can produce these nuclei in the process of *spallation*; they are produced by collisions of cosmic rays with the interstellar medium. Therefore, these nuclei are sometimes referred to as *secondary nuclei*. Spallation effects in our solar system are orders of magnitude lower compared to cosmic rays, explaining the difference we see in the relative abundance of these two groups. The second difference is that nuclei with an atomic number $Z > 1$ are much more abundant with respect to hydrogen in cosmic rays. This phenomenon is not yet well understood but might be attributed to the difficulty to ionize hydrogen, necessary for acceleration processes.

The flux of cosmic rays seen on Earth is expressed in units of $[\text{m}^{-2}\text{s}^{-1}\text{sr}^{-1}]$. We can see in Figure 3.2 that the cosmic ray flux follows a power law energy spectrum

$$dN \propto E^\gamma dE, \quad (3.1)$$

where γ is called the *spectral index*. Because of the steepness of the spectrum, it is often multiplied by a higher power of energy as can be seen in Figure 3.2*.

*The broad range in both energy and flux, visible in Figure 3.2, should convince the reader that many types of

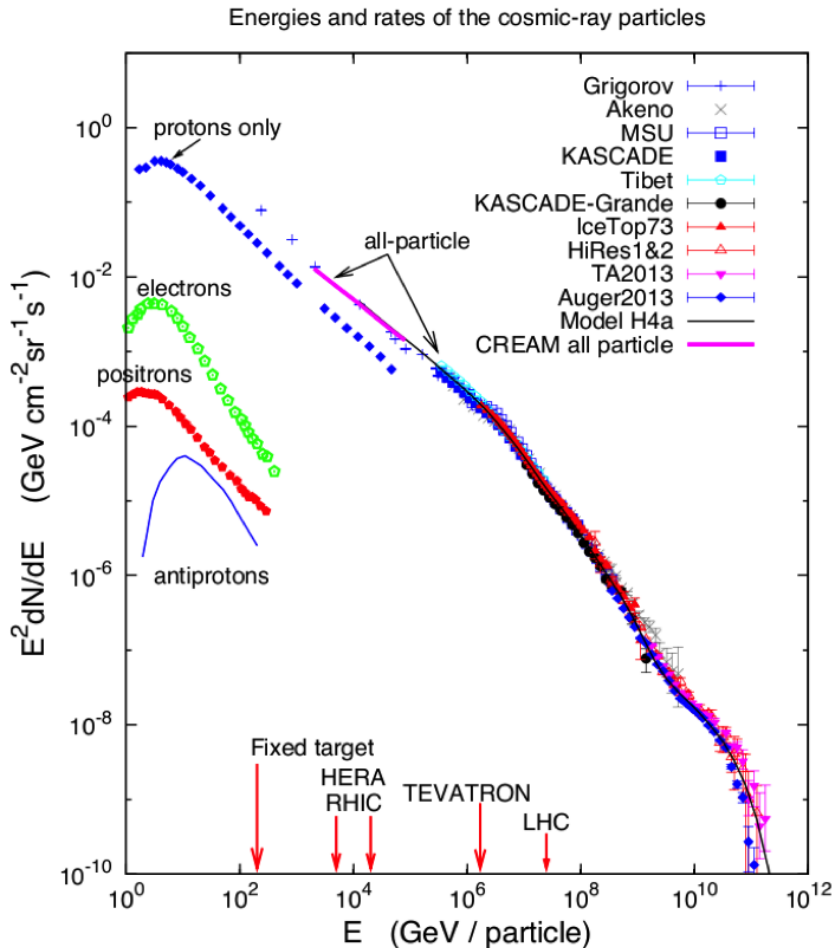


Figure 3.2: Spectrum of cosmic rays at Earth. The all-particle spectrum measured by different experiments is plotted together with the proton-only spectrum. Subdominant contributions to the total flux from electrons, positrons and antiprotons as measured by the PAMELA experiment are also shown. The primary particle energies are compared to accelerator experiments by showing what energy the primary particle should have to reach a similar center-of-mass energy compared to these accelerators, see Eq. 2.2. Figure from Ref. [100].

We can divide the global spectrum in four regions. Between 10 GeV and 1 PeV the differential spectral index is around -2.7. From 10 PeV to 1 EeV it's around -3.1. Below 10 GeV, there is a strong suppression of cosmic rays due to an effect called *solar modulation*^{*}. Above 10 EeV, the spectrum again flattens to an index around -2.6 and an apparent cutoff region is present at around 10^{20} eV. The transition of this first to second region at around 3 PeV is referred to as the *knee*. The second to third region transition is called the *ankle*. It might be possible to describe the full cosmic-ray spectrum with sources within our galaxy. However, a more generally accepted theory is that the knee in the spectrum originates from the end of a population of particles that are accelerated within our Milky Way [101]. Around 100 PeV is the *second knee*, believed to be a feature of the iron drop-off (see Section 3.1.2.1).

The origin of cosmic rays has been a topic of discussion for many years. We now know that most particles originate from sources in the local galaxy, having spent on average 10^7 years in diffusive motion in the interstellar medium [101]. This is consistent with the similar features of the relative abundances of cosmic rays and elements from our solar system. However, there is no general consensus about the origin of the cosmic rays with energies above 3 EeV. In the following, the abovementioned energy regions are discussed in more detail.

3.1.2.1 Galactic component

It is believed that low-energy cosmic rays have a galactic origin. The most probable acceleration mechanism is by shocks driven by expanding supernova remnants (SNRs) [102]. This is supported by observations of a lower gamma-ray emissivity from π^0 decay from Magellanic Clouds compared to the Milky-Way [103] and the detection of a typical π^0 -decay in the γ -spectrum from SNRs [104].

With their approximate energy density of around 0.5 eV/cm³ in our local galaxy, the supernova energy density results into a total power of around

$$L_{CR} = 7 \times 10^{40} \text{ erg/s}, \quad (3.2)$$

where erg is a unit often used in astronomy[†]. If one assumes a supernova explosion of around one per every 30 years, then the total power output of type II supernovae with a mass output of around ten times the mass of the Sun at a velocity close to 5×10^8 cm/s would result in a power of

$$L_{SN} \sim 3 \times 10^{42} \text{ erg/s}. \quad (3.3)$$

These numbers are not set in stone and hold large uncertainties, but it shows that with an acceleration efficiency on the order of a couple of percent, supernova explosions could be a prominent source of energetic cosmic rays, if not the dominant one.

It is still unclear if the galactic component is solely due to SNRs or other possible sources, such as pulsars, have a measurable contribution.

From the ratio of primary to secondary nuclei, it can be inferred that cosmic rays travel distances thousands of times greater than the thickness of the disk of the galaxy. There is also an apparent decrease in the amount of matter that is traversed by cosmic rays with higher energies than with lower. Higher-energy cosmic rays seem to spend less time in the galaxy than lower-energy ones which suggests that cosmic rays are accelerated before most propagation occurs [95].

The way the cosmic ray spectrum is fit is not set in stone. Here I will use the convention used by Gaisser, Stanev and Tilav described in Ref. [101]: the spectrum is subdivided in three populations. The first population corresponds to the particles that are primarily accelerated by

detectors are necessary to study the behavior of cosmic rays. Low-energy particles are abundant and high-energy particles are much more rare. Both the energy and the incoming flux will determine the type and size of the detector.

^{*}In the solar system, a stream of charged particles (electrons, protons and alpha particles) is released from the Sun, creating a magnetic field. Cosmic rays coming into the solar system interact with these particles and magnetic field where the influence is greatest on particles with the lowest energies.

[†]1 erg = 10^{-7} J.

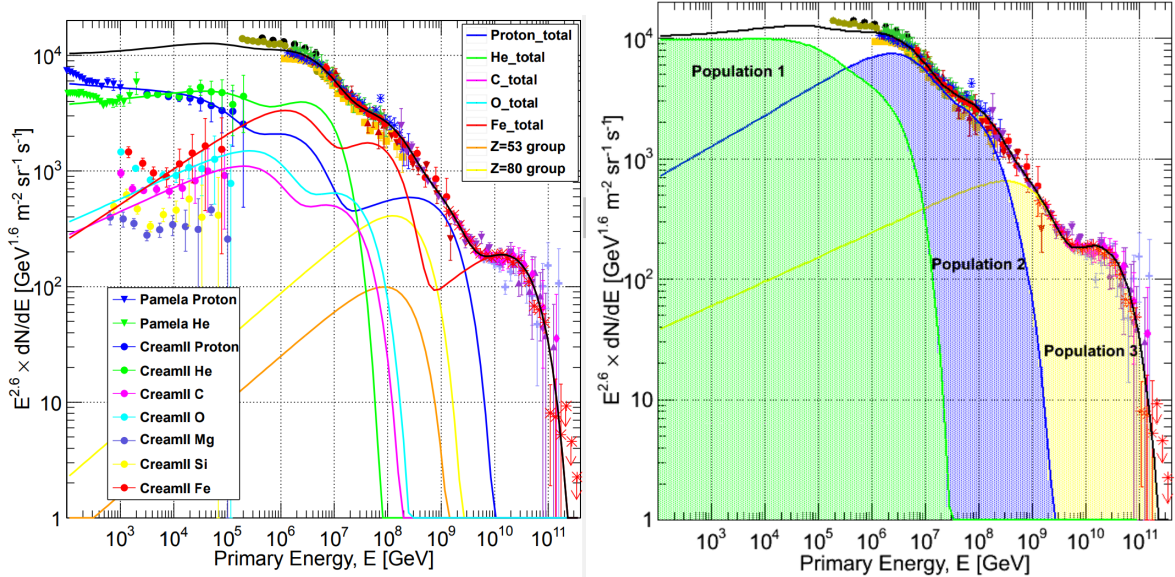


Figure 3.3: Overview of the categorization of the cosmic-ray spectrum as done in Ref. [101]. The individual components are shown on the left, and the total contribution of the three proposed populations are shown on the right.

supernova remnants, with the knee signaling the cutoff of this population. The second population is a higher-energy galactic component of unknown origin. The third generation will be described in more detail in Section 3.1.2.2. Assuming that the primary spectrum depends on the *magnetic rigidity**,

$$R = \frac{pc}{Ze}, \quad (3.4)$$

where Ze is the charge of a nucleus of total energy $E_{tot} = pc$. The magnetic rigidity relates to the gyroradius of a particle, r_g , in a given magnetic field B as

$$r_g = \frac{R}{B}. \quad (3.5)$$

If there is a characteristic rigidity, R_e , above which a particular acceleration process reaches a limit, then the feature will show up in total energy first for protons, then for helium and so forth for heavier nuclei according to

$$E_{tot} = Ze \times R_e. \quad (3.6)$$

This effect is visualised in Figure 3.3 and indicates that as one population reaches its maximum, the composition becomes heavier. The second knee, reported by KASCADE-Grande [105] and GAMMA [106] could be explained with an “iron knee” bump.

3.1.2.2 Extragalactic component

Very-high-energy cosmic rays are almost certainly from extragalactic origin and result in a flux at the highest energies that is exceedingly small. The number of events at energies above 5 EeV is around one per square kilometer per century. There are only two experiments in the world capable of detecting the highest-energy cosmic rays in a statistically meaningful way: Telescope Array, located in the Northern Hemisphere (instrumented area of ≈ 700 km²) and the Pierre Auger Observatory in the Southern Hemisphere (instrumented area of ≈ 3000 km²).

Both experiments see a suppression of the flux above 6×10^{19} eV. The cutoff is consistent with the expected Greisen-Zatsepin-Kuzmin (GZK) effect [107, 108] where cosmic rays interact with the cosmic microwave background radiation (CMB)

* An assumption that is experimentally favored over other assumptions. Rigidity is an appropriate variable for interpreting changes in the spectrum due to propagation and acceleration in magnetic fields.

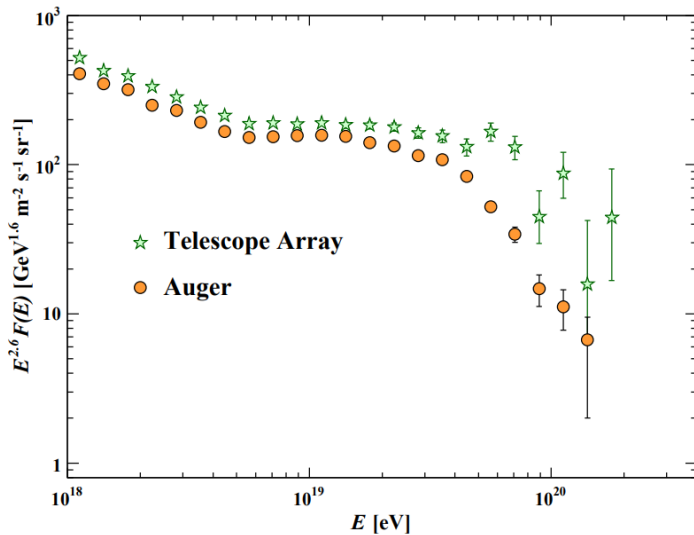


Figure 3.4: Expanded view of the highest energy portion of the cosmic-ray spectrum from data of the Telescope Array and the Pierre Auger Observatory [42].

$$\gamma_{CMB} + p \rightarrow \Delta^+ \rightarrow p + \pi^0 \quad (3.7)$$

or

$$\gamma_{CMB} + p \rightarrow \Delta^+ \rightarrow n + \pi^+. \quad (3.8)$$

The Pierre Auger experiment reported to see higher compositions at the highest energies [109]. If the particle is a nucleus with A nucleons, then the GZK limit applies to its nucleons, which carry only a fraction $1/A$ of the total energy. For iron nuclei this would for example result in a limit of 2.8×10^{21} eV. In contrast, the TA experiment interpreted their data as implying a light primary composition (mainly p and He) at the highest energies. Both experiments use a different interpretations for crucial quantities of these measurements and a thorough joint analysis conducted by both experiments states that, at the current level of statistics and understanding of systematics, both data sets are compatible with being drawn from the same parent distribution [42].

The exact origin of Ultra High Energy Cosmic Rays (UHECR) is uncertain. We will see in Section 3.1.3.1 that the maximum energy from shock acceleration by a supernova remnant is insufficient to explain UHECRs. Particles can be accelerated if the trajectory of the particles can be changed and energy can be transferred multiple times. The magnetic fields responsible for the course change of these particles have to be sufficient in magnitude in order for these particles not to escape and go beyond the reach of the source responsible for the acceleration. This limitation is expressed by the gyroradius of the accelerator, $r_L = E/ZeB$ similar to Eq. 3.5, requiring it to be smaller than the physical radius of the accelerator: $r_L < R$ or $E < ZeBR$.

Even if only qualitative, this relation provides an interesting criterion to identify possible sources of UHECRs by looking at the accelerator related term BR . This was done in a classic paper by Hillas [110], illustrated in the more recent Figure 3.5. Accelerators necessary to explain the amount of UHECRs are not populated (enough) in our galaxy, making them more likely to be of extra-galactic origin. Active galactic nuclei, gamma ray bursts, starburst galaxies, and galaxy clusters, which are currently thought to be the sources of UHECRs, are therefore also briefly explained.

To this date, it has not been proven that these sources all contribute and if they are the sole contributors. There are also more exotic theories on the origin of UHECRs, such as the decay of superheavy particles [112].

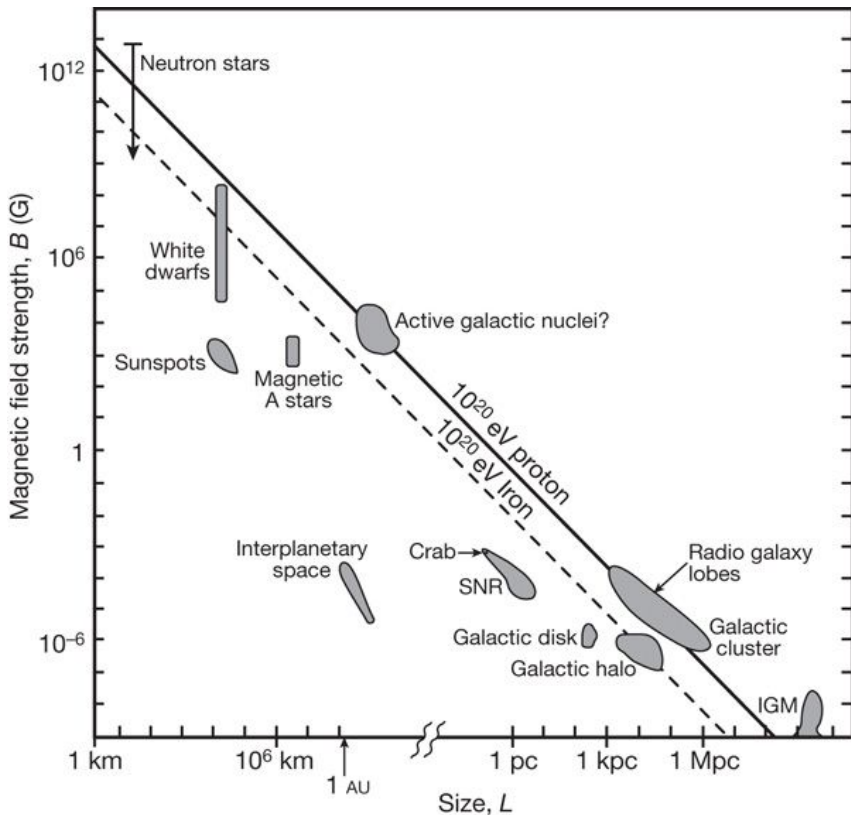


Figure 3.5: The Hillas plot of potential cosmic ray accelerators determines objects according to size and magnetic field. Objects to the left of the diagonal lines cannot accelerate particles to 10^{20} eV (proton: solid, iron: broken). Image obtained from Ref. [111].

The Pierre Auger Observatory also reported evidence for an anisotropic distribution of the arrival directions of the highest-energy cosmic rays from a direction where the distribution of galaxies is relatively high and does not coincide with the galactic plane [113]. These observations, together with our lack of known possible sources within our galaxy for these ultra-high energies is compelling evidence that these particles have an origin from outside our galaxy. From pion decay, there is also an expected flux from extragalactic neutrinos (more information in Section 3.3.3 and ??). The flux, spectrum and angular distribution of the excess neutrino signal detected by IceCube between ≈ 50 TeV and ≈ 2 PeV are also inconsistent with those expected for Galactic sources [114].

3.1.3 Acceleration mechanism

How cosmic rays got their signature slope in the energy spectrum and its intricate details have been under discussion for multiple decades. To this date, there is no clear detailed picture how these particles are accelerated. It is beyond the scope of this work to give a comprehensive overview of all possible acceleration mechanisms or possible sources. Most calculations are left out and for a more detailed discussion, the reader is referred to specialized books or the references in the text.

The acceleration of the particles can be subdivided into two questions. First, where are the particles accelerated? Does it happen on large scales, cosmological distances in galaxies or near specific sources? Secondly, how are these particles exactly accelerated? What is the driving mechanism? Since primary cosmic rays are all electromagnetically charged particles, these mechanisms should clearly be sought for in places where electric and/or magnetic fields play a dominant role. Below, a summary of the possible sources is given.

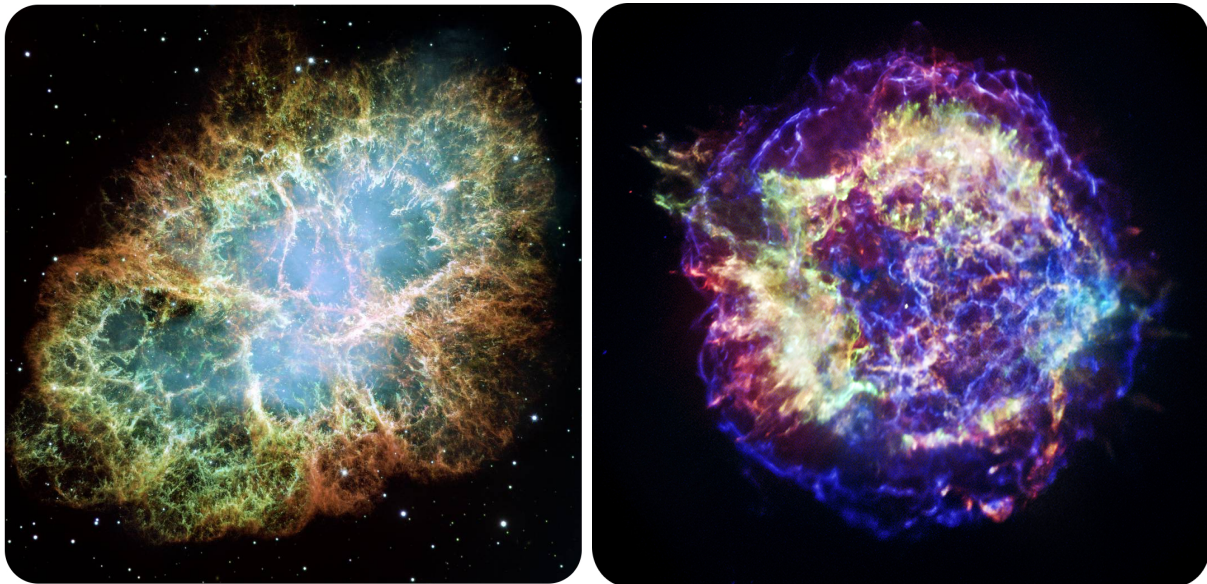


Figure 3.6: *Left:* the Crab Nebula is a supernova remnant approximately one thousand years old. The supernova was noted by Chinese astronomers in the year 1054 AD. *Right:* Chandra X-ray observatory picture of the Cassiopeia A supernova remnant (pictures from NASA).

3.1.3.1 Supernova (remnants)

Supernovae can be broadly subdivided in two categories: type I and type II. Type I supernova explosions happen in binary star systems. In those systems, one of the two stars is a carbon-oxygen white dwarf that accretes matter from the second star. When the total mass of the white dwarf reaches the Chandrasekhar limit of around 1.44 solar masses, it cannot longer hold itself under the gravitational pressure and collapses in on itself. Within seconds, the carbon component in the white dwarf starts nuclear fusion and enough energy is released to produce an explosion brighter than the Sun with a factor of around 5 billion. A resulting shock wave can reach up to around 3% of the speed of light.

Type II supernova explosions differ by being single star systems. When a star reaches the end of its lifecycle, the subsequent fusion reactions reach a halt. If the star has enough mass (at least 8 times the mass of the Sun), it is possible for the inner core to again reach the Chandrasekhar limit and collapse in on itself due to the lack of *electron degeneracy*. Without the outward pressure of nuclear fusion reactions and the support of the core, the outer layers of the star collapse under the gravitational pressure. The compression of the electrons and protons into neutrons results in a very hot, dense, neutron core. The velocity of the inward falling layers can reach a staggering 23% of the speed of light and recoil when hitting the remaining core. The outward going shockwave hits the remaining outer layers forming the supernova explosion*. This violent core collapse is an additional neutrino production mechanism.

Because of their brightness, supernovae within our galaxy can be seen with the naked eye (provided they are not obscured). The last recorded supernova from our galaxy was by Kepler in 1604 but earliest recordings go back to 185 AD by Chinese astronomers†.

The question remains how supernovae can serve as cosmic ray accelerators. In 1949, Fermi

*To get a better feeling of how extraordinary these events really are, I'd like to illustrate what it would be like if one could be close to a supernova event. From Figure 3.11, one can calculate that the number of solar neutrinos going through our hand per second is around *one trillion*. Yet they are so weakly interaction that, on average, only one will interact with an atom in our body every few years. Supernova explosions are vast, releasing around 10^{57} neutrinos. This number is large enough that even if an observer is a distance of 2.3 AU away from the event, he would still receive a fatal radiation dose of *neutrinos alone*. As another example: looking at a supernova at a distance of 1 AU is 10^9 times brighter than detonating a hydrogen bomb pressed against your eyeball.

†From observations of other galaxies, supernovae are expected to occur, on average, once every thirty years. Not all of these will be visible to the naked eye, but would almost certainly be observable with modern astronomical telescopes.

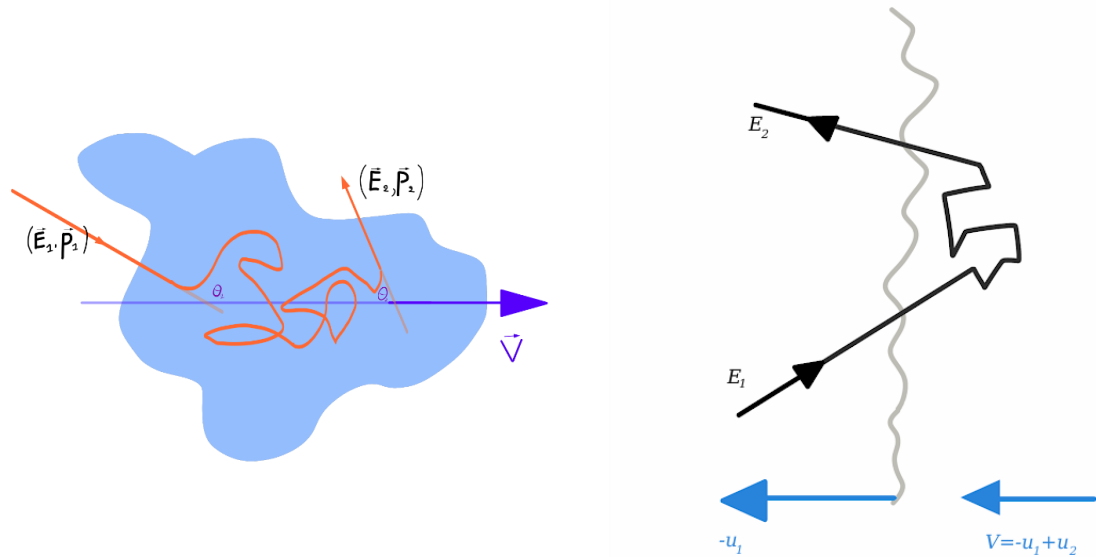


Figure 3.7: *Left:* magnetic cloud showing second-order Fermi acceleration. *Right:* shock waves typically have magnetic inhomogeneities both preceding (downstream) and following them (upstream). If a charged particle travels through the shock wave, it can gain velocity through first-order Fermi acceleration. In the illustration, a particle travels from upstream to downstream and back upstream. At every back and forth movement, the particle effectively gains energy. For a particle with a velocity u_1 relative to the shock front, the front seems to come at him with velocity $-u_1$. The downstream medium has a velocity relative to the shock front of $u_2 < u_1$ making it seem coming towards the particle with velocity $u_1 - u_2$.

proposed a mechanism where particles can gain energy by collisions with moving interstellar ionized gas clouds. Only later, it was realized that a large, plane shock front moving with a certain velocity is able to accelerate charged particles much more efficiently. This first mechanism results in an energy transfer proportional to the squared velocity of the cloud and is thus called *second order Fermi acceleration*. Shock front acceleration energy transfer is proportional to the velocity and is called *first order Fermi acceleration*. Supernova remnants provide an explanation for the origin of these shock fronts.

First- and second-order Fermi acceleration

Suppose we have a magnetic cloud in the interstellar medium travelling with a certain velocity \vec{V} and a particle with velocity \vec{v} enters the cloud under an angle θ_1 (see Figure 3.7). If we assume collisionless scattering (no energy is dissipated from the particle to the cloud) due to the magnetic fields in the cloud, the magnitude of the momentum in the rest frame of the cloud will not change ($E'_1 = E'_2$, where the apostrophe denotes the cloud rest frame). From special relativity we know that:

$$\begin{aligned} E'_1 &= \gamma (E_1 - p_{1,\parallel} V) \\ &= \gamma E_1 (1 - \beta \cos \theta_1), \end{aligned} \tag{3.9}$$

with $\beta = V/c$ and γ the Lorentz factor. Similarly, and using $E'_1 = E'_2$

$$\begin{aligned} E_2 &= \gamma E'_2 (1 + \beta \cos \theta'_2) \\ &= \gamma^2 E_1 (1 - \beta \cos \theta_1) (1 + \beta \cos \theta'_2) \end{aligned} \tag{3.10}$$

and

$$\frac{\Delta E}{E} = \frac{E_2 - E_1}{E_1} = \frac{1 - \beta \cos \theta_1 + \beta \cos \theta'_2 - \beta^2 \cos \theta_1 \cos \theta'_2}{1 - \beta^2} - 1. \quad (3.11)$$

By hypothesis, the escaping particles are isotropic in the cloud frame: $\langle \cos \theta'_2 \rangle = 0$. One can show that $\langle \cos \theta_1 \rangle = -\frac{\beta}{3}$ [95], leading to

$$\frac{\Delta E}{E} = \frac{4}{3} \frac{\beta^2}{1 - \beta^2} \approx \frac{4}{3} \beta^2, \quad (3.12)$$

showing that for molecular clouds, the energy gain is indeed proportional to the square of β , thus second-order Fermi acceleration.

If a particle is incoming to an expanding shock (see Figure 3.7), one can prove that $\langle \cos \theta_1 \rangle$ is equal to $-2/3$ and $\langle \cos \theta'_2 \rangle$ is equal to $2/3$, leading to

$$\frac{\Delta E}{E} = \frac{\frac{4}{3}\beta + \frac{13}{9}\beta^2}{1 - \beta^2} \approx \frac{4}{3}\beta, \quad (3.13)$$

where β is now equal to $u_1 - u_2$, as explained in the caption of Figure 3.7. We have shown that for shock fronts the energy gain is indeed proportional to β for first-order Fermi acceleration.

Power

The energy gain of a “single collision” results in a powerlaw spectrum when considering a process in which a test particle increases its energy by an amount proportional to its energy with each encounter. Let us assume $\Delta E = \xi E$, then, after n encounters:

$$E_n = E_0 (1 + \xi)^n, \quad (3.14)$$

where E_0 is the energy when the particle first enters the accelerator medium. To reach a certain energy E' , the particles must undergo a number of collisions

$$n(E') = \frac{\ln \left(\frac{E'}{E_0} \right)}{\ln (1 + \xi)}. \quad (3.15)$$

To reach energies of E' or higher, the number of collisions will be proportional to

$$\begin{aligned} N(\geq E') &\propto \sum_{m=n}^{\infty} P_{present}(m) = \sum_{m=n}^{\infty} (1 - P_{esc})^m \\ &= (1 - P_{esc})^n \left((1 - P_{esc}) + (1 - P_{esc})^2 + \dots \right) \\ &= \frac{(1 - P_{esc})^n}{P_{esc}}, \end{aligned} \quad (3.16)$$

where $P_{present}$ is the probability of a particle still being present in the accelerator and P_{esc} the probability of the particle to escape per collision. Making use of $a^{\ln b} = e^{\ln a \ln b} = b^{\ln a}$ and inserting Eq. 3.15 yields

$$N(\geq E') \propto \frac{1}{P_{esc}} \left(\frac{E'}{E_0} \right)^{-\gamma}, \quad (3.17)$$

with

$$\gamma = \frac{\ln \left(\frac{1}{1 - P_{esc}} \right)}{\ln (1 + \xi)} \approx \frac{P_{esc}}{\xi}. \quad (3.18)$$

The power law spectrum becomes visible in the derivative of the number of particles in energy

$$\frac{dN}{dE} \sim E^{-(\gamma+1)}, \quad (3.19)$$

in agreement with Eq. 3.1 (although γ is not the same variable here). Shock wave fronts have an expected $\gamma \approx 1$, giving rise to a different spectrum to what is seen on Earth but which can be explained by propagation from the source to Earth (see 3.1.4). The spectrum from Fermi shock acceleration is thus expected to follow an E^{-2} powerlaw behavior.

Maximum energy

The highest energies that particles can be accelerated to can be defined by

- the differential energy gain per collision dE/dt , and
- the total time the particle can be accelerated.

The energy gain is given by

$$\frac{dE}{dt} = \frac{\xi E}{T_{cycle}}, \quad (3.20)$$

where T_{cycle} is the characteristic time for one acceleration cycle. T_{cycle} depends on the diffusion coefficients and velocities of the upstream and downstream regions and is set to $T_{cycle} \geq 20E/(3u_1ZeB)$ by Lagage and Cesarsky [115] for a strong shock and arguing that the diffusion length, λ_D , cannot be smaller than the Larmor radius of the particle. Particles with a Larmor radius greater than the irregularities holding a magnetic field are not prone to be heavily influenced by them. Lagage and Cesarsky therefore concluded that

$$E_{max} \leq \frac{3}{20} \frac{u_1}{c} ZeB(u_1 T_{ST}), \quad (3.21)$$

where T_{ST} is the Sedov-Taylor time where particles are less prone to escape and is ~ 1000 years. For $u_1 \sim 10^9$ cm/s [116] and $B \sim 3\mu G$ the Lagage and Cesarsky limit reads

$$E_{max} \leq Z \times 2.4 \times 10^{14} \text{ eV}. \quad (3.22)$$

3.1.3.2 Active Galactic Nuclei

Active Galactic Nuclei (AGNs) are no stars at the end of their life cycle but active black holes located in the center of galaxies. It is believed that most massive galaxies have supermassive black holes in their centers by the accretion of matter from surrounding large gas clouds [117, 118]. However, this is still under debate. AGN masses in current models range from 10^6 to 10^{10} solar masses [119].

The efficient conversion of gravitational potential energy to kinetic energy and radiation make AGNs the most luminous persistent sources of electromagnetic radiation in the universe. As such, they serve as very good tools to discover distant objects. The accretion discs heat up due to friction from the inward falling and produce light peaking in the ultraviolet waveband. Certain emission lines are also expected due to the radiation from excited cold atomic material. Some accretion discs produce jets, which point opposite to each other. Their direction is defined by either the spin of the black hole, the accretion disc or a combination of both. The most powerful AGNs are classified as *quasars* and AGNs with a jet pointing toward the Earth are called *blazars*.

Charged particles can have a large magnetic rigidity in AGNs and the relativistic jets could provide the necessary mechanisms to accelerate particles to ultra-high energies. The Pierre Auger collaboration hinted to a correlation of the highest-energy cosmic rays with the positions of nearby active galactic nuclei [120].

3.1.3.3 Gamma Ray Bursts

The most catastrophic deaths of massive stars or mergers of two neutron stars or of a neutron star and a black hole result into Gamma Ray Bursts (GRBs). GRBs are named after the burst of gamma rays that is followed by a longer-lived afterglow of electromagnetic radiation at longer wavelengths. These bursts are the most energetic explosions in the electromagnetic spectrum and occur when a high-mass star collapses to form a neutron star or black hole. A typical burst releases as much energy in a few seconds than the Sun does in its entire 10 billion-year lifetime

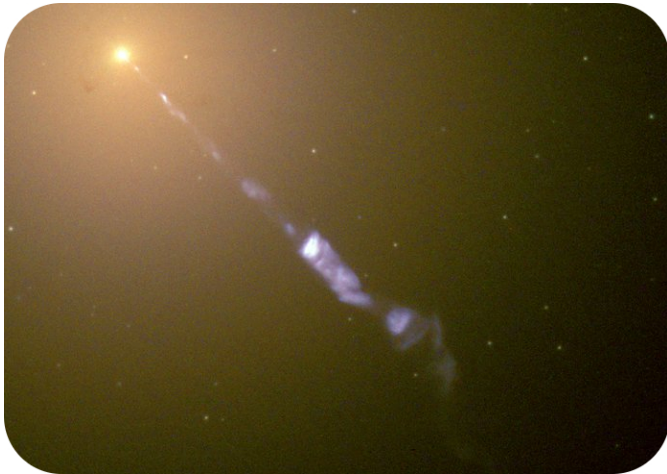


Figure 3.9: Image from the Hubble telescope where we see a jet streaming out from the center of galaxy M87.

and temporarily outshines the rest of the galaxy*. GRBs are isotropically distributed, making them extragalactic in origin [122].

An often used model to explain how charged particles could reach extremely high energies is called the *fireball model*. This internal-external shock model assumes that kinetic energy of an ultra-relativistic flow is dissipated in internal collisions.

Although there is still much ongoing discussion, GRBs are usually subdivided into two groups: *long gamma ray bursts* ($t_{burst} > 2$ s) and *short gamma ray bursts* ($t_{burst} < 2$ s). Long bursts originate from collapsars: a massive star core-collapse forms a black hole and surrounding matter is pulled into an accretion disk. Short bursts hint to progenitors that are extremely compact, where neutron-neutron star or neutron star-black hole mergers are the most probable explanation. The recent detection of gravitational waves can provide a significant contribution to the understanding of these sources [123, 124, 125, 126, 127].

3.1.3.4 Starburst galaxies

Galaxies that undergo an episode of large-scale star formation, are called *starburst galaxies*. Most of these are in the midst of a merger or close encounter with another galaxy. Several experiments have shown their gamma ray emission at several hundred GeV to be two to three orders of magnitude of that in our own galaxy [128, 129]. Galactic scale winds from the central regions are possible sources for cosmic ray acceleration.

3.1.3.5 Galaxy clusters

When galaxies are bound together by gravity, they are referred to as *galaxy clusters*. They can contain around 100 to 1000 galaxies and have typical mass ranges around $10^{14} - 10^{15}$ solar masses. Through merging and accretion of dark matter and baryonic gas, galaxy clusters are expected to generate powerful shock waves on large scales. Shocks with significant velocities could provide the necessary conditions for cosmic ray acceleration [130].

3.1.4 Propagation

After creation, particles also encounter propagation effects on their way to Earth. For example, charged particles can be deviated in magnetic fields close to or far from their source and the Earth's magnetic field. The particles can interact with expelled matter from the source soon after their creation. Other possibilities are gas clouds **hoe nauwkeurig is dit?**, leading to spallation effects or a loss of energy. The models describing these effects will not be given in this work.

*GRBs were first discovered in the late 1960s by accident. The Vela satellites had additional gamma ray detectors designed to detect very fast bursts of gamma rays that were expected to be produced by nuclear tests in space [121].

However, it is noteworthy to mention that in these models the measured cosmic ray flux becomes much softer than the source flux. The discrepancy between spectral indices around $-2.7/-3$ and a theoretical source flux around -2 is usually attributed to these propagation effects. For more information, I refer the reader to Ref. [95].

3.2 Air showers

When primary cosmic ray particles hit the Earth's atmosphere, they give rise to a large shower of secondary particles. At low- to mid-energy ranges, the abundance of cosmic rays is large enough for these showers to be analyzed with balloon or satellite experiments. As indicated in Section 3.1.2, the flux of high-energy cosmic rays is so small that there is a need for very large-scale detectors, measuring square kilometers in instrumented area.

The interaction length of nuclei with high energies is too small for them to be able to travel as close as a couple of tens of kilometers in height as measured from the ground. They will interact with an atmospheric nucleus and produce secondary particles. These particles in their turn decay or interact further with the atmosphere and give rise to an *extensive air shower* (EAS) if the production of new particles is large enough. Some of these particles will be stopped, but others are capable of reaching the Earth or even penetrate deep inside it. Although air showers are of significant importance in cosmic ray studies, we will only give a brief summary of the most noteworthy features and its main importance for this analysis. An air shower has three components: the hadronic, muonic and electromagnetic. The hadronic component can be seen as the core of the shower, consisting of high-energy hadrons. The interactions and subsequent decays of these hadrons fuel the electromagnetic and muonic parts. A schematic overview is given in Figure 3.10. If the primary particle is a photon, the shower is made up almost exclusively of an electromagnetic component. Because the lateral size of an electromagnetic cascade is caused by multiple scatterings of electrons and positrons, the lateral size of these showers is relatively small (radius around 1 km for a vertically downgoing 100 TeV photon). In hadronic cascades, on the other hand, the lateral size is caused by the transverse momenta of the secondary particles making these showers much larger (radius around 4 km for a vertically downgoing 100 TeV proton) [131].

3.2.1 Hadronic component

When a proton interacts with a nucleus, it interacts with another proton or a neutron and will most often produce charged or neutral pions

$$\begin{aligned} p + N &\rightarrow p + N + k\pi^+ + k\pi^- + r\pi^0, \\ p + N &\rightarrow n + N + (k+1)\pi^+ + k\pi^- + r\pi^0, \end{aligned} \quad (3.23)$$

where N stands for a nucleon of an atmospheric nucleus and k and r are the multiplicities of the produced pions. The extension to heavier nuclei from this is straightforward. On average, one-third of the hadron production will be neutral pions ($k/r \approx 3$), which decay immediately into electromagnetic particles

$$\pi^0 \rightarrow \gamma + \gamma \quad (98.8\%) \text{ or} \quad (3.24)$$

$$\pi^0 \rightarrow e^+ + e^- + \gamma \quad (1.17\%). \quad (3.25)$$

The other two-thirds will be charged particles that have a lot longer lifetime, making them much more probable to interact with air nuclei. After having traveled a distance corresponding to their mean interaction length, charged particles interact again with air nuclei if their energy is large enough. 90% of these charged particles are new pions and 10% of the daughter particles are kaons. Pions almost exclusively decay to muons ($\pi^+ \rightarrow \mu^+ + \nu_\mu$) and the most dominant kaon decay modes are (similar for K^-) [42]

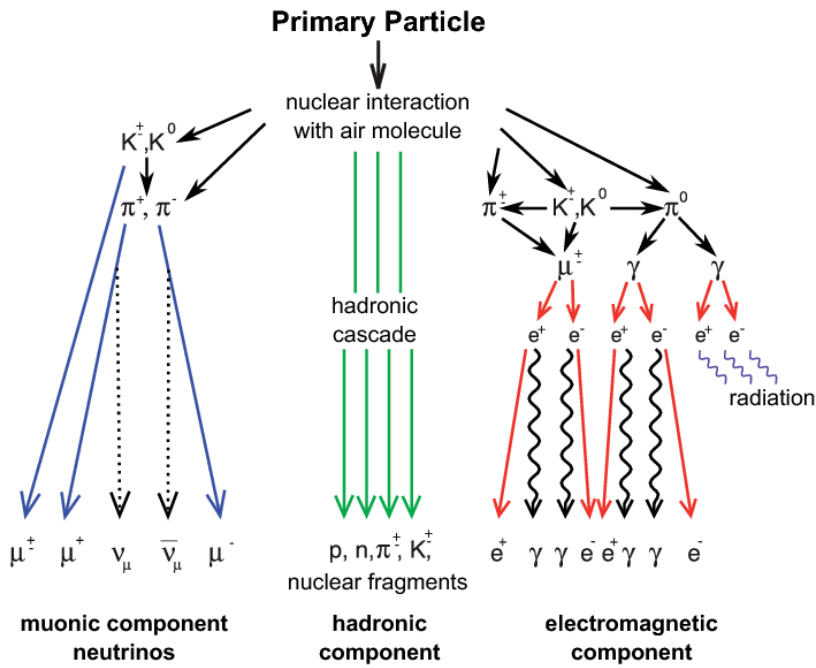


Figure 3.10: Schematic view of an extensive air shower with a clear distinction between the three components. Image from the KASKADE collaboration.

$$\begin{aligned}
 K^+ &\rightarrow \pi^+ + \pi^0 & (20.7\%), \\
 K^+ &\rightarrow \mu^+ + \nu_\mu & (63.6\%), \\
 K^+ &\rightarrow \pi^0 + e^+ + \nu_e & (5\%), \\
 K^+ &\rightarrow \pi^0 + \mu^+ + \nu_\mu & (3.4\%),
 \end{aligned} \tag{3.26}$$

where the first decay mode fuels the hadronic component further. The remaining decay modes enter in the EM and muonic components. The total number of hadrons reaching sea level is very small and when they do, they are immediately stopped.

3.2.2 Muonic component

Muons are the dominant component of particles reaching sea level (around 80%). Most muons that are produced in an EAS are able to reach so far due to their relativistic velocities and lifetime of $2.2 \mu s^*$. They have relatively low ionization losses compared to electrons, making them very penetrating and therefore referred to as the *hard component*. Muons can also decay and contribute to the electromagnetic component via

$$\begin{aligned}
 \mu^+ &\rightarrow e^+ + \nu_e + \bar{\nu}_\mu, \text{ and} \\
 \mu^- &\rightarrow e^- + \bar{\nu}_e + \nu_\mu.
 \end{aligned} \tag{3.27}$$

3.2.3 Electromagnetic component

At each hadronic interaction, slightly more than a third of the energy goes into the electromagnetic component. Since most hadrons re-interact, eventually most of the primary energy finds its way into the electromagnetic component. Muons also produce delta electrons or electron-positron pairs from pair production (see Section 4.4.5).

*The half-survival length of 5 GeV muons is $L = \ln(2) \times \gamma \times 2.2 \mu s \times 0.9998 \times c = \gamma \times 456 \text{ m} \approx 23 \text{ km}$. The relativistic time dilation is of crucial importance here!

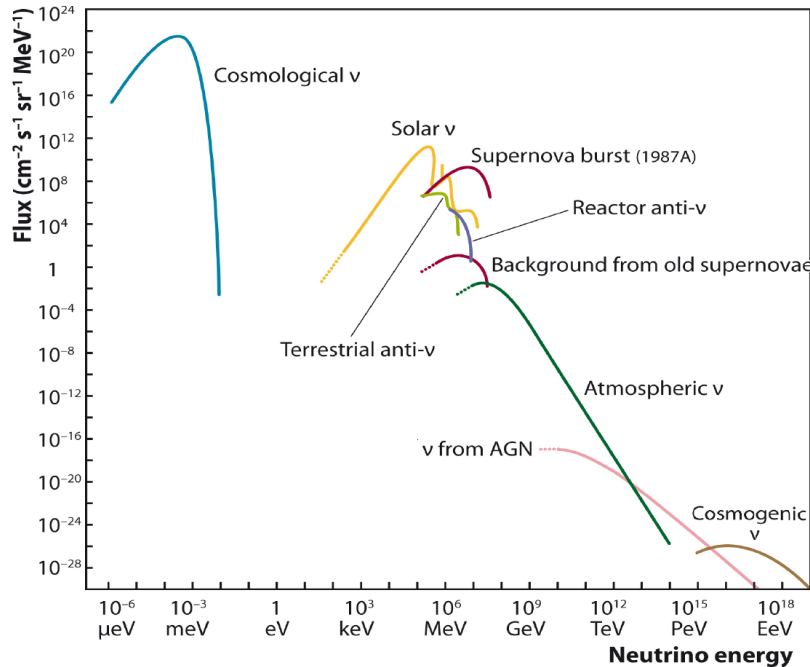


Figure 3.11: Plot illustrating several neutrino sources that cover a huge range of energy. Illustration from Ref. [132].

At energies above a few MeV, photons interact with the electric field of atmospheric nuclei in a process called pair production and convert into an electron-positron pairs. High-energy electrons and positrons primarily emit photons via bremsstrahlung. These two processes are repeated until the photons fall below the pair production threshold and bremsstrahlung energy loss starts to dominate. Because electrons lose their energy fast, they are almost immediately stopped when they reach dense matter (Earth's surface) and hence referred to as the *soft component*.

3.3 Neutrinos

As by-products of cosmic ray collisions with matter, neutrinos provide incontrovertible evidence for hadronic acceleration. Since these particles are weakly-interacting, they can escape much denser environments and hold crucial information about the origins of their production environments. Because these particles barely interact, their detection is difficult. Similarly to cosmic rays, neutrinos cover a broad range in energy (see Figure 3.11), calling for different types of detectors to cover this large spectrum.

Cosmic rays are deflected in magnetic fields and therefore, their arrival direction at Earth does not hold much pointing information (Figure 3.12, left). Light ranging from radio to gamma rays in the electromagnetic spectrum is of crucial importance in astrophysics but has its limitations: photons can be absorbed by interstellar medium, or are trapped in opaque sources. At higher energies ($\approx 10^{14}$ eV), photons interact with the CMB and produce electron-positron pairs ($\gamma + \gamma \rightarrow e^+ + e^-$). Unless the sources are closeby, no photons are capable of reaching Earth (see Figure 3.13, right). Neutrinos escape from the sources more easily and are not deflected by magnetic fields, making them key messengers in identifying cosmic ray accelerators. In the following, we will go over the different types of neutrinos that are detectable on Earth.

3.3.1 Conventional

Neutrinos are produced in large abundances in air showers (see Section 3.2; Eq. 3.26 and 3.27). The neutrinos that are produced with low to high energies (\approx MeV to PeV range) are called *atmospheric* or *conventional* neutrinos. They are primarily produced in pion or kaon decay. Due to helicity effects, pion and kaon decay to electrons/electron neutrinos is strongly suppressed

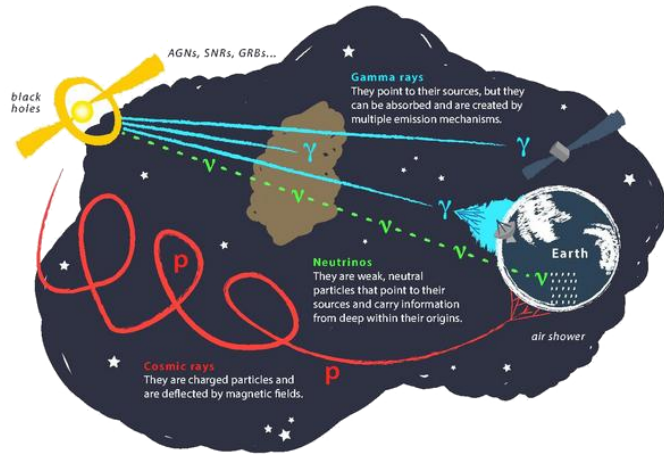


Figure 3.12: Artist impression of the path that several types of particles travel before reaching Earth.

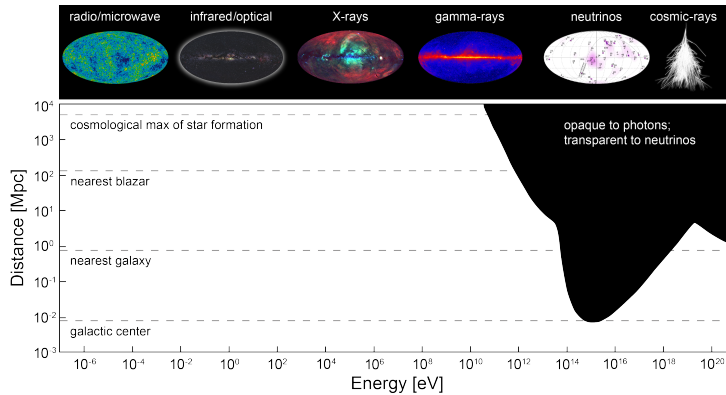


Figure 3.13: Illustration of the visibility of sources in function of their distance and the photon energy. The dip in the photon visibility comes from the pair production peak when photons interact with the CMB. Both illustrations from the IceCube collaboration.

compared to decays into muons/muon neutrinos. As a result, the ratio of electron neutrinos to muon neutrinos is about 2

$$\frac{N(\nu_\mu + \bar{\nu}_\mu)}{N(\nu_e + \bar{\nu}_e)} \approx 2, \quad (3.28)$$

which should be clear when we look at the example of pion decay where the muon decays as well



The most cited to calculations for the atmospherical neutrino flux were done by Honda et al. [133].

3.3.2 Prompt

Charmed mesons, also called D mesons, are the lightest particles that contain charm quarks*. Hints of charm particles were first seen in cosmic rays in 1971 by Niu et al. [135]. The production

* $D^0 : c\bar{u}, \bar{D}^0 : u\bar{c}, D^+ : c\bar{d}, D^- : d\bar{c}$

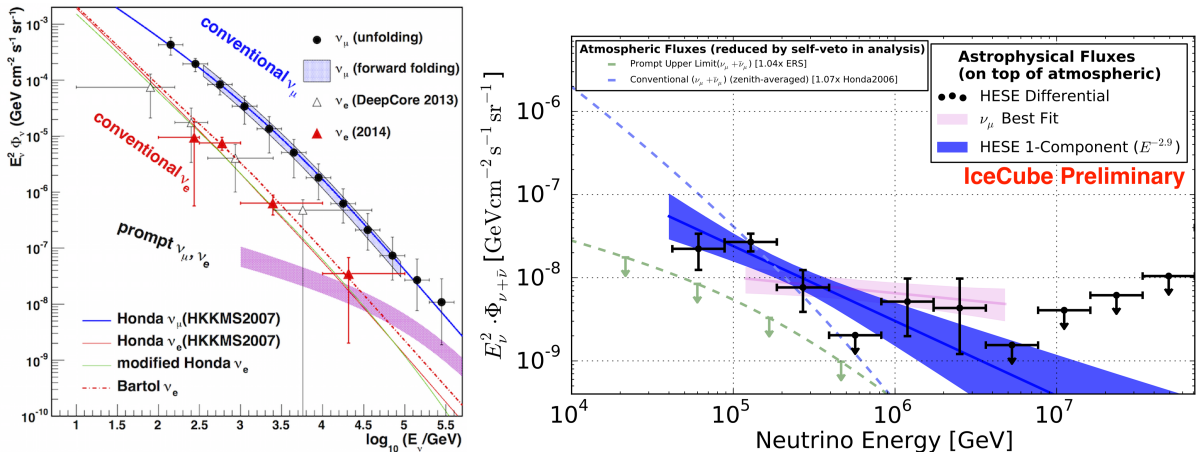


Figure 3.14: *Left:* Measurement from the IceCube collaboration showing the difference in ν_e and ν_μ flux. *Right:* Measured differential astrophysical flux using contained events (points) and a fit to that data (blue line and band), compared with the best fit obtained from through-going ν_μ (pink line and band). From Ref. [134].

of these particles is strongly suppressed, but is expected to exhibit a harder spectrum than conventional neutrinos do. These mesons have short lifetimes (hence the name: prompt) and decay into neutrinos independent of their energy and arrival direction. Therefore, their energy spectrum is expected to follow that of primary cosmic rays. Their contribution at higher energies can be non-negligible or even become dominant. To this date, it has not been possible to observe this prompt component, but it remains an interesting signal in diffuse neutrino searches and could contribute significantly to background expectations, usually in analyses looking for high-energy neutrinos. The most cited to calculations for the prompt neutrino flux were done by Endberg et al. [136].

3.3.3 Astrophysical

Astrophysical neutrinos are expected to be created when cosmic rays interact close to their interaction sites. Because they are neutral and are unlikely to be absorbed, astrophysical neutrinos are expected to reveal more information about these sources. To first order, these neutrinos would follow the spectrum of cosmic rays at their production. As indicated in Section 3.1.3.1, this is equal to an E^{-2} powerlaw spectrum from Fermi shock acceleration. The majority of these neutrinos are expected to arise from decays from pions that were created in these cosmic-ray interactions ($\pi \rightarrow \mu + \nu_\mu$) followed by the muon decay ($\mu \rightarrow e + \nu_e + \nu_\mu$). The resulting flavor ratio fraction is $\nu_e : \nu_\mu : \nu_\tau = 1 : 2 : 0$ at the source. Neutrino oscillations* across cosmological distances give an expected $\nu_e : \nu_\mu : \nu_\tau = 1 : 1 : 1$ expectation at Earth. Given the tension between different analyses, as can be seen in Figure 3.14, it is still unclear if the spectrum at high energies can be described with a single power law or something more complex.

The spectrum is expected to follow a harder spectrum compared to the conventional and prompt neutrinos and dominate at the highest energies.

Recently, a collaborative effort of IceCube, Fermi-LAT, MAGIC and others observed a coincidence of high-energy neutrinos and a blazar, making them very good candidates of sources of astrophysical neutrinos [137].

3.3.4 Other neutrino sources

The abovementioned neutrino sources are most important for high-energy neutrino research. Other, more abundant sources such as cosmological, solar, terrestrial and reactor neutrinos,

*Explained in Section 1.3.4.

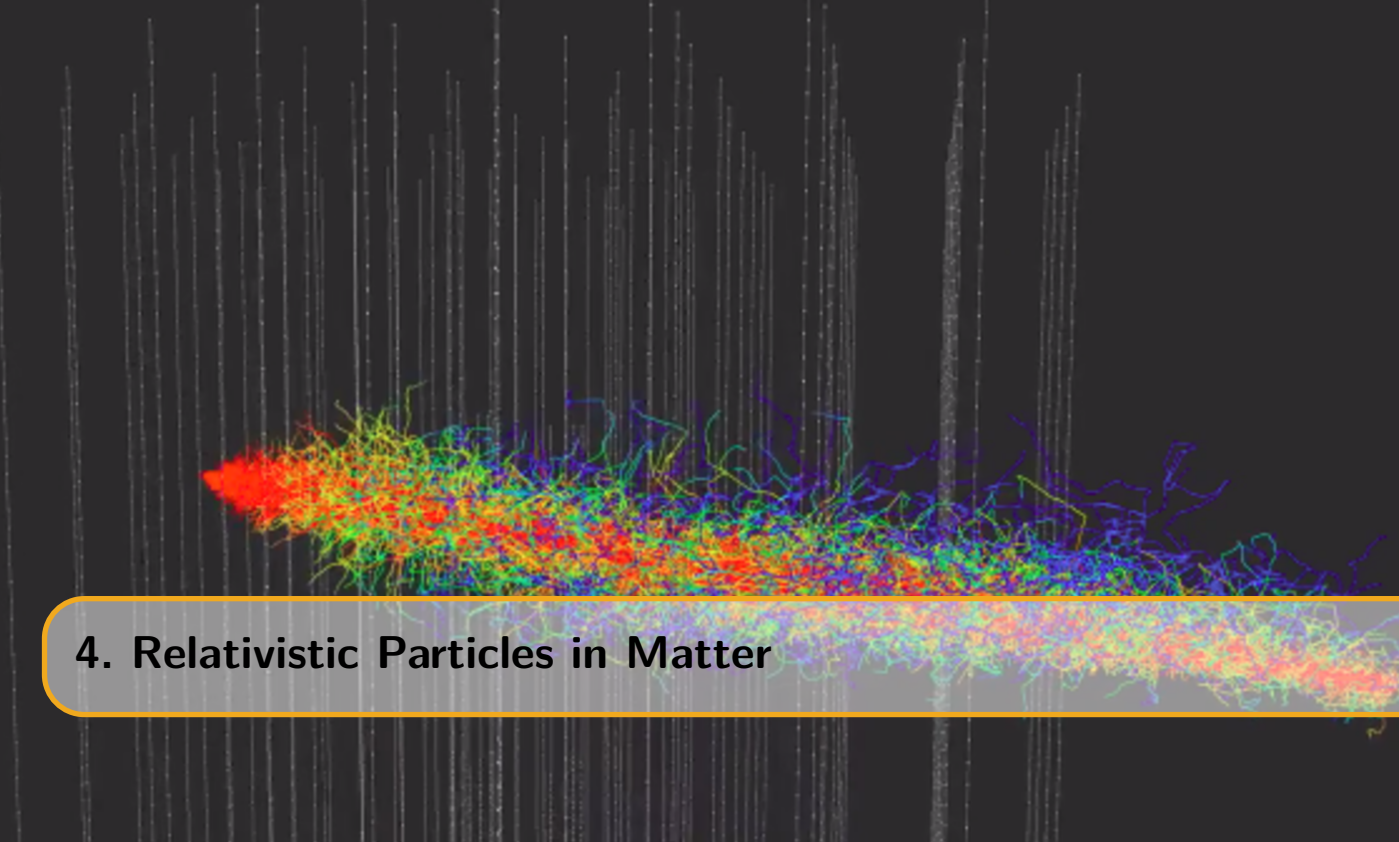
play less of a role in kilometer scaled detectors such as the IceCube detector (see Chapter 5). Supernova and GZK neutrinos have not yet been observed but are a part of the experiment's search strategies and therefore briefly explained below.

3.3.4.1 Supernova neutrinos

The core collapse of stars where electrons and protons are compressed into neutrons as described in Section 3.1.3.1 dissipates most of its energy in the production of neutrinos ($e^- + p^+ \rightarrow n + \nu_e$) [138]. Since the IceCube detector is designed to detect neutrinos with an energy greater than 100 GeV, supernova neutrinos with an energy of a couple of MeV are only visible to the detector due to a collective raise of the dark noise of the equipment. The sensitivity ranges from 20 standard deviations at the galactic edge (30 kpc) and 6 standard deviations at the Large Magellanic Cloud (50 kpc) [139].

3.3.4.2 GZK neutrinos

The GZK-effect was introduced in Section 3.1.2.2 where it was explained how high-energy cosmic rays interact with the CMB. The pions that are produced in this process can decay to neutrinos. These neutrinos are expected to have an energy above ~ 10 PeV. To this date, no neutrino events with an unquestionable GZK origin have been observed [140]. There are, however, ongoing experiments trying to measure the flux of these extremely energetic neutrinos (see Section 5.7.2.3).



4. Relativistic Particles in Matter

*Hofstadter's Law: It always takes longer than you expect, even when you take into account
Hofstadter's Law*

Charged particles that travel faster than the speed of light in that material produce light in a process that is called the *Cherenkov effect*. The production of photons makes it possible to detect particles with a non-zero charge (electrons, muons, SMPs, etc.) in a neutrino detector such as the IceCube experiment. This cubic-sized detector is able to register the light that is produced from charged particles in air showers and charged particles that are created when neutrinos interact with the ice around or inside the detector. In this chapter, an overview is given of the Cherenkov effect and the different other physical processes that are visible in the IceCube detector. These signatures have to be accounted for in the background prediction when looking for particles with an anomalous charge. Finally, the energy loss formulae of charged particles in matter are given.

4.1 Cherenkov effect

From Einstein's works on special and general relativity, it follows that the speed of light in vacuum, c , is a universal constant. The speed of light in matter can be significantly lower than that. If a particle travels through a dielectric medium at a speed that is greater than the phase velocity of light in that medium, electromagnetic radiation is emitted. This radiation is called *Cherenkov radiation* and is named after the first person who was able to detect it experimentally, Pavel Cherenkov. He was awarded the Nobel Prize in 1958 for his findings together with Frank and Tamm for their theoretical work on the subject [141].

The velocity of a propagating wave is given by the three-dimensional wave equation

$$\nabla^2 \psi = \frac{1}{v^2} \frac{\partial^2 \psi}{\partial t^2}, \quad (4.1)$$

where ψ is the wave function and v its group velocity. From Maxwell's equations and some vector calculus, it is straightforward to find that the wave equation for electromagnetic radiation becomes

$$\nabla^2 E = \mu \epsilon \frac{\partial E}{\partial t}, \quad (4.2)$$

where E is the electric field and μ and ϵ the permeability and permittivity of the medium, respectively. From these equations it is clear that for light in a dielectric medium

$$v = \frac{1}{\sqrt{\mu\epsilon}} = \frac{1}{\sqrt{\mu_r\epsilon_r}} \frac{1}{\sqrt{\mu_0\epsilon_0}} = \frac{1}{\sqrt{\mu_r\epsilon_r}} \times c \leq c, \quad (4.3)$$

where $1/\sqrt{\mu_0\epsilon_0} = c$ and μ_r and ϵ_r are the relative (to vacuum) permeability and permittivity, respectively and are ≥ 1 . These terms are also written as the refractive index of the medium, $n = \sqrt{\mu_r\epsilon_r}$ and result in

$$v = c/n. \quad (4.4)$$

When a charged particle moves inside a dielectric medium, it excites the molecules of the medium to the higher levels and excited states. The molecules emit photons in the form of electromagnetic radiation upon returning back to their ground state. According to the *Huygens principle*, the emitted waves move out spherically at the phase velocity of the medium (which can be less than the speed of light in vacuum). If the motion of the particle is slow, the radiated waves bunch up slightly in the direction of motion, but they do not cross. However, if the particle moves faster than the light speed, the emitted waves add up constructively, leading to a coherent radiation at angle θ_c with respect to the particle direction; Cherenkov radiation. The coherent interference is enough to be visible to the naked eye*. The signature of the effect is a cone of emission in the direction of particle motion. Figure 4.1 shows a schematic view of the Cherenkov radiation, illustrating the typical spherical wavefront and the resulting radiation†.

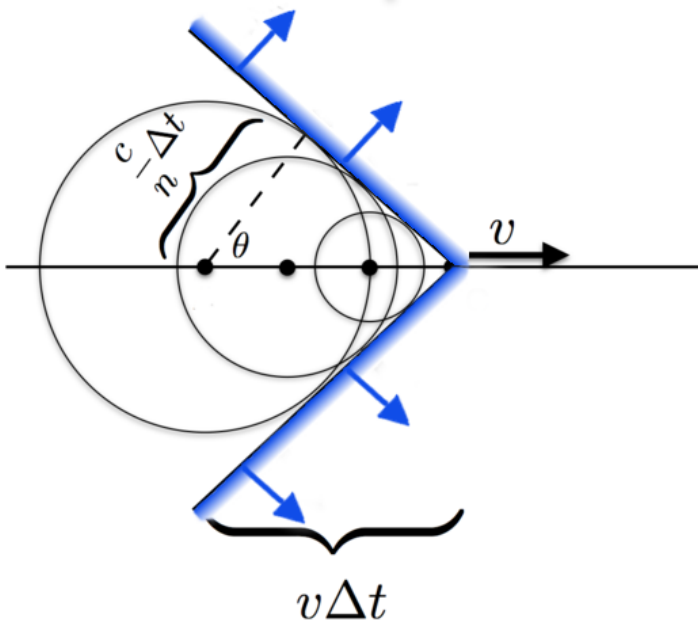


Figure 4.1: Schematic view of Cherenkov radiation from a particle traveling at a velocity v .

From the figure we can derive that

$$\cos \theta_c = \frac{\frac{c}{n}\Delta t}{v\Delta t} = \frac{c}{vn} = \frac{1}{\beta n}. \quad (4.5)$$

Because $-1 \leq \cos \theta_c \leq 1$, the velocity of the charged particle must be $v \geq c/n$. Typical values of n are on the order of 1-2, requiring the particles to be relativistic in order to emit Cherenkov radiation. The number of photons produced per unit path length of a particle with charge ze

*The typical blue light in the cooling water at nuclear reactors is also due to this Cherenkov radiation.

†The typical cone shape of this effect can be easily seen when observing ducks. If a duck is traveling in a straight line in the water, individual concentric waves can be distinguished and a cone shaped wave is produced behind them.

and per unit energy interval of the photon was calculated by Frank and Tamm, and is often referred to as the Frank-Tamm equation [42]

$$\begin{aligned} \frac{d^2N}{dEdx} &= \frac{\alpha z^2}{\hbar c} \sin^2 \theta_c = \frac{\alpha^2 z^2}{r_e m_e c^2} \left(1 - \frac{1}{\beta^2 n^2(E)} \right) \\ &\approx 370 \sin^2 \theta_c (E) \text{ eV}^{-1} \text{cm}^{-1} \quad (z = 1), \end{aligned} \quad (4.6)$$

where r_e is the classical electron radius, m_e the electron mass and α the fine-structure constant. Equivalently, this equation can be written in function of the wavelength of the photon

$$\frac{d^2N}{dxd\lambda} = \frac{2\pi\alpha z^2}{\lambda^2} \left(1 - \frac{1}{\beta^2 n^2(\lambda)} \right), \quad (4.7)$$

where it is clear that the charge of the particle will influence the total Cherenkov light yield. A charge of $1/3e$ will reduce the light output with a factor of 9 compared to a particle with a charge equal to the electron charge, e .

Examples of experiments that make use of this Cherenkov effect are air Cherenkov telescopes such as MAGIC, H.E.S.S and VERITAS that look for the direct and indirect Cherenkov light from gamma rays and cosmic rays. Because the refractive index of air is close to 1 (1.000293 at sea level and smaller with increasing height) the opening angle of the Cherenkov cone is small ($\approx 1^\circ$). The particles need to be very relativistic in order for Cherenkov radiation to occur*.

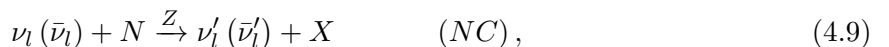
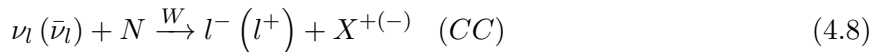
In water and ice, the refractive index is ≈ 1.33 , making $\beta_{min} = 0.75$ and $E_{min} = 1.51 \cdot m_0$. Experiments using water or ice as the interaction medium are Super-Kamiokande, ANTARES and the IceCube experiment.

Most of the light that is emitted from charged particles traveling through matter originates from this Cherenkov effect, provided that their energy is not too high. At higher energies, the amount of secondary particles with an energy high enough to produce Cherenkov effects themselves, becomes so large that this becomes the primary source of light (see Section 4.4). This analysis focusses on SMPs that lie below this threshold and we see from Eq. 4.7 that the charge of the SMP enters in the photon production quadratically. SMPs with a lower charge are therefore expected to produce less photons than minimum ionizing muons.

4.2 Neutrino interactions

The IceCube experiment is a neutrino detector, but neutrinos have no electromagnetic charge. Neutrinos are only visible through their production of secondary particles with an electromagnetic charge and emit Cherenkov radiation in the ice. Here, we briefly describe how these interactions take place.

Neutrinos interact with matter through both charged current (CC) and neutral current (NC) processes. In the former, the mediator particle is a charged W boson resulting in a charged lepton in the final state. In the latter, the mediator particle is the neutral Z boson. Both interaction types have a resulting hadronic component as daughter particles. The interactions can be written as



*Let us assume the refractive index of air at sea level, then, from $E^2/m^2 = \gamma^2 = 1/(1 - \beta^2)$, it follows that the minimal energy is ≈ 41 times its rest mass. Since the refractive index decreases in function of height, the energies of particles interacting with the atmosphere must be even higher.

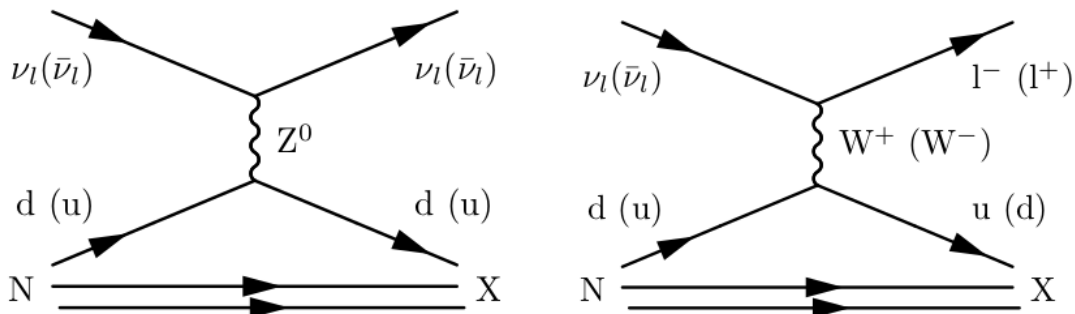


Figure 4.2: Feynman diagrams of NC (left) and CC (right) neutrino interactions. l is the lepton flavor (e, μ, τ), N denotes the initial hadronic state of the nucleus and X the final hadronic state. The antineutrino interactions are given in brackets.

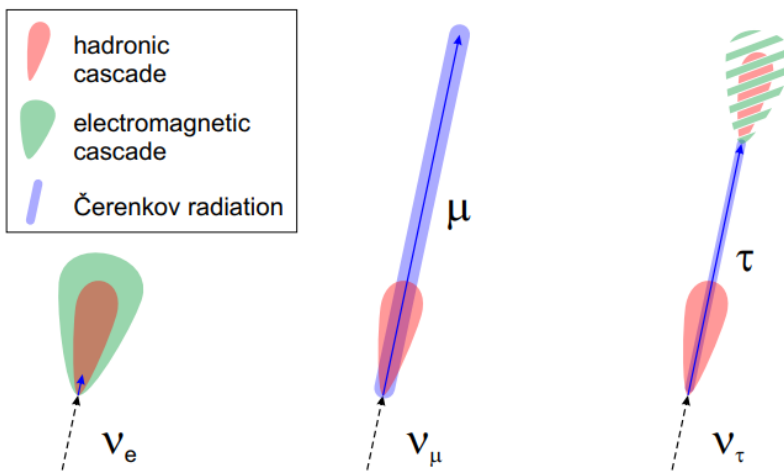


Figure 4.3: Schematic view of the neutrino signatures in matter. At each interaction point there is a hadronic cascade (red). Every hadronic cascade has electromagnetic sub-showers which are not illustrated here. Muons and energetic taus can give rise to tracks. The electromagnetic and hadronic cascades have a more spherical shape but are exaggerated for illustrative purposes in the figure. Illustrations from Ref. [142].

where l is the lepton flavor (e, μ, τ), N denotes the initial hadronic state of the nucleus and X the final hadronic state. These interactions are illustrated in Figure 4.2.

The charged leptons and hadrons lead to light production via gamma ray production and Cherenkov radiation. With the right material, it is possible to detect this light production and reconstruct some of the neutrino's characteristics.

4.3 Propagation

As described in Section 4.2, neutrinos give rise to several types of interactions in the surrounding medium. There are three characteristic signatures, which are the main interest in the IceCube detector (illustrated in Figure 4.3).

4.3.1 Cascades

4.3.1.1 Electrons and photons

In a charged current neutrino interaction, the energetic electron gives rise to a shower of gamma rays (bremsstrahlung) and positrons and electrons (pair production). Positrons and electrons in their turn emit new gamma rays and this process continues until the photon energies fall below

the pair production threshold. Because electrons/positrons lose their energy fast, they are almost immediately stopped, giving an *electromagnetic cascade* an almost spherical shape.

Let us assume E_0 is the energy of the incoming electron. In a very simplistic toy model one can say that an electron emits one photon after one radiation length, X_0 . A photon will decay into an electron-positron pair after approximately one radiation length too*. At every decay or radiation process, it is assumed that the daughter particles carry 1/2 of the energy. After t steps, the energy is equal to

$$E(t) = \frac{E_0}{2^t}. \quad (4.10)$$

The number of particles will be equal to

$$N(t) = 2^t. \quad (4.11)$$

At a critical energy E_c , the multiplication process stops (as pair production dominates over bremsstrahlung) and we find

$$t_{max} = \frac{\ln\left(\frac{E_0}{E_c}\right)}{\ln 2}, \quad (4.12)$$

the total longitudinal length of an electromagnetic shower is thus approximately equal to

$$X = X_0 \frac{\ln\left(\frac{E_0}{E_c}\right)}{\ln 2}. \quad (4.13)$$

This logarithmic dependence on the energy of the initial particle will therefore result into elongations of a couple of meters at most. Typical values in ice are $X_0 \approx 40$ cm and $E_c \approx 80$ MeV.

4.3.1.2 Hadrons

In the case of neutral current events, the breakup of the struck nucleus leads to charged byproducts. These byproducts can reinteract in the medium and produce neutral pions that decay into gamma rays. These particles again die out quickly, resulting in a spherical emission of light for *hadronic cascades*. The basic development of hadronic cascades in space is very similar to that of electromagnetic ones, but with important differences in energy loss, particle content, lateral spread and fluctuations. Hadronic cascades contain particles heavier than electrons, that have a higher Cherenkov threshold. A fraction of them are slow neutrons, which do not produce any light. Neutral pions produce gamma rays. Charged pions, on the other hand, can decay into muons and muon neutrinos; long-ranged particles that do not contribute to the cascading process. Finally, a non-negligible fraction of the energy is lost in the hadronic binding processes.

The light yield will be smaller than the one obtained from an electromagnetic cascade of equal initial energy and with much larger event-by-event variations.

4.3.2 Muon tracks

Muons are produced in charged current muon-neutrino interactions and travel much further than electrons and positrons. The relativistic muon will produce light according to the Frank-Tamm equation, Eq. 4.7, resulting in *direct Cherenkov radiation*. Ionization, bremsstrahlung, pair production, and photonuclear interactions (see Section 4.4) are also capable of producing relativistic secondary particles that produce *indirect Cherenkov radiation*. Both effects result in a Cherenkov cone with a diffuse light emission from the track in all directions behind it.

*In fact one radiation length implies $1/e$ times the initial energy. Assuming the electron loses half its energy to the photon, then $0.63/0.5 \approx 1$. After one radiation length, a high energy photon loses $\approx 7/9$ times its energy via bremsstrahlung, again we assume ≈ 1 .

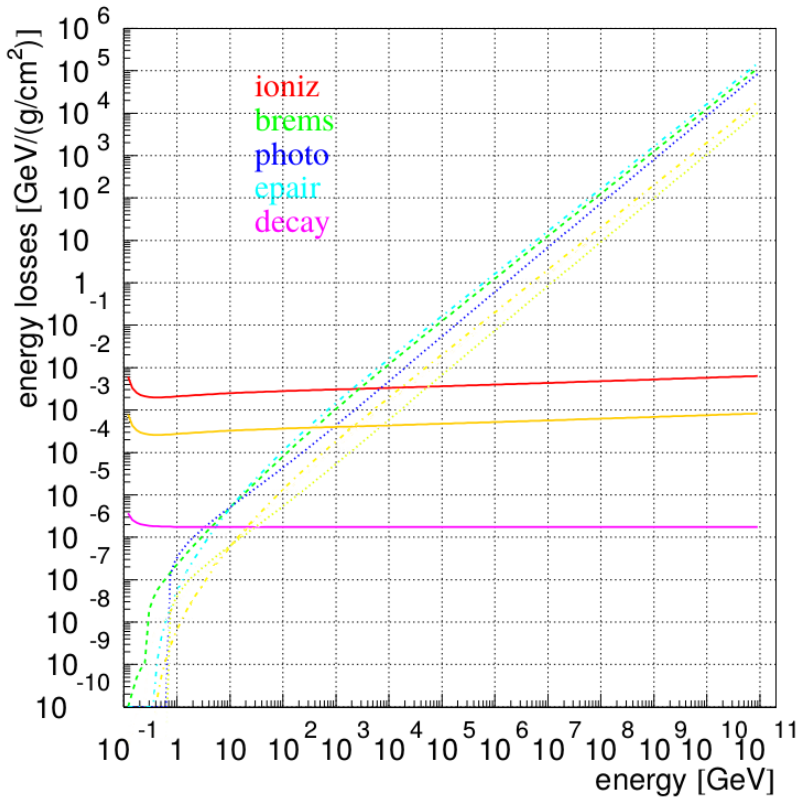


Figure 4.4: Muon energy loss from ionization (upper solid curve, red), bremsstrahlung (dashed, green), photonuclear (dotted, blue), pair production (dashed-dotted, cyan) and decay (lower solid curve, purple). Additionally, the expected energy losses of a muon with charge 1/3 are shown in orange/yellow. Ionization, photonuclear and pair production scale with z^2 , giving a factor 9 difference. Bremsstrahlung, which has a z^4 dependence is left out.

4.3.2.1 Energy loss

Below 1 TeV, muons will lose most of their energy to ionization losses. A charged particle traversing matter ionizes the material around it. When the energy transfer is high enough, electrons can be stripped away from their atoms, resulting in *delta electrons*. As can be seen in Figure 4.4, ionization losses have only a very weak energy dependence. It is therefore very difficult to distinguish for example a 50 GeV from a 500 GeV muon as the direct Cherenkov light production will be similar (Eq. 4.7) and the energy loss is from the energy-independent ionization.

Above 1 TeV, however, the muon, on average, loses more energy to stochastic* effects. Here, effects such as bremsstrahlung, pair production and the photonuclear effect dominate over ionization (see Section 4.4). Therefore, indirect Cherenkov production starts to dominate and makes the energy estimation much easier.

The average energy loss from ionization and stochastic effects along the muon trajectory can be parametrized by [143]

$$-\frac{dE}{dx} = a + b \cdot E_\mu, \quad (4.14)$$

where a and b are obtained by fitting and can be found in Table 4.1. Here a corresponds to the ionization energy loss (given by Eq. 4.17), and b corresponds to the sum of e^+e^- pair production, bremsstrahlung, and photonuclear contributions. The muon range can be found by integrating Eq. 4.14

*In this context we mean that the energy losses are not deterministic: it is impossible to know when an interaction of this kind will occur. One can only make estimations of their *expected* effects.

Table 4.1: Best fits for muon energy loss parameters a and b from Eq. 4.14. Fits from Ref. [144].

Medium	$a \left(\frac{\text{GeV}}{\text{mwe}} \right)$	$b \left(\frac{10^{-3}}{\text{mwe}} \right)$
Air	0.281	0.347
Ice	0.259	0.363
Fr. Rock	0.231	0.436
St. Rock	0.223	0.463

[†] Mwe stands for “meter water equivalent”, a unit often used in cosmic ray physics. A detector shielded by matter equal to 100 mwe would be equally shielded from cosmic rays if it were 100 meters below water.

$$R_\mu \approx \frac{1}{b} \ln \left(\frac{E_\mu}{E_{th}} + 1 \right), \quad (4.15)$$

with $E_{th} = a/b = 720$ GeV, the energy threshold above which stochastic effects are dominant.

SMPs will have very similar signatures in the IceCube detector as we have assumed that they behave leptonically (Section 2.4). The tracks will be dim compared to muon tracks due to the charge dependence in the Cherenkov effect (Section 4.1).

4.4 Energy loss formulae

As mentioned in Section 4.3.2.1, secondary interactions such as bremsstrahlung, pair production and photonuclear effect, become non-negligible at certain energies. At high energies (> 1 TeV for muons) the Cherenkov light of the secondary particles will have a significant contribution additional to the Cherenkov light coming from the primary particle. These effects are taken into account in IceCube simulations and are of great importance for high-energy muons. Since these interactions are electromagnetic in nature, they will also play a role for SMP particles, yet these effects are small for the SMPs with a primary focus on lower energies.

In this section we go over the four main components of secondary interactions. This section is largely based on the findings in Ref. [144]. The energy of the secondary particles will be expressed by $\nu = vE$, with E the energy of the incident particle and v the fraction of the energy transfer. Secondary interactions occur at all energy levels and become continuous in nature below a certain energy threshold. Therefore, in many codes v_{cut} is implemented as a lower bound equal to 0.05 and a ν_{cut} equal to 500 MeV [145].

4.4.1 Ionization

Fast charged particles that move through matter interact with the electrons of atoms in the material. The interaction excites or ionizes the atoms. The Feynman diagram of this interaction is given in Figure 4.5 (left).

The cross section is expressed as

$$\frac{d^2N}{d\nu dx} = \frac{1}{2} K z^2 \frac{Z}{A} \frac{1}{\beta^2} \frac{1}{\nu^2} \left[1 - \beta^2 \frac{\nu}{\nu_{max}} + \frac{1}{2} \left(\frac{\nu}{E(1+1/\gamma)} \right)^2 \right], \quad (4.16)$$

with $\nu_{max} = \frac{2m_e(\gamma^2 - 1)}{1 + 2\gamma \frac{m_e}{m_t} + \left(\frac{m_e}{m_t} \right)^2}$

where negligible terms are left out and K is equal to $4\pi N_A r_e^2 m_e c^2$, N_A is Avogadro’s number, r_e the classical electron radius, m_e the electron mass, z the charge of the particle (in units of the

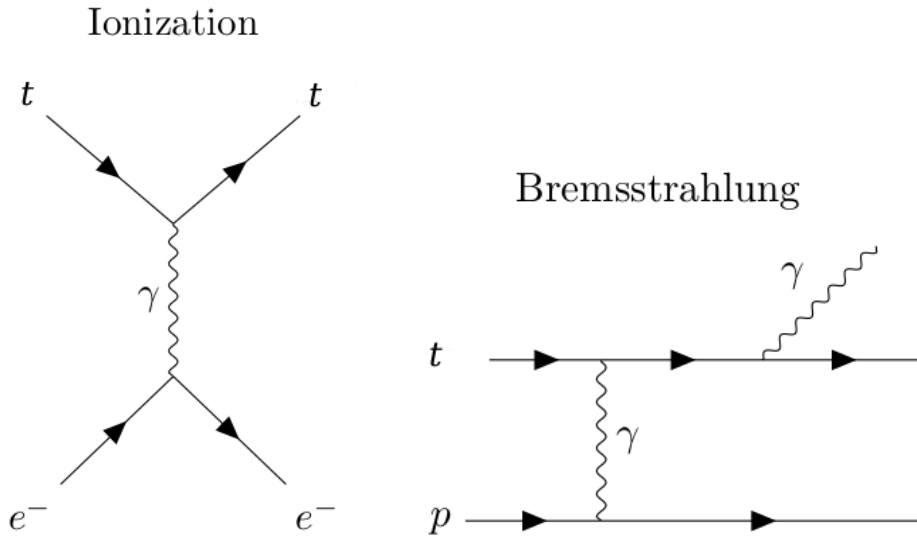


Figure 4.5: Feynman diagrams of an ionization interaction (*left*) and bremsstrahlung (*right*). t denotes the primary particle.

electron charge), Z the atomic number of the absorber, A the atomic mass of the absorber and m_t the mass of the throughgoing particle.

This interaction leads to an energy loss of the traveling particle and is expressed by the Bethe-Bloch formula [42]

$$-\left\langle \frac{dE}{dx} \right\rangle = K z^2 \frac{Z}{A \beta^2} \left[\frac{1}{2} \ln \left(\frac{2m_e \beta^2 \gamma^2 \nu_{upper}}{I(Z)^2} \right) - \frac{\beta^2}{2} \left(1 + \frac{\nu_{upper}}{\nu_{max}} \right) + \frac{1}{2} \left(\frac{\nu_{upper}}{2E(1+1/\gamma)} \right)^2 - \frac{\delta}{2} \right],$$

where $\nu_{upper} = \min(\nu_{cut}, \nu_{max})$

(4.17)

where I is the mean excitation energy of the absorber. The density correction δ can be found in the corresponding literature [144].

For particles in the region of $0.1 \leq \beta\gamma \leq 1000$ this is the dominant factor in the mean energy loss.

4.4.2 Bremsstrahlung

Charged particles that decelerate by another charged particle lose kinetic energy that is converted into radiation. This phenomena is known as *bremsstrahlung* and is illustrated in Figure 4.5 (right). The cross section may be represented by the sum of an elastic component and two inelastic components,

$$\sigma = \sigma_{el} + \Delta\sigma_a^{in} + \Delta\sigma_n^{in},$$
(4.18)

where σ_{el} denotes the cross section for the Coulomb scattering of the particle off the atomic nucleus and the two other terms are corrections that account for additional processes, in which the bremsstrahlung is accompanied by a change of electron or nuclear structure of the atom in the final state.

4.4.2.1 Elastic component

$$\sigma_{el}(E, v) = \frac{\alpha}{v} \left(2z^2 Z \frac{m_e}{m_t} r_e \right)^2 \left(\frac{4}{3} - \frac{4}{3}v + v^2 \right) \left[\ln \left[\frac{m_t}{\delta} \right] - \frac{1}{2} - \Delta\sigma_a^{el} - \Delta\sigma_n^{el} \right],$$

where $\delta \approx \frac{\mu^2 \omega}{2E(E - \omega)}$,

(4.19)

where α is the fine structure constant and ω the photon's frequency with $\hbar = 1$. The atomic and nuclear formfactors are equal to

$$\begin{aligned}\Delta\sigma_a^{el}(\delta) &= \left[1 + \frac{1}{\delta\sqrt{e}BZ^{-1/3}/m_e} \right] \\ \Delta\sigma_n^{el}(\delta) &= \left[\frac{D_n}{1 + \delta(D_n\sqrt{e} - 1)/m_t} \right].\end{aligned}\quad (4.20)$$

Values for B and D_n can be found in Ref. [146], here, e is the base of the natural logarithm (≈ 2.718) and other constants are as defined in Eq. 4.17. Other parametrizations can be found in the corresponding literature [144].

4.4.3 Inelastic component

The effect of nuclear excitation can be evaluated as

$$\Delta\sigma_n^{in} = \frac{1}{Z} \Delta\sigma_n^{el}; (Z \neq 1), \quad (4.21)$$

where $\Delta\sigma_n^{el}$ is defined in Eq. 4.20.

In the case of atomic excitation, one accounts for bremsstrahlung whereby photons radiate from the primary particle and where photons radiate from the electrons of the atom. This factor is equal to

$$\Delta\sigma_a^{in} \approx \frac{1}{Z} \ln \left[\frac{m_t/\delta}{\delta m_t/m_e^2 + \sqrt{e}} \right] - \ln \left[1 + \frac{m_e}{\delta\sqrt{e}B'Z^{-2/3}} \right], \quad (4.22)$$

where $B' = 1429$ for $Z > 2$, $B' = 446$ for $Z = 1$ and e is again the base of the natural logarithm.

4.4.4 Photonuclear

The photonuclear interaction of leptons is the process by which a lepton scatters inelastically with a nucleon or nucleus. Through a virtual photon exchange, hadrons are produced, as is illustrated in Figure 4.6. The cross section formula is given by

$$\begin{aligned}\frac{d\sigma}{dv} &= \frac{z^2\alpha}{2\pi} A\sigma_{\gamma N}v \left\{ 0.75G(x) \left[\kappa \ln \left(1 + \frac{m_1^2}{t} \right) \right. \right. \\ &\quad - \frac{\kappa m_1^2}{m_1^2 + t} - \frac{2m_t^2}{t} + \frac{4m_t^2}{m_1^2} \ln \left(1 + \frac{m_1^2}{t} \right) \\ &\quad \left. \left. + 0.25 \left[\left(\kappa + \frac{2m_t^2}{m_2^2} \right) \ln \left(1 + \frac{m_2^2}{t} \right) - \frac{2m_t^2}{t} \right] \right. \right. \\ &\quad \left. \left. + \frac{m_t^2}{2t} \left[0.75G(x) \frac{m_1^2 - 4t}{m_1^2 + t} + 0.25 \frac{m_2^2}{t} \ln \left(1 + \frac{t}{m_2^2} \right) \right] \right\},\right.\end{aligned}\quad (4.23)$$

$$\text{where } t = Q_{max}^2 = \frac{m_t^2 v^2}{1-v}, \quad \kappa = 1 - \frac{2}{v} + \frac{2}{v^2}, \\ m_1^2 = 0.54 \text{ GeV}^2, \quad \text{and} \quad m_2^2 = 1.8 \text{ GeV}^2.$$

Parameters that aren't defined here can be found in the corresponding literature [144].

4.4.5 Pair production

Pair production occurs when the virtual photon radiated from the primary particle or proton splits into an electron-positron pair or muon-antimuon pair. The differential cross section is equal to

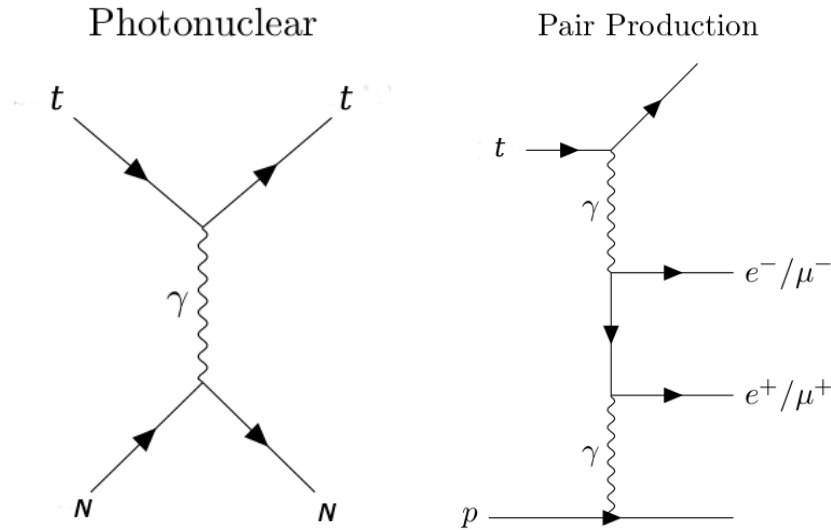


Figure 4.6: Feynman diagrams of a photonuclear interaction (*left*) and pair production (*right*). t denotes the primary particle.

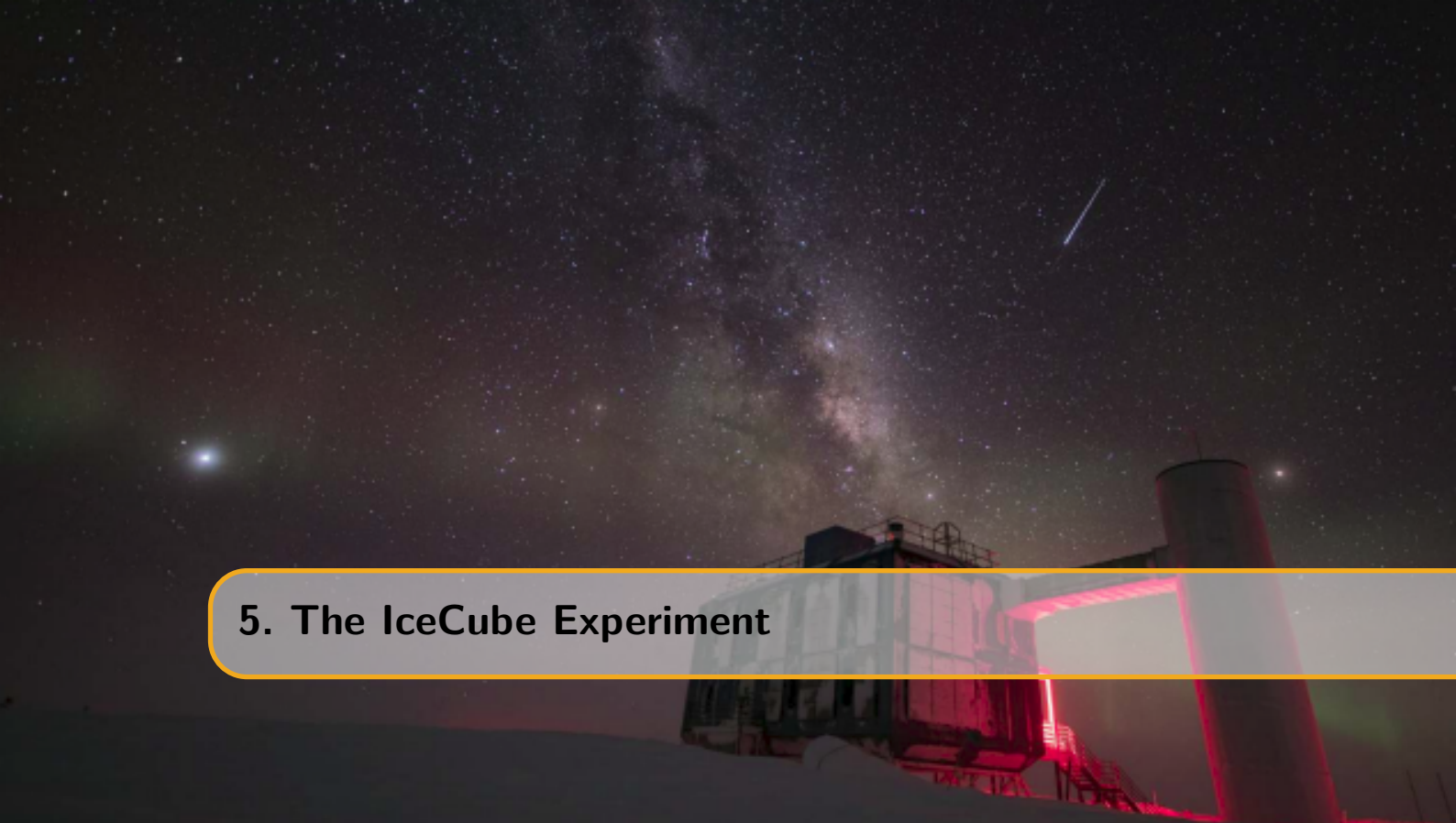
$$\frac{d\sigma(E, v, \rho)}{dv d\rho} = \frac{2}{3\pi} Z(Z + \zeta)(z\alpha r_e)^2 \frac{1-v}{v} \left(\Phi_e + \frac{m_e^2}{m_\mu^2} \Phi_\mu \right), \quad (4.24)$$

where $v = (\epsilon_+ + \epsilon_-)/E$, $\rho = (\epsilon_+ - \epsilon_-)/(\epsilon_+ + \epsilon_-)$,

and ϵ_+ and ϵ_- denote the energies of the positively and negatively charged electrons/muons. The parameters not described in detail can be found in the corresponding literature [144].

4.4.6 Conclusion

From the previous discussion we can conclude that the charge enters in the energy loss formulae quadratically for ionization, pair production and the photonuclear effect. Bremsstrahlung scales with a factor of z^4 , making it negligible compared to the other energy losses. The influence of the mass of the particle enters these equations in a non-trivial manner but has a minimal effect, again with bremsstrahlung as the exception. There, the mass enters with $1/m_t^2$, making it completely negligible for heavy particles. The effects from secondary particle production in the light yield are only substantial at very relativistic SMPs ($\approx 10^4$ times the rest mass). Due to the assumed E^{-2} signal flux (see Chapter 2), their relative contribution to the sample is very small but accounted for.



5. The IceCube Experiment

Computers are useless; they can only give you answers ~ Pablo Picasso

IceCube is a neutrino observatory located near the Amundsen-Scott South Pole Station close to the geographic South Pole. Experiments that search for astrophysical neutrinos need to be constructed with enormous instrumented volumes. IceCube is the first gigaton neutrino detector ever built and was designed specifically for this case. It is buried beneath the surface of the Antarctic ice, starting from around 1450 meters of depth and extending to around 2500 meters (~ 300 meters above bedrock). The ice acts as a medium for both the interaction of a neutrino and light propagation. This chapter serves as a general overview of the several components of IceCube detector together with an introduction to the data processing.

The main goal of the IceCube experiment is to learn more about the distant sources that we believe to be responsible for the production of the highest-energy cosmic rays. As indicated in Section 3.3, neutrinos are crucial in gaining information about these far away sources. Large-scale detectors are necessary to observe the faint flux of neutrinos with very high energies. Detecting the Cherenkov radiation (Chapter 4) from neutrino interactions is the best way to observe these weakly interacting particles. Because hadronic, electromagnetic and muonic components from these interactions require a medium that extends to a couple of kilometers and has good light propagation characteristics, the South Pole ice sheet acts as a near ideal component of the detector. As a proof of concept, the AMANDA (Antarctic Muon And Neutrino Detector Array) experiment was built between 1996 and 2000 to show that neutrinos with energies above 50 GeV could be detected in the Antarctic ice [147, 148]. After construction was finalized, this detector consisted of 677 optical modules mounted on 19 separate strings that are spread out in a rough circle with a diameter of around 200 meters. The strings were deployed by first “drilling” holes in the ice with a hot-water hose, showing that this specific drilling technique works and can be used on larger scales. After some years of data taking, it was clear that high-energy neutrinos could be observed, paving the way for the much larger IceCube project [149].

5.1 Geometry

The IceCube detector consists of three main parts that act as different purpose physics detectors. The *in-ice* IceCube detector is the main component and consists of 4680 digital optical modules.

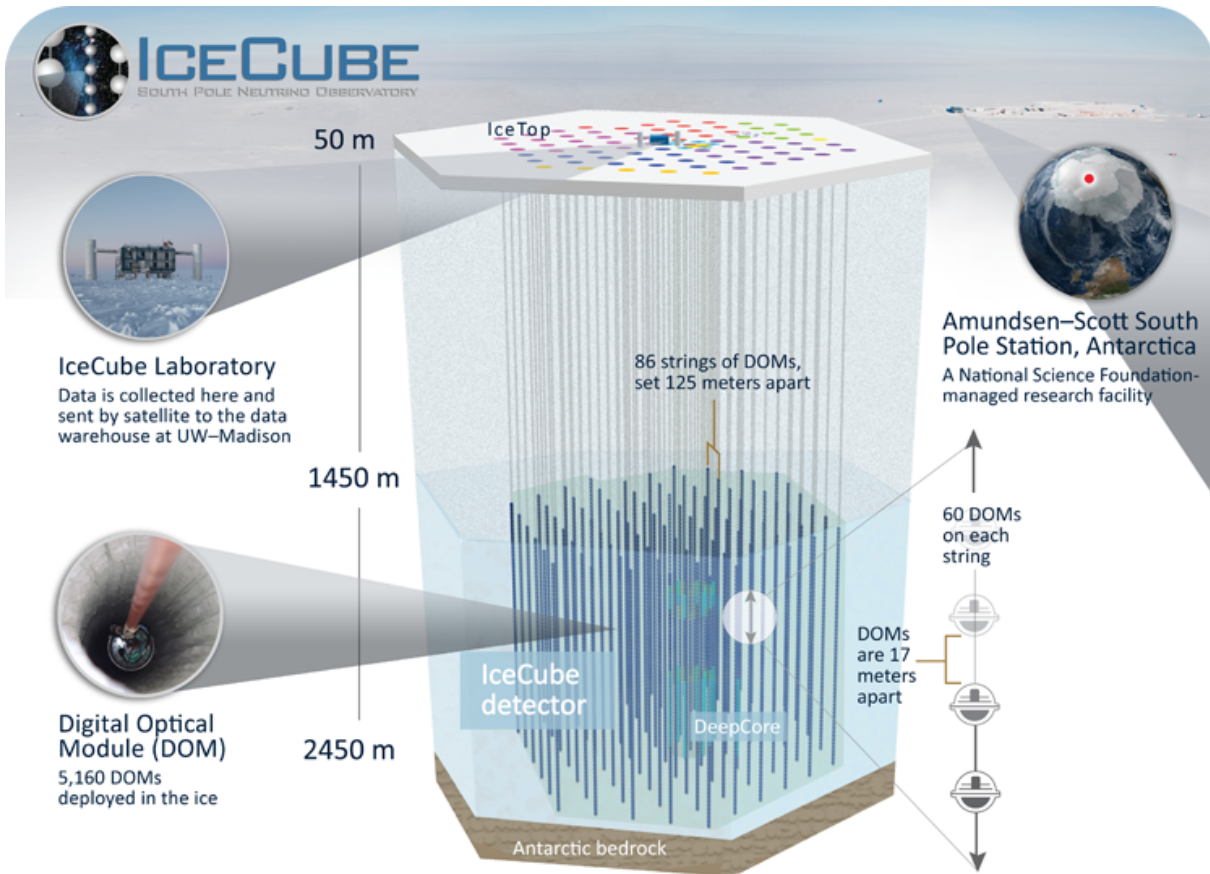


Figure 5.1: Illustration of the IceCube South Pole neutrino observatory.

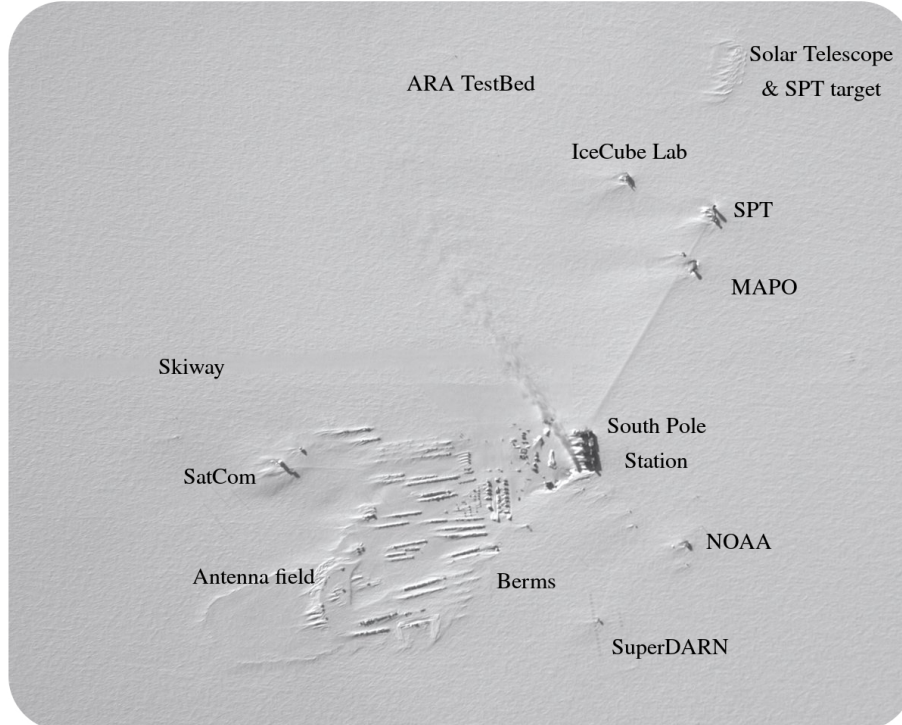


Figure 5.2: Aerial view of the South Pole. The main buildings and experimental setups are indicated in the figure. The exhaust of the South Pole Station is also visible.

In its core, a denser subdetector, *DeepCore*, significantly enhances the capabilities for low-energy events of the observatory in a limited volume. The center of the DeepCore array consists of 480 sensors. On the surface of the ice, water tanks with optical modules inside are spread out over an area of approximately 1 km^2 and make up the *IceTop detector*. This surface array was built as a cosmic ray detector and veto for the in-ice array. The three components combined make the facility a multipurpose physics detector. Figure 5.1 shows the layout of the detector.

5.1.1 In-ice array

The in-ice array consists of 4680 digital optical modules (DOMs) that are able to register light that is scattered and propagated through the ice (more info about these modules can be found in Section 5.2.1). The DOMs are attached to cables and are frozen in the ice. In total, 78 of these “strings” were frozen into boreholes and spread out over a cubic kilometer in a hexagonal shape. Because only the deep ice is transparent, the DOMs are attached to the strings starting from a depth of 1450 meters to 2450 meters. The strings, as viewed from above, are spaced about 125 meters apart and along each string, 60 DOMs are attached with a vertical separation of 17 meters. This design was chosen in order to meet up to the primary science requirement of detecting astrophysical neutrinos in the energy range of $\mathcal{O}(\text{TeV})$ – $\mathcal{O}(\text{PeV})$.

5.1.2 DeepCore

A subset of in-ice DOMs is deployed along eight extra strings in the central region of the in-ice array. The optical modules are deployed deeper than 1750 meter with a denser instrumented volume. Seven additional strings, belonging to the standard in-ice strings, are also combined with the DeepCore strings to optimize the instrumented volume for this detector. The inter-string spacing on the eight specialized DeepCore strings varies from 41 meters to 105 meters. The DOM-to-DOM spacing is 7 meters for the bottom 50 optical modules (which are deployed at depths of 2100 to 2450 meters). The remaining 10 DOMs on each string are located at depths above 2000 meters deep with a spacing of 10 meters. This extra “layer” serves as a veto for downgoing atmospheric muons. Each string is instrumented with 60 DOMs, resulting in a total of 480 DOMs. Instrumentation in the ice between 2000 to 2100 meters proved to be less useful due to the *dust layer* (see Section 5.5) and was therefore left out. Six out of the eight specialized strings are also instrumented with DOMs using PMTs of higher quantum efficiency. The two remaining strings are instrumented with regular IceCube DOMs. A layout of the in-ice array is given in Figure 5.3.

The DeepCore design allows us to detect neutrinos of much lower energies in the range of $\mathcal{O}(10 \text{ GeV})$ – $\mathcal{O}(100 \text{ GeV})$. Experiments for neutrino oscillation experiments, WIMP dark matter annihilation, galactic supernova neutrinos and point sources are made possible, or more feasible, with this dense subarray [150].

5.1.3 IceTop

IceTop is a cosmic ray air shower array, located on the surface of the ice and 2835 meters above sea level. As discussed in Chapter 3, air showers die out when they are propagating to Earth’s surface but as a consequence of the high altitude of IceTop, showers are observed near maximum*, resulting in a good energy resolution for the detector. This is important if one wants to measure changes in composition as a function of energy. In total, 162 ice-filled tanks are distributed in 81 stations (two tanks per station) in a grid similar to the in-ice array. Like the denser DeepCore infill, there are eight stations in the center of IceTop placed more closely together.

The two tanks per station are separated 10 meters apart from each other and each tank contains two IceCube DOMs. One is operated at a “low-gain” and one at “high-gain”, making them more suitable for air shower detection. The tanks measure the Cherenkov light that is produced in the ice of a tank due to the particles in a shower (electrons, positrons, muons and hadrons). The IceTop design allows to fully cover the knee of the energy spectrum and is

*The height of the shower where the maximum number of particles are produced in an air shower is often referred to as the “shower maximum”.

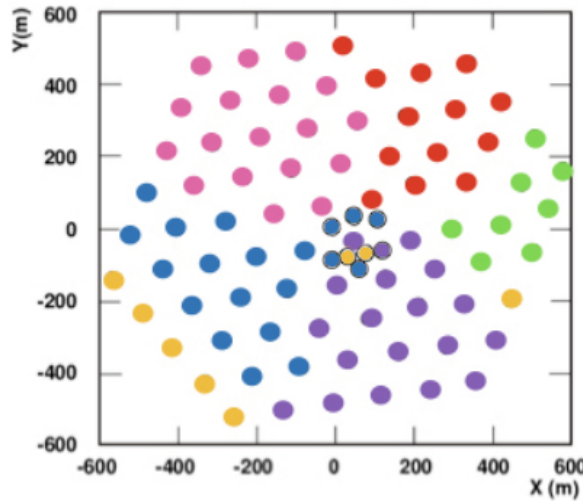


Figure 5.3: Layout of the IceCube (regular) and DeepCore strings (black edge). The string color scheme represents different deployment seasons (04-05: orange, 05-06: green, 06-07: red, 07-08: pink, 08-09: purple, 09-10: blue, 10-11: yellow). Figure from Ref. [151], with minor corrections.

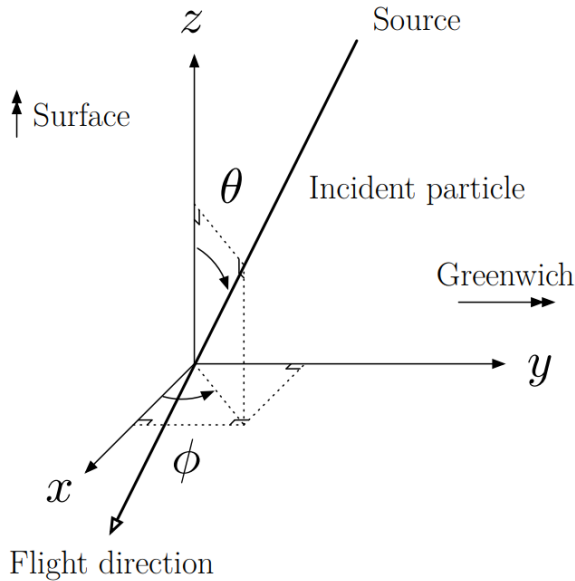


Figure 5.4: The IceCube coordinate system.

primarily sensitive from PeV to EeV energies. The denser infill allows the threshold to be lowered to 100 TeV. The detector is used in studies of the composition, high- p_T muons, etc.

5.1.4 IceCube coordinate system

When referring to positions and directions, one has to define a coordinate system that is able to uniquely define these variables. The system used in the IceCube collaboration is shown in Figure 5.4.

The center of the coordinate system is set close to the geometric center of the detector, at about 2000 m below the surface of the ice. The y-axis of the coordinate system is aligned with the Prime Meridian pointing toward Greenwich (United Kingdom). The x-axis is set perpendicular to the y-axis pointing in a 90° clockwise direction. The z-axis is set perpendicular to the xy-plane, pointing upwards, normal to the Earth's surface.

A particle's direction is defined with zenith and azimuth angles, θ and ϕ respectively. The zenith angle is measured relative to the positive z-axis and the azimuth angle is measured

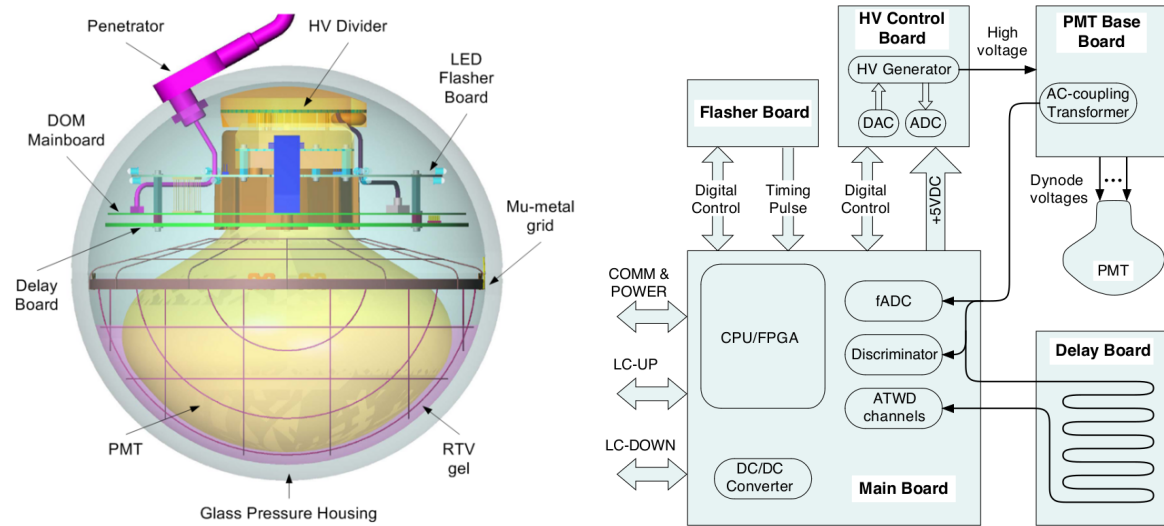


Figure 5.5: *Left:* illustration of the mechanical DOM components. *Right:* Scheme of the functional connections.

counterclockwise from the positive xy-plane.

5.2 Hardware components

5.2.1 Digital optical modules

The Digital Optical Modules, or DOMs, convert light into electrical signals and have the necessary hardware installed to perform some basic processing of the electrical pulses. A downward facing 10"-diameter photomultiplier tube (PMT) is set with a high voltage of 2 kV, resulting in a gain of 10^7 [152]. The amplitude of the resulting waveforms ranges from 1 mV up to and beyond the linearity limit of the PMT (~ 2 V) with the width ranging from 12 ns to 1500 ns. This wide dynamic range of the waveform is processed by onboard electronics: the main board and delay board. The main board controls all the devices in the DOM (high voltage power supply for the PMT, the flasher board and pressure, temperature, and power supply voltage monitor sensors), digitizes the PMT waveforms, communicates with the data acquisition (DAQ) on the surface, houses an internal clock that is regularly calibrated with the DAQ on the surface and exchanges pulses with the adjacent DOMs. An illustration of the mechanical components of the optical module and a schematic view of the data flow starting from the PMT is shown in Figure 5.5. The optical module is housed in a 13"-glass sphere of 0.5" thick made from borosilicate. It is separated into two halves and held together with an aluminium waistband. The sphere was tested up to 690 bar hydrostatic pressure and is able to withstand the enormous pressure that the DOM is exposed to deep within the ice and during freezing (see Section 5.3). A penetrator inside the glass sphere brings out three wires pairs housed in a cable. One wire pair is connected to the string and ultimately to the IceCube Laboratory (see Section 5.2.4), the other two wires to the neighboring DOMs directly above and below for local coincidence pulses (see Section 5.2.3). A detailed description is given in the detector paper [152].

5.2.1.1 PMTs

The 10" (or 25 cm) diameter PMT comes in two types: Hamamatsu R7081-02 for standard IceCube DOMs and a high-quantum-efficiency (HQE) version, Hamamatsu R7081-02MOD for the specialized DeepCore strings [153]. The peak quantum efficiency is around 25% (34% for HQE) at a wavelength of approximately 390 nm. However, the total acceptance of the optical module is the convolution of the quantum efficiency with the glass transmission (93% at 400 nm, decreasing to 50% at 340 nm and 10% at 315 nm at a normal incidence). The resulting acceptance is illustrated in Figure 5.6. The PMTs face downwards and are housed in a mu-metal

grid to shield them from the Earth magnetic field and a silicone gel necessary for optical coupling and mechanical support.

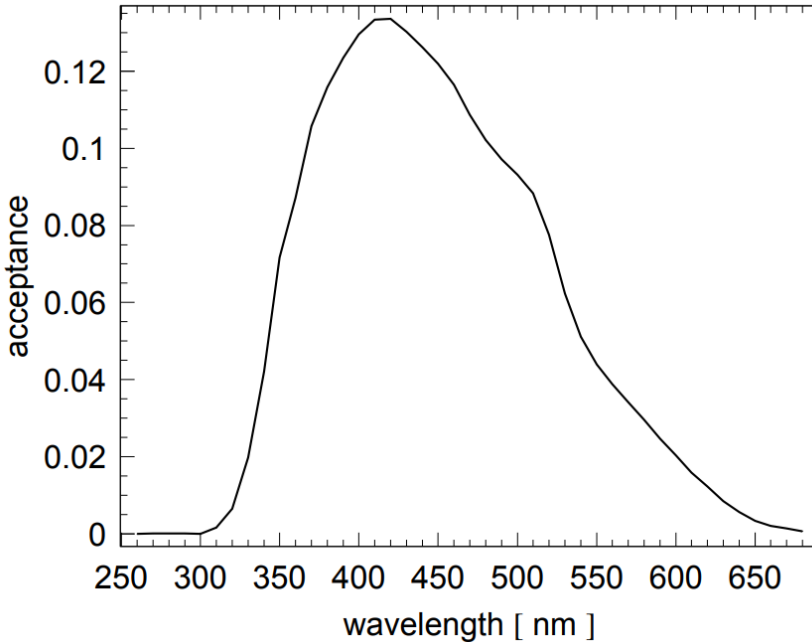


Figure 5.6: Fraction of photons arriving from a direction parallel to the PMT axis in function of the photon wavelength. Glass and gel transmission, PMT quantum and collection efficiencies are all included. Figure from Ref. [154].

5.2.1.2 Main board and delay board

The PMT signals are sent to two ATWD (Analog Transient Waveform Digitizer) and one fast ADC (fADC) with a delay of about 75 ns. This delay is necessary because signals are only processed if the signal exceeds a voltage that corresponds to 0.25 PE (one PE is the voltage that typically corresponds to the voltage produced by a single photoelectron). Once this threshold is crossed, the signal is compressed and included in a “DOMlaunch” or “hit”. Signals that pass the local coincidence requirement (see Section 5.2.3) have their full waveforms compressed, whereas for isolated events only a time stamp and brief charge summary is sent. For each hit, an FPGA (Field Programmable Gate Array) opens up one of the two ATWD chips. Each of the two chips is provided with three amplifier gains with nominal values of 16, 2 and 0.25. Most pulses use the highest-gain channel while the other lower-gain recordings are used as needed when pulses reach 75% of the range of a higher-gain channel. The ATWD recording duration is 427 ns, which should include light that is produced within tens of meters of a DOM. The slower fADC is used when light reaches the DOM after the ATWD time window and samples continuously. The FPGA is programmed to save an interval of 6.4 μ s after the launch. ATWD chips sample the input voltage at 300 Msps, followed by a 10-bit digitization. The fADC captures the information with a 10-bit 40 Msps.

The two sets of ATWD chips are operated alternately in order to reduce deadtime. After 50 ns, the second chip is available to be launched during the digitization step of the first. The digitization procedure is terminated for isolated hits and the ATWD is reset, reducing the DOM dead time.

The delay board consists of a 10 m-long copper trace that delays the signal for 75 ns, necessary to be able to record the full waveform before the discriminator threshold of 0.25 PE is exceeded.

5.2.1.3 Flasher board

To be able to characterize the ice and simulate light propagation, each DOM was instrumented with 12 LEDs that are aimed in six different azimuth angles (with 60° spacing) and along two

different zenith angles. The LEDs were chosen to have a wavelength spectrum centered at around 400 nm to approximate the typical wavelength of detected Cherenkov photons. Flasher data is used for:

- verifying the timing response of the DOMs throughout the analysis software chain;
- measuring the position of the deployed DOMs in ice;
- measuring the optical properties of the ice (see Section 5.5);
- verifying the performance of shower reconstruction algorithms in measuring position, direction and energy.

5.2.2 Calibration

Regular calibration of the components is necessary to be able to convert the DOM waveforms to reliable and comparable physical units. Optical efficiencies of the optical modules were determined in the lab before deployment and are also done *in situ* with calibration procedures.

Some of these procedures do not allow for simultaneous data-taking and are performed as little as possible, without losing significant confidence in the calibration of the devices. For example, in-ice DOMs are calibrated yearly with the DOMCal procedure, whereas global time calibration can be done in parallel with data-taking and is provided by the RAPCal procedure.

As they result in the vast majority of the background hits, *dark noise* needs to be properly understood for low-energy neutrino analyses, supernova searches, and detector simulations. The total rate of dark noise averages at around 560 Hz for in-ice DOMs and 780 Hz for HQE DOMs. The origins of the noise are non-trivial and include electronic noise, thermionic emission, Cherenkov light from radioactive decays, field emission within the PMT, and scintillation/luminescence in the glass of the PMT and pressure sphere. They are simulated with a combination of uncorrelated (Poissonian) noise and a correlated component. The temperature dependence of the noise rate was determined by combining a measured temperature profile of the South Pole ice cap with a fit of the Poissonian expectation of the total dark noise rate to every individual DOM, and was verified in lab measurements. The seasonal variations of the dark noise rates are below 1%, but are tracked over time and updated yearly in a database.

More information about these and other calibration procedures can be found in Ref. [152].

5.2.3 Cable systems

The DOMs are the eyes of the detector, but the cable system connects all the modules together and links them to the readout hardware at the surface. The in-ice cables, 2505 m long, are each connected to 60 DOMs and terminate at a Surface Junction Box (SJB) between IceTop tanks. IceTop tanks also connect to the SJB. A surface cable was trenched 1 m deep at the time of deployment and runs to the IceCube Laboratory. One cable consists of 20 “quads”, a construction of four twisted wires. Four quads provide special instrumentation and local coincidence between connections and one is a spare. The remaining 15 quads are each connected to four DOMs with two wire pairs. A wire pair connects two adjacent DOMs and is attached to connectors at 30 breakouts spaced 34 m apart as can be seen in Figure 5.7. Each DOM is connected to three wire pairs. One wire pair is used for bi-directional communication to the surface and power. The two remaining wires are dedicated to determine *Local Coincidence (LC)*. Each DOM is connected to its nearest neighbor above and below. If nearest or next-to-nearest neighbors are hit within a time window of $\pm 1 \mu\text{s}$, the hits are said to be in Hard Local Coincidence (HLC). Isolated hits are referred to as Soft Local Coincidence (SLC). Most DOM hits originate from dark noise (see Section 5.2.2) and are not in HLC. Light originating from particles traveling through matter is more likely to trigger DOMs in close proximity. Therefore, LC requirements are able to drastically reduce the noise rate.

5.2.4 IceCube laboratory

The central building to which the modules of all the detectors are connected is the IceCube Laboratory (ICL). Cables/strings from the arrays run up two cable towers on either sides of the

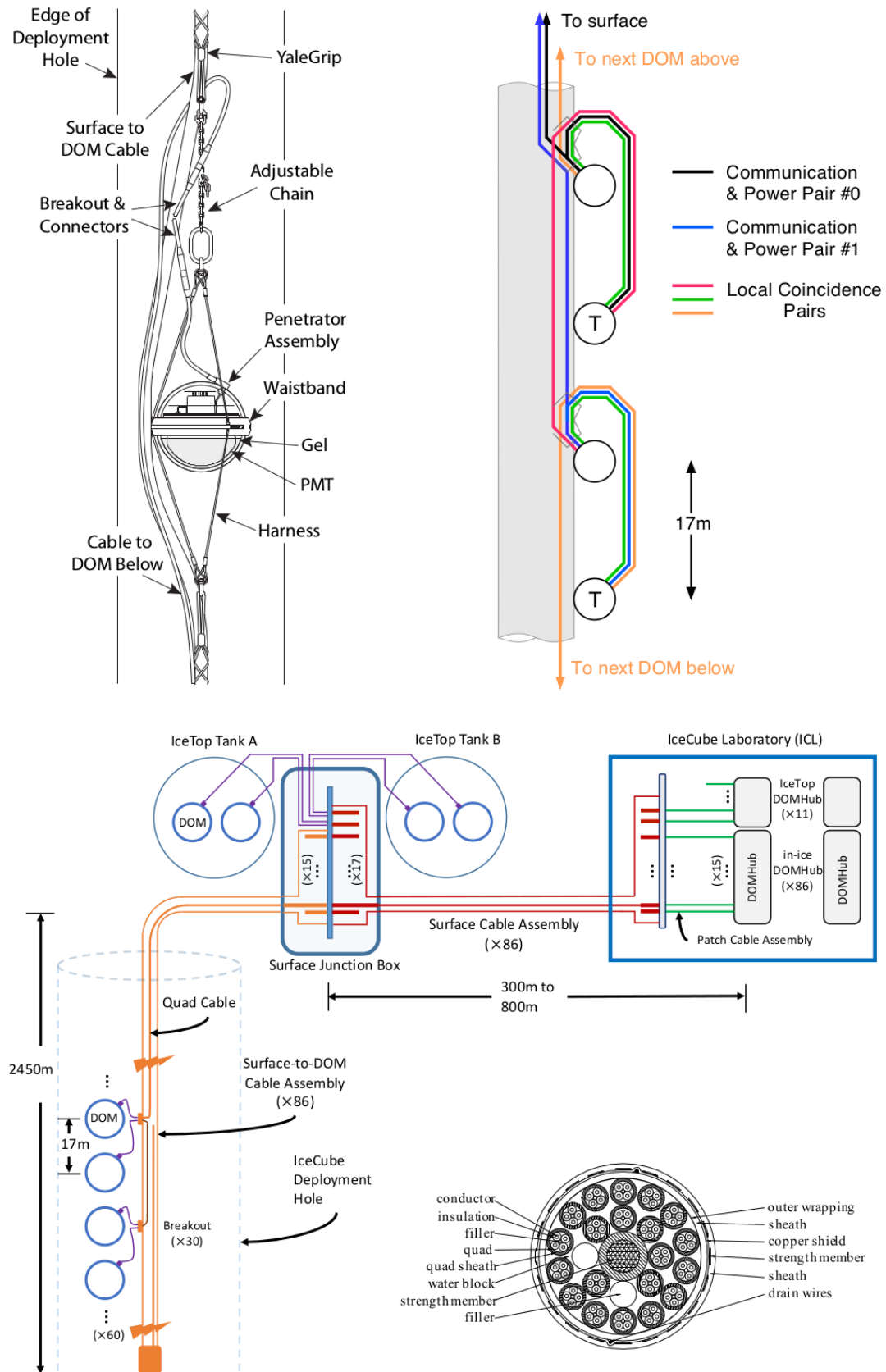


Figure 5.7: *Top:* Sketch of DOM cabling and schematic overview. The modules are connected to their nearest neighbors and the string. *Bottom:* General schematic overview of the IceCube cabling system and the connection between all components together with an in-ice cable cross section. Illustrations from Ref. [152].

structure. A picture of the ICL is shown as the header image of this chapter (pg. 65); one of the towers is visible. Inside the main part of the building is a server room to which the cables in the towers are connected. All data acquisition and online filtering computers are housed inside the server room together with the main IceCube computing system called the “South Pole System” (more information on this in Section 5.4).

5.3 Deployment

In total, 86 holes had to be drilled for all IceCube and DeepCore strings. The surface consists of a 50 m snow and firn region with a gradual transition to ice. The ice was melted with a 5 MW Enhanced Hot Water Drill (EHWD) capable of drilling about 1 hole per 48 hours. The holes were 60 cm in diameter, providing enough clearance for the optical modules that were 35 cm in diameter, and with contingency time for delays that meant holes could shrink due to refreezing. Because melting snow and firn with hot water is not practical, a specialized drill with copper tubing through which hot water flows was used to melt the firn by contact.

The IceCube drilling was completed in seven field seasons during Antarctic summers (early November to mid-January). The first season started in 2004-2005 and construction ended in 2010-2011.

After drilling one hole, all 60 DOMs were lowered one by one and connected to each other with the penetrator assembly as shown in Figure 5.7. After deployment of all DOMs, the remaining 1.5 km of in-ice cable was lowered into the hole (known as the “drop phase”). The top of the cable was then secured by an anchor trenched in the snow and connected to the Surface Junction Box.

In total, 5484 (5160 IC + 324 IT) optical modules were deployed and as of 2018, there are 5396 still in data-taking mode (98.4%). There were 55 DOMs that failed almost immediately during freeze-in, while 34 DOM failures occurred after deployment. This number includes modules on a wire pair that are taken out when the partner DOM on the same pair failed. The mean failure rate is estimated to be around $(4.1 \pm 1.2) \text{ yr}^{-1}$, which results in a survival fraction of $(97.4 \pm 0.3)\%$ in 2030.

5.4 Data taking

First processing of the photon detection is done inside the DOM. After digitization, the waveforms are sent along the cable/string to which all DOMs are attached and that runs to the ICL. Each one of the strings is connected to one of the DOMHubs, which together with servers that run various online systems, comprises the South Pole System (SPS). An overview is given in Figure 5.8.

The data acquisition (DAQ) system is run on the DOMHubs and recognizes patterns in hits that are most likely caused by particle interactions with the use of the implemented triggers and filters (see below). This combination of hits is called an “event”. Most of the DAQ data rate originates from atmospheric muons with an event rate averaging 2.7 kHz. The total bandwidth saved to tape/disk (see Section 5.4.3) is approximately 1 TB/day.

To implement possible changes in the detector settings, triggers, or filters, a full physics run spans over one year, starting in May and ending in May the following year. Data is recorded in smaller 8 hour runs, where each run has a unique run number. Over the years, with the use of both online and on-site automatic alerts, the total uptime of the detector has a steady increase of clean uptime (usable data) from 89.75% in 2011 to 98.89% in 2018.

5.4.1 Triggers

Aside from the discriminator thresholds in the module (see Section 5.2.1.2), a system of triggers is set up to further reduce the noise rate and refine searches for physics events. Below, a short description of the triggers is given. An overview of the trigger settings is given in Table 5.1.

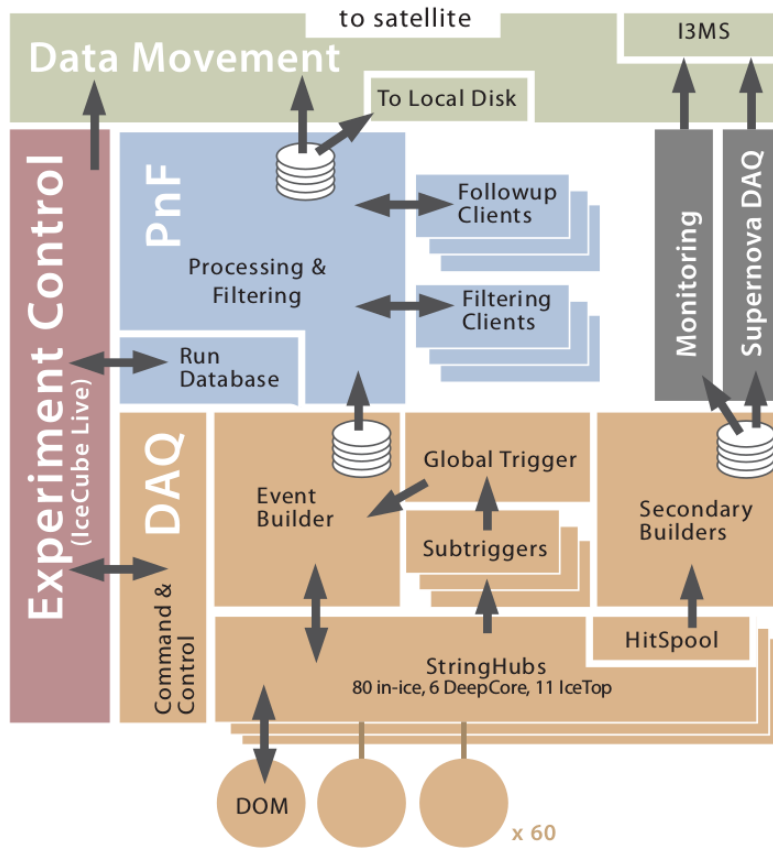


Figure 5.8: Schematic overview of the data flow in the primary IceCube online systems.

- The most important trigger is the Simple Multiplicity Trigger (SMT) used for the IceCube, DeepCore and IceTop arrays. The trigger setting requires a certain number of hits within a time window of the order of a couple of μs without any locality requirements.
- The Volume Trigger requires less HLC hits, but they have to be clustered in a certain cylindrical volume.
- Locality conditions are powerful for low-energy events that do not reach far in the detector but are more prone to produce hits in a small volume and time window. Therefore, a dedicated String Trigger was designed for low-energetic upgoing events passing along a single string.
- IceCube is also sensitive to hypothetical massive particles moving at subrelativistic speeds: magnetic monopoles. Therefore, a dedicated Slow Particle (SLOP) trigger has been developed. It searches for triplets of HLC pairs within a window, T_{\max} , and removes HLC pairs within a time window, T_{prox} , to remove hits originating from particles traveling at the speed of light. Other velocity and geometric requirements are set with the inner angle between triplets, α_{\min} and the “velocity” along the sides of the triangle.
- A Fixed Rate Trigger (FRT) reads out hit data from the full detector at fixed intervals, useful for DOM noise studies.

If a trigger condition is fulfilled, the start of the trigger window is determined as the first HLC hit of the active volume of the trigger. The minimum length of the triggered window slides along with the hits until there is no more HLC after the last hit within the set minimum time window. The length of a triggered set of hits can therefore be longer than the minimum trigger window. As one event is able to fulfill multiple trigger requirements, the (sub)triggers are merged into one Global Trigger while keeping the information on the individual triggers. This data is subsequently sent to the Event Builder that writes DAQ events (also called *Q frames*) to a temporary file that is saved when it reaches a certain size. These events are eventually re-split into physics events (*P*

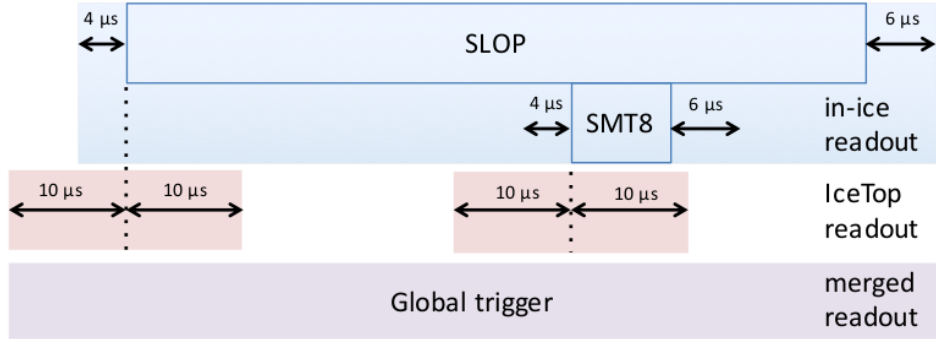


Figure 5.9: Example of a global trigger construction. Multiple triggers are combined due to their overlap with the long SLOP trigger.

Table 5.1: Parameter settings of triggers (as of May 2016) and typical trigger rates.

Trigger	DOM set	$N_{\text{HLC hits}}$	Trigger Window (μs)	Readout Window IC	Window (μs) IT	Topology	Rate (Hz)
SMT	in-ice	8	5	-4, +6	± 10	-	2100
SMT	DeepCore	3	2.5	-4, +6	± 10	-	250
SMT	IceTop	6	5	± 10	± 10	-	25
Volume	in-ice	4	1	-4, +6	± 10	cylinder ($r = 175 \text{ m}$, $h = 75 \text{ m}$)	3700
Volume	IceTop	4	0.2	± 10	± 10	cylinder ($r = 60 \text{ m}$, $h = 10 \text{ m}$)	4
String	in-ice	5	1.5	-4, +6	± 10	7 adjacent vertical DOMs	2200
SLOP	in-ice	N_{triplet}	$T_{\text{prox}} = 2.5$	$-4, +6$	± 10	$\alpha_{\min} = 140^\circ$, $v_{\text{rel}}^{\max} = 0.5$	12
			$T_{\min} = 0$				
			$T_{\max} = 500$				
FRT	all	-	-	Combined: 10000	-	-	0.003

frames) corresponding to a certain subtrigger before reconstruction and analysis. An example of a Global Trigger, here mostly determined by the very long SLOP trigger, is shown in Figure 5.9.

All triggers read out all SLC/HLC hits of all DOMs, even the ones not directly involved in the trigger construction. For this, they use the StringHub software component located on every DOMHub that is able of caching SLC and HLC hits in memory. Hits before and after the trigger window are also saved to the event to add information of early and late pulses. This is typically 4 μs before and 6 μs after the trigger window for in-ice triggers.

5.4.2 Filters

Events are sent through the online Processing and Filtering (PnF) system for additional processing. First, the triggered events have their waveforms further compressed using the Super Data Storage and Transfer format (SuperDST), which uses only 9% of the storage size of the full waveform information. Very fast, basic reconstructions are run on the SuperDST waveforms to compute the vertex position, energy, direction and goodness-of-fit that are necessary for the filter selections of possible interesting events.

Around 25 filters search for a wide range of different types of particle interactions, ranging from low-energy neutrinos for oscillation measurements to the highest-energy neutrino interactions illuminating large parts of the detector. Some filters are designed to look for neutrino events of wide astrophysical interest to the scientific community and trigger alerts that are distributed to followup observatories worldwide. One example is the “EHE alert” that searches for Extremely High Energy neutrinos that are most likely of astrophysical origin [155]. Another example is the Gamma Follow Up alert that notifies the MAGIC and VERITAS collaborations when significant bursts of neutrinos from known high-energy gamma-ray sources over periods up to 3 weeks occur [156]. Other filters look for events that could be caused by muons, WIMPs, monopoles, etc. The filters that were used in this analysis are given in Section ??.

As a bonus, filtering reduces the data volume to a level of around 90 Gb/day, which is small enough to transfer to the North using a satellite.

5.4.3 Data handling

Most of the data is processed with the PnF system. The geometry, calibration, and detector status (GCD) information from each 8 hour run is sent via the same satellite transfer that is used for the continuously running PnF system. All the raw waveforms were written to tape before that system was retired in 2015. Since then, disks have been used to store the remaining archival data. This raw data is shipped to the North every year and is used if reprocessing of data is necessary. An example is the SPE correction for all runs starting from 2010 to 2016 referred to as *pass2 data* [157].

Files are stored in IceCube specific files and are called *i3files*.

5.5 Antarctic ice

The ice, in which the optical modules are frozen, acts as the propagation medium for the light that is produced by relativistic particles. Therefore, the parameterization of the ice is of great importance for good reconstructions and reliable simulations. The relativistic particles that travel through the ice produce photons in a Cherenkov cone of around 41° (see Section 4.1). How these photons further propagate from the point of emission to the receiving sensors is determined by the absorption and scattering within the ice. The most important parameters necessary to describe the photon propagation in ice are:

- the average distance to absorption,
- the average distance between successive scatters of photons, and
- the angular distribution of the new direction of a photon at each given scattering point.

There has been a large effort into measuring and modeling the Antarctic ice that is still ongoing. A good summary (although is a bit outdated as it does not include ice anisotropy effects, cable shadowing and DOM tilts) can be found in Ref. [154].

5.5.1 Ice simulation

The ice is modeled by the six-parameter ice model introduced in Ref. [158]. Flasher data from LEDs is used to fit the model to data (see Section 5.2.1.3). In this model, the ice is described by a table of depth-dependent parameters $b_e(400)$ and $a_{dust}(400)$ related to scattering and absorption at a wavelength of 400 nm. These two parameters depend on the relative temperature $\delta\tau$, which changes in function of depth, and six global parameters. The effective scattering coefficient is equal to $b_e = b \cdot (1 - \langle \cos \theta \rangle)$, where b is the geometrical scattering coefficient that determines the average distance between successive scatters and θ is the deflection angle at each scatter. The absorption coefficient a determines the average distance traveled by a photon before it is absorbed and is the sum of two components: one due to dust and the other a temperature dependent component for pure ice.

$$b_e(\lambda) = b_e(400) \cdot \left(\frac{\lambda}{400} \right)^{-\alpha}, \quad (5.1)$$

$$a(\lambda) = a_{dust}(\lambda) + Ae^{-B/\lambda} \cdot (1 + 0.01 \cdot \delta\tau), \quad (5.2)$$

with $a_{dust}(\lambda) = a_{dust}(400) \cdot \left(\frac{\lambda}{400} \right)^{-\kappa}$.

α, κ, A and B are determined in Ref. [158]*, $\delta\tau$ is equal to

$$\delta\tau(d) = T(d) - T(1730\text{m}), \quad (5.3)$$

with $T(d) = 221.5 - 0.00045319 \cdot d + 5.822 \cdot 10^{-6} \cdot d^2$,

*The remaining two parameters D and E were not used here.

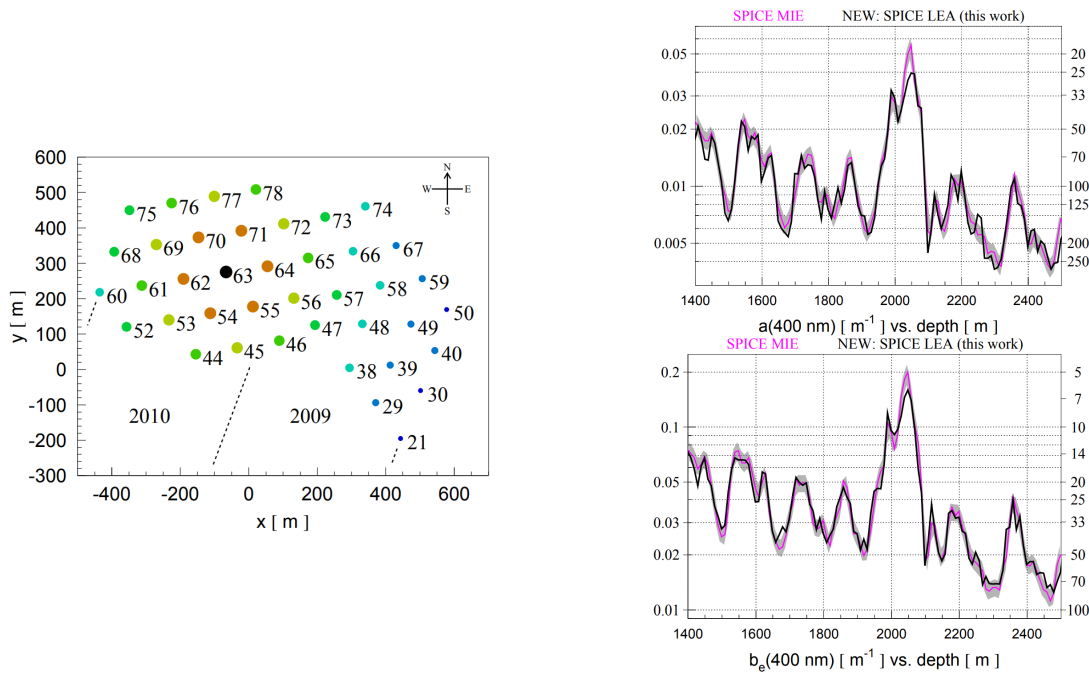


Figure 5.10: *Left:* Top view of the 2008 detector configuration when DOMs on string 63 were used to flash LEDs in a flasher run. Same colors are used for strings located at a similar distance to the central string. *Right:* values of $b_e(400)$ and $a(400)$ vs. depth for two different ice models. The scale and numbers to the right of each plot indicate the corresponding effective absorption $1/a$ and scattering $1/b_e$ lengths in [m]. Both illustrations from Ref. [159].

where d is the relative depth compared to the center of AMANDA (1730 m depth). Using flasher data with 400 nm wavelengths, it is possible to measure the values of $b_e(400)$ and $a_{dust}(400)$ at certain depths and use the six-parameter ice model to extrapolate scattering and absorption for other wavelengths.

In 2008, a flasher run was launched where each DOM on string 63 was producing flashes. The layout of the detector at the time of the flasher run and results of fits to $b_e(400)$ and $a(400)$ vs. depth can be found in Figure 5.10. At a depth between 2000 meters and 2100 meters, a large increase in scattering and absorption is clearly visible. A *dust layer*, presumably originating from volcanic ash, is characterized by an increase of dust in the ice, responsible for the higher scattering and absorption factors.

Over the years, multiple different ice models have been constructed. For this analysis the SPICELea* model has been set as nominal. This is the most recent model that has significant Monte Carlo background simulations available. It includes an angular sensitivity estimation due to the *hole ice*, a column of ice approximately 30 cm in radius immediately surrounding the strings with an increased amount of scattering. More information about this model can be found in Ref. [159].

5.5.2 Systematic uncertainties

The characteristics of the ice are complex. Dust particles, the tilt in the ice sheets, etc. result into non-negligible uncertainties in the ice model. Data from the flasher runs are compared to simulation and this verification was used to quantify the uncertainty on the measured values of $b_e(400)$ and $a(400)$. From this, it was determined that $(+10\%, 0), (0, +10\%)$ and $(-7.1\%, -7.1\%)$ uncertainties on the scattering and absorption coefficients, respectively, was a conservative estimation.

*SPICE stands for South Pole Ice. Lea is an addition to distinguish the different model types, but has (as far as the author knows) no special meaning.

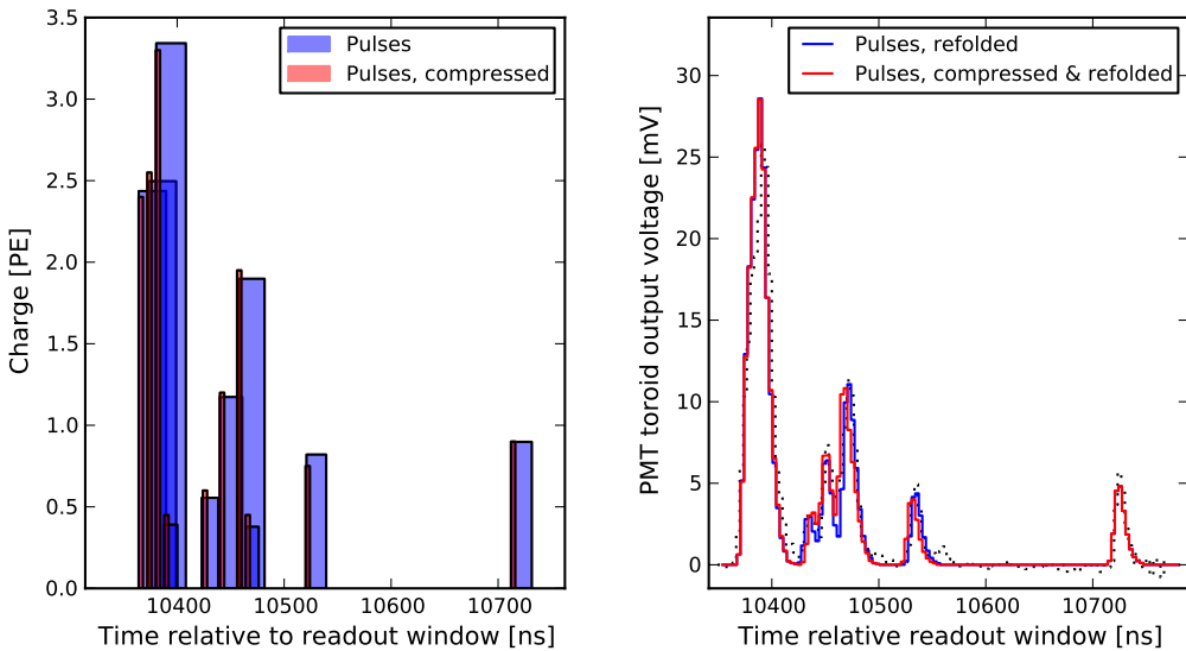


Figure 5.12: *Left:* pulse information illustrated with blue bars; the leading-edges time, width, and charge of the pulse are given by the left edge, width, and height of the bar, respectively. The red bars show the same after SuperDST compression. *Right:* Reconstructed pulses using the full pulse profiles in blue are compared to an approximation of the original waveform that is obtained by convolving the pulse times and charges with an average single-photoelectron pulse shape. Figures from Ref. [160].

5.6 IceCube event topology

The compressed waveforms are refolded to approximations of the original waveforms using average single-photoelectron pulse shapes as can be seen in Figure 5.12. The timing, shape and amplitude of the reconstructed waveforms in all the DOMs in an event are used to characterize the event topologies in the detector. Different interactions give rise to several possible signatures in the detector. Energetic muons propagate several hundred meters in the ice and give rise to tracks, whereas electrons and hadrons are stopped almost immediately, giving rise to cascades (see Section 4.3).

The track-like events, originating from charged-current muon neutrino interactions, provide an angular resolution at a typical angle of 1° for well-contained and reconstructed tracks at 1 TeV and improves to $\sim 0.3^\circ$ for neutrinos with an energy of 1 PeV [161]. Cascades, originating from electromagnetic or hadronic cascades, result in a more spherical light generation in the detector. Well-contained shower events have an average deposited energy resolution of around 15%. These event types are shown in more detail in Figure 5.13.

5.7 Future upgrades

The last couple of years there has been a large focus on improving the physics work that can be done in the IceCube experiment. Several projects are in the pipeline, are under R&D, and/or have been funded to improve the full analysis case of the detector(s).

Lower-energy neutrinos can be detected with a denser infill with other optical modules (the Upgrade, see Section 5.7.1), cosmic ray measurements can be improved with a complementary scintillator array to the IceTop tanks [163] and small air cherenkov telescopes [164]. Also, the detection of ultra-high-energy neutrinos could be made possible with a larger infill of the current IceCube in-ice array (Gen2) or radio antennas. Below a brief summary of projects that could be of potential importance to this analysis is given.

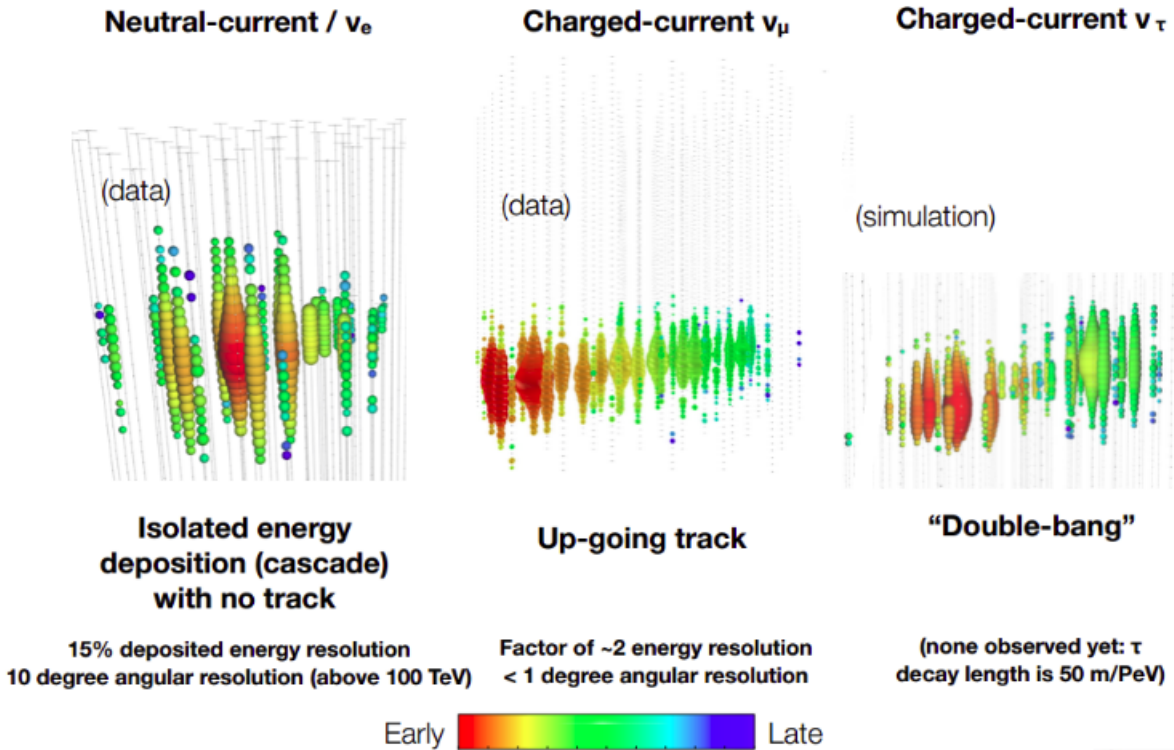


Figure 5.13: Neutrino interactions in the IceCube detector have two distinct types of interactions: cascades and tracks. Energetic taus are theorized to have double-bang signatures but have not undeniably been seen. Colors determine the timing of hits in the optical modules in the ice. Illustrations from the IceCube collaboration [162].

5.7.1 IceCube Upgrade

In 2018, a funding proposal for a dense 7-string infill of DeepCore was accepted by the NSF and was effective from the beginning of October later that year. This infill would have DOMs separated 2.4 m apart and start from a depth of 2140 m, reaching to 2440 m deep in the ice along seven new strings (see Figure 5.14). This very dense array would allow low-energy and oscillation experiments to reach much better sensitivities. Also, very dim tracks such as the ones from particles with an anomalous charge lower than e , might be easier to distinguish from low-energy muons that produce more Cherenkov light.

Because this project involves a restart of the drill, it also serves as a testbed for new optical modules. The Upgrade is the first step towards the much bigger Gen2 project. New types of optical modules would be used with higher angular acceptances than the currently used DOMs that have one large downward facing PMT. Examples are D-Eggs, which have two PMTs at each end of an ellipsoid glass [165], and mDOMs, where multiple smaller PMTs are positioned in a ball-shaped optical module [166].

A camera system could also be included in the new optical module designs and should help to improve the properties of the ice after refreezing [167]. Another camera system, the Precision Optical Calibration Module (POCAM) should further improve our understanding of the ice characteristics and accurately determine the efficiency and angular acceptance of the IceCube DOMs [168].

Deployment is currently planned for the 2022/2023 season.

5.7.2 IceCube Gen2

Although the IceCube in-ice array has successfully been able to determine the flux of astrophysical neutrinos and show the detection of a coincident neutrino with a blazar in an active state, a next generation larger detector infill would greatly improve the detection possibilities of astrophysical

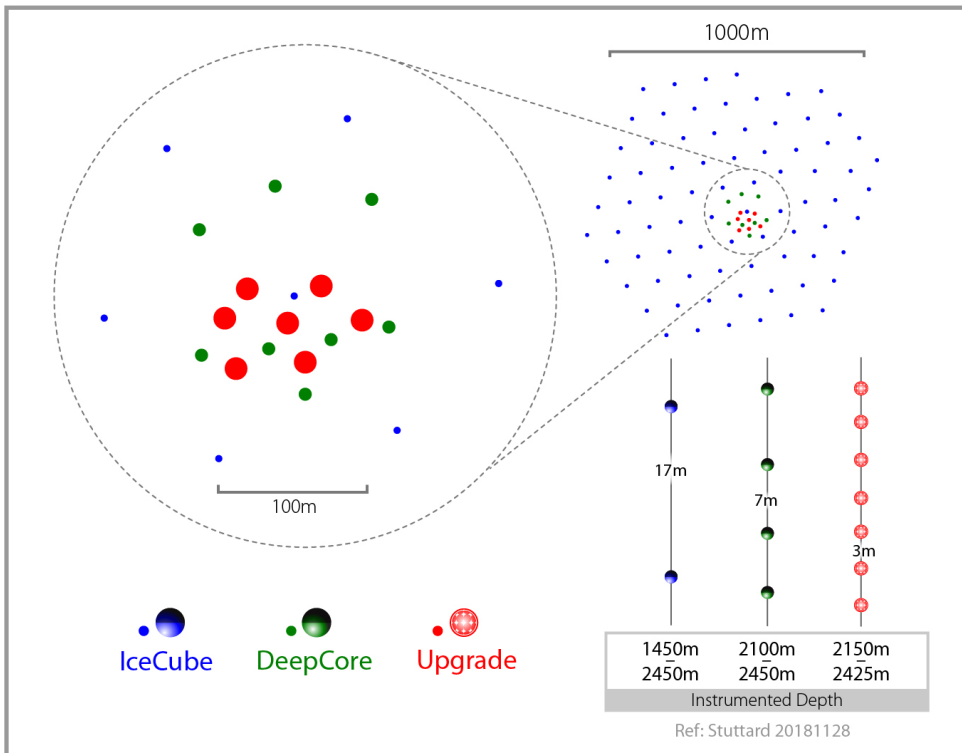


Figure 5.14: Top view of the Upgrade infill (red circles) within the DeepCore array (green) and the whole IceCube detector (blue). The area of the circles is representative of the instrumented photocathode density on a given string. Illustration from the IceCube collaboration.

neutrinos [169]. A 10 km^3 volume of clear glacial ice would allow for a much higher detector acceptance of high-energy neutrino interactions, helping in searches for point sources, better characterizing the spectral and flavor properties, and search for cosmogenic neutrinos among others. Point sources and cosmogenic neutrinos have, for now, not been observed even though the detector has been running stable for a couple of years. There is also only a small set of unambiguous astrophysical neutrinos. It would take extremely large running operations from the current detector (without hardware failures that are prone to happen more and more) to gather enough events for meaningful statistics. A much larger instrumented volume, such as the one proposed, is predicted to have an increase in sensitivity to transient source densities and rated by about two orders of magnitude [170]. Also, a large extension of the active volume could help to look for long tracks originating from SMPs. Although much is undecided, the plans are to have an extra surface array for cosmic ray detection and a radio array for the highest energy neutrinos along the in-ice array.

Deployment is planned for ???

5.7.2.1 In-ice infill

The current design for the Gen2 string configuration would be ~ 120 cables with an inter-string spacing around 250 m to 300 m. This much coarser spread of strings will result in a loss of sensitivity for neutrino events of the order of couple of TeV but would not affect the measurements of the very energetic astrophysical neutrinos. Measurements of the absorption lengths in function of the depth in the ice indicate that the instrumentation of the strings could be extended with an additional 250 m in total. This total depth is comparable to the current depth of the IceCube detector, meaning the surface area should reach to an exposed area of $\sim 10 \text{ km}^2$. This would result in a drastic sensitivity improvement of (near-)horizontal muons traversing the ice that are too energetic to be contained in the current detector.

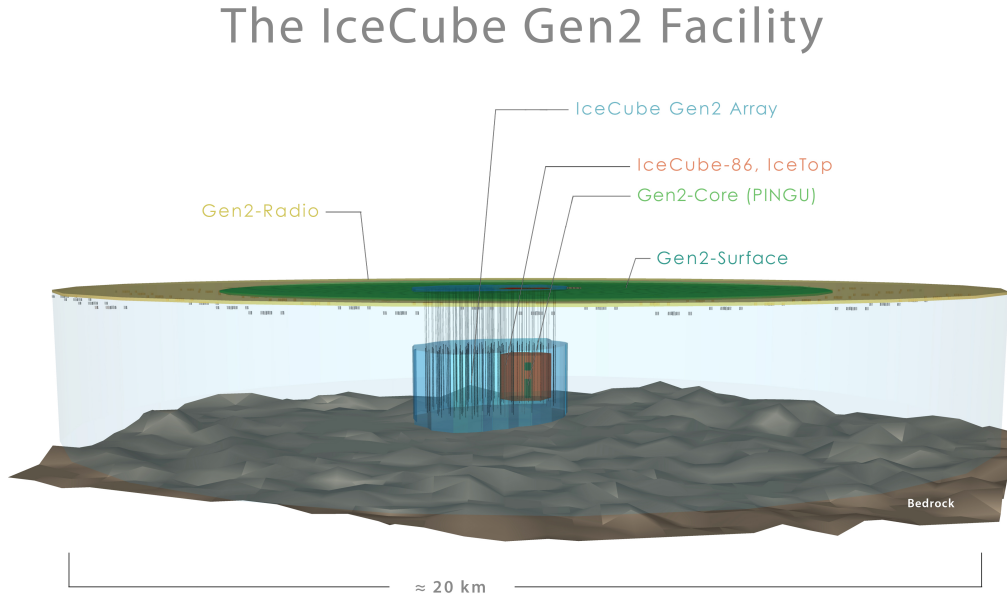


Figure 5.15: Impression of the possible Gen2 layout. The current IceCube in-ice and IceTop arrays are shown in red/brown. The 10x larger Gen2 in-ice array is given in blue. Possible layouts for the radio array (yellow) and surface array (green) are also listed. From the IceCube collaboration. PINGU zit hier bij, maar nog geen idee of dat er van ga komen of dat het bij de upgrade gaat blijven...

5.7.2.2 Surface array

The size of the IceTop array is too limited for most analyses to be used as a veto for most analyses. Therefore, the prospects of a surface array for the Gen2 extension would have much larger designs [171]. The geometry and optimal type of detector that should be used for this configuration is still under design.

5.7.2.3 Radio array

To achieve an improved sensitivity to neutrinos in the $10^{16} - 10^{20}$ eV energy range, including GZK neutrinos, an additional radio-pulse neutrino detector could be constructed. At the critical energy of around 100 PeV, the origins of cosmic rays transitions from the highest-energy galactic sources to the even more extragalactic cosmic rays. A good review of radio emission from cosmic rays is given in Ref. [172]. There are ongoing experiments that act as a proof-of-principle for the radio technique in the ice: ARA (Askaryan Radio Array) [173], close to the IceCube detector at South Pole (see Figure 5.2) and ARIANNA (Antarctic Ross Ice Shelf Antenna Neutrino Array) [174] on the Ross Ice Shelf at the antarctic coast.

5.8 Beyond the Standard Model searches

The IceCube experiment consists of about 300 people from 50 institutions spread over 12 countries. A wide variety of senior scientists, graduate students, technicians, software specialists and engineers works on the continuous running operations to keep the detector running in both hardware and software. Most other people focus on physics analyses that range from low-energy oscillation physics to the rare highest-energy neutrino interactions in the ice. Below I give a general and very brief overview of some IceCube analyses that search for beyond-the-Standard-Model physics.

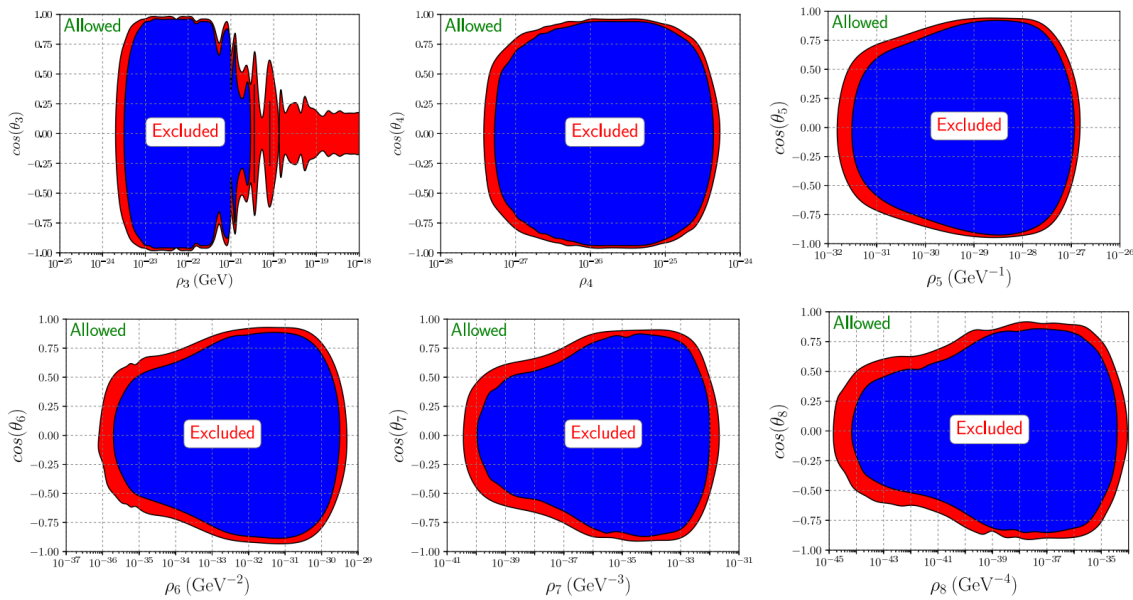


Figure 5.16: Regions excluded at 90% (99%) C.L. in the LIV parameter space in red (blue). ρ is related to the strength of the LIV and $\cos(\theta_d)$ is a combination of coefficients defining LIV in the effective Hamiltonian of Standard Model Extension [175]. The subscript d refers to the power of the corresponding operator in the Hamiltonian. More information in Ref. [176].

5.8.1 Lorentz invariance violation

is dit nu goed uitgelegd of niet?

Lorentz symmetry is one of the foundations of the SM: fundamental laws in nature are thought to be independent of the observer's inertial frame. Some SM extensions allow for spontaneous breaking of Lorentz symmetry and can lead to Lorentz-invariance violating (LIV) effects. Examples are string theory or quantum gravity. Some effects that would follow from these extensions are incorporated in the Standard Model Extension (SME) [175] and although the size of LIV effects should be suppressed by the Planck scale ($\approx 10^{19}$ GeV). They could manifest themselves in, e.g., oscillations of atmospheric neutrinos that would modify the observed energy and zenith angle distributions of atmospheric muon neutrinos observed by the IceCube experiment. The LIV effects are often parametrised by two parameters: ρ_d and $\cos(\theta_d)$ (which are explained in the capture of Figure 5.16), where d refers to the power of the operator in the Hamiltonian. The energy reach of the IceCube detector makes it possible to go to dimensions up to 8 whereas most other experiments are sensitive up to dimension $d = 3$ or $d = 4$. This analysis was done first in the 40-string configuration [177] and later redone with the full detector configuration [176]. Results for $3 \leq d \leq 8$ are shown in Figure 5.16.

5.8.2 Dark matter

The large amount of evidence to support the existence of dark matter (DM) was given in Section 1.5. Many ongoing experimental efforts try to search for these elusive particles*. Collider experiments try to produce these particles by SM interactions (*production searches*), other experiments try to measure their interaction with SM particles through nuclear recoil (*direct detection*). It should also be possible to search for the SM products that are produced when annihilation of DM occurs and the corresponding daughter particles find their way to Earth (*direct detection*). Most searches focus on specific regions in the sky that are more prone to produce a measurable signal. As one characteristic of DM is its non-zero mass, they are expected to be gravitationally trapped in the halo of galaxies or to accumulate in heavy celestial objects nearby such as the Sun or the Earth itself. Since most SM particles never reach us, neutrinos are the only possible messengers. Figure 5.17 shows a comparison of upper limits on $\langle \sigma_A v \rangle$ versus

*Assuming that they are in fact particles.

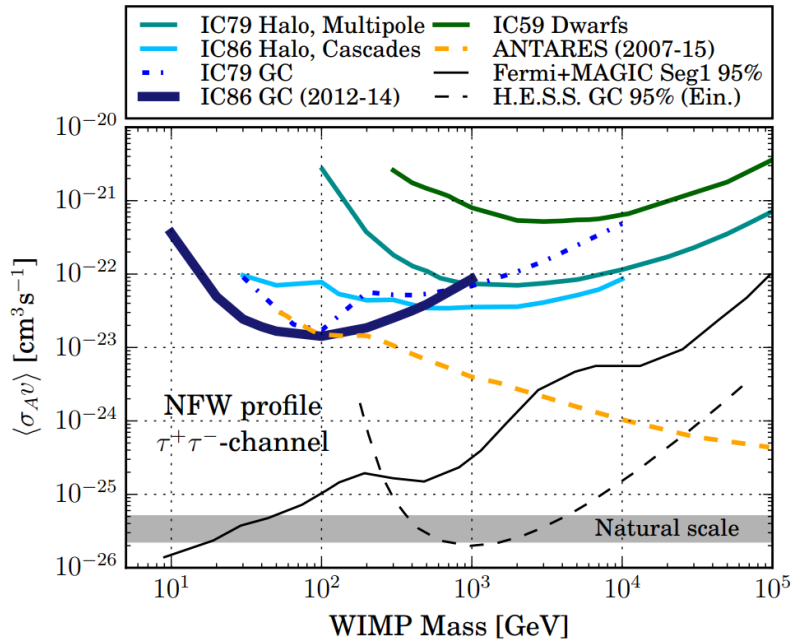


Figure 5.17: Upper limits of $\langle\sigma_A v\rangle$ in function of the WIMP mass from different experiments.

WIMP mass*, for the annihilation channel $\chi\chi \rightarrow \tau^+\tau^-$ producing tau neutrinos. $\langle\sigma_A v\rangle$ is the WIMP-WIMP annihilation cross section and determines the strength of the expected neutrino flux. The analysis mentioned in the figure searched for signals from the center of the Milky Way [178]. Other IceCube analyses have searched for dark matter in the Sun [179, 180] and in the Earth [181].

5.8.3 Magnetic monopoles

The quantum theory of magnetic charge started with a paper by P. Dirac [182] in which he theorized the existence of magnetic monopoles in a similar fashion as he did to successfully predict the positron. If q_m is the magnetic charge and q_e the electric charge, Dirac found that the following condition should hold

$$q_m q_e = 2\pi n \quad (n \in \mathbb{Z}), \quad (5.4)$$

and could therefore explain why the electric charge is always quantized, i.e. in integer multiples of an elementary charge. The smallest possible magnetic charge would be†

$$g_D = 2\pi/e = e/2\alpha \approx 68.5e, \quad (5.5)$$

with $\alpha = e^2/\pi$ in natural units. Magnetic monopoles appear automatically in certain Grand Unified Theories that would give rise to these particles after spontaneous symmetry breaking of the GUT group, similar to the Higgs mechanism [183, 184]. Masses are typically of the order of 10^{16-17} GeV. They are searched for in IceCube analyses in multiple velocity ranges. Monopoles with velocities close to the speed of light in vacuum produce extremely bright tracks due to their high Dirac charge as shown in Eq. 5.5. At lower velocities ($\approx 0.5c$ to $0.76c$) secondary knock-off δ -electrons could have velocities above the Cherenkov threshold and produce light. Luminescence light from excitation of the ice dominates at low relativistic velocities ($\approx 0.1c$ to $0.5c$). For each of these speed ranges, searches for magnetic monopoles at the IceCube experiment are either in

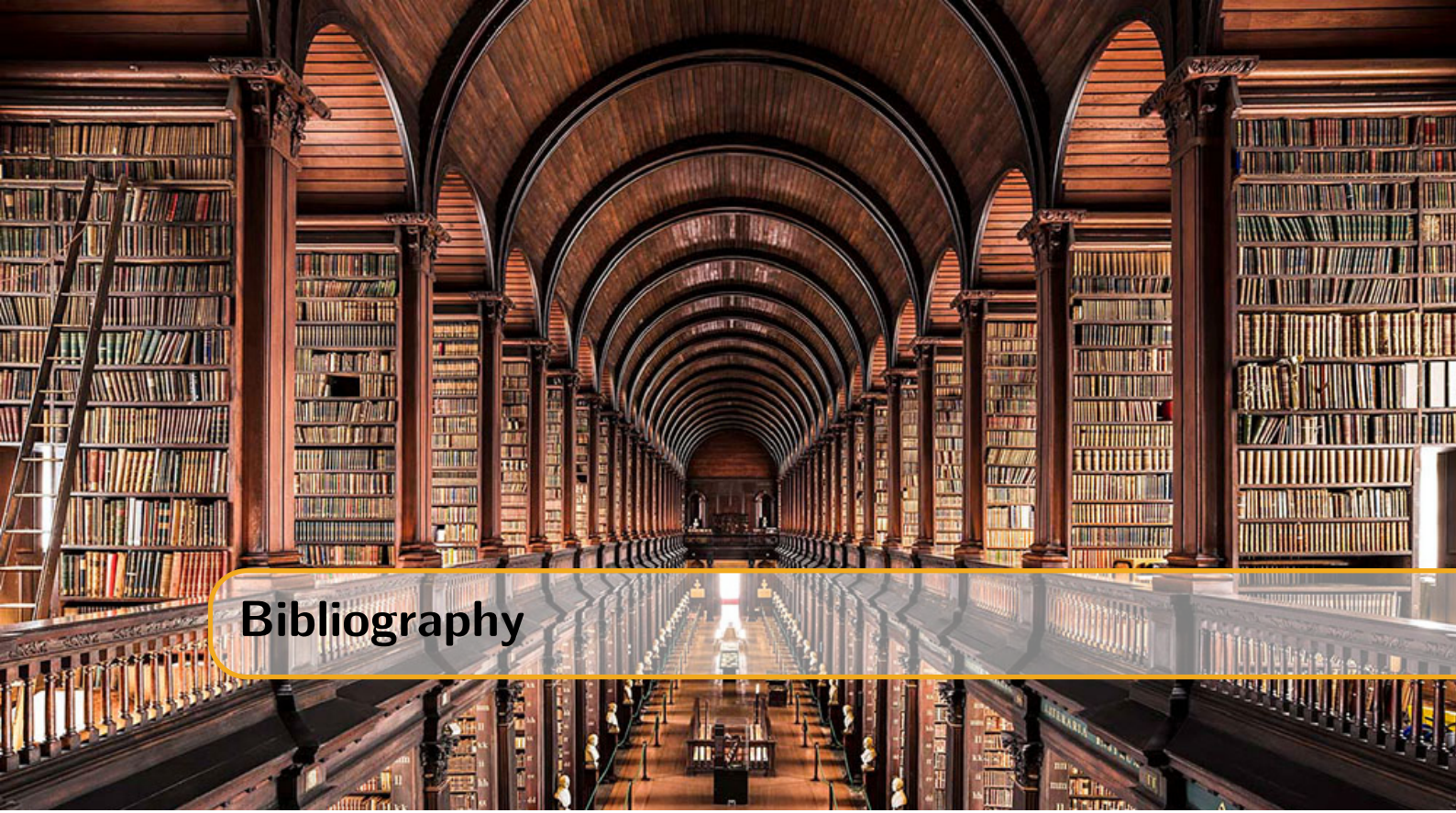
*WIMP stands for Weakly Interacting Massive Particle and is one possible candidate for dark matter.

†At the time of writing his paper, Dirac believed the smallest electric charge was from the electron. Since now we know the down quark holds an electric charge equal to $1/3e$, the minimal magnetic charge would be equal to $3g_D$.

progress (luminescence) or have already set the world's best upper limits on the flux of magnetic monopoles over a wide range of velocities [185].

5.9 Discussion

Nodig om over te gaan van deel 1 naar deel 2? Zou zeggen van wel. Kort.



Bibliography

- [1] B. Povh et al. *Particles and nuclei: An Introduction to the physical concepts*. 1995. DOI: 10.1007/3-540-36684-9 (cited on page 11).
- [2] Michael E. Peskin and Daniel V. Schroeder. *An Introduction to quantum field theory*. Reading, USA: Addison-Wesley, 1995. ISBN: 9780201503975, 0201503972. URL: <http://www.slac.stanford.edu/~mpeskin/QFT.html> (cited on page 11).
- [3] M. Tanabashi et al. “Review of Particle Physics”. In: *Phys. Rev. D* 98 (2018), page 030001 (cited on page 11).
- [4] Alessandro Bettini. *Introduction to elementary particle physics*. 2008. ISBN: 9780521880213. URL: <http://www.cambridge.org/catalogue/catalogue.asp?isbn=9780521880213> (cited on page 11).
- [5] CERN. URL: <https://home.cern/about/physics/standard-model> (cited on page 12).
- [6] Arthur B. McDonald. “Nobel Lecture: The Sudbury Neutrino Observatory: Observation of flavor change for solar neutrinos”. In: *Rev. Mod. Phys.* 88 (3 July 2016), page 030502. DOI: 10.1103/RevModPhys.88.030502. URL: <https://link.aps.org/doi/10.1103/RevModPhys.88.030502> (cited on page 13).
- [7] CMS. URL: <http://cms.web.cern.ch/news/jets-cms-and-determination-their-energy-scale> (cited on page 13).
- [8] A. Kircher. *Athanassii Kircherii... Magnes, sive De arte magnetica opus tripartitum...* sumptibus H. Scheus, 1641. URL: <https://books.google.be/books?id=1aZ3FcTAYdUC> (cited on page 14).
- [9] G. Farmelo. *The Strangest Man: The Hidden Life of Paul Dirac, Mystic of the Atom*. Basic Books, 2009. ISBN: 9780465019922. URL: <https://books.google.be/books?id=q sodmIGD0fMC> (cited on page 15).
- [10] F. Mandl and G. Shaw. *Quantum Field Theory*. Wiley, 2013. ISBN: 9781118716656. URL: <https://books.google.be/books?id=jTBzQfctvHAC> (cited on page 16).
- [11] Flip Tanedo. URL: <https://www.quantumdiaries.org/2012/02/14/why-do-we-expect-a-higgs-boson-part-ii-unitarization-of-vector-boson-scattering/> (cited on page 19).

- [12] S. L. Glashow, J. Iliopoulos, and L. Maiani. “Weak Interactions with Lepton-Hadron Symmetry”. In: *Phys. Rev.* D2 (1970), pages 1285–1292. DOI: 10.1103/PhysRevD.2.1285 (cited on page 23).
- [13] J. H. Christenson et al. “Evidence for the 2π Decay of the K20 Meson”. In: *Physical Review Letters* 13 (July 1964), pages 138–140. DOI: 10.1103/PhysRevLett.13.138 (cited on page 23).
- [14] Ziro Maki, Masami Nakagawa, and Shoichi Sakata. “Remarks on the Unified Model of Elementary Particles”. In: *Progress of Theoretical Physics* 28.5 (1962), pages 870–880. DOI: 10.1143/PTP.28.870. eprint: /oup/backfile/content_public/journal/ptp/28/5/10.1143/ptp.28.870/2/28-5-870.pdf. URL: <http://dx.doi.org/10.1143/PTP.28.870> (cited on page 23).
- [15] Claudio Giganti, Stéphane Lavignac, and Marco Zito. “Neutrino oscillations: the rise of the PMNS paradigm”. In: *Prog. Part. Nucl. Phys.* 98 (2018), pages 1–54. DOI: 10.1016/j.ppnp.2017.10.001. arXiv: 1710.00715 [hep-ex] (cited on page 23).
- [16] C. D. Anderson. “The Positive Electron”. In: *Phys. Rev.* 43 (1933), pages 491–494. DOI: 10.1103/PhysRev.43.491 (cited on page 24).
- [17] Paul A. M. Dirac. “The quantum theory of the electron”. In: *Proc. Roy. Soc. Lond.* A117 (1928), pages 610–624. DOI: 10.1098/rspa.1928.0023 (cited on page 24).
- [18] S. H. Neddermeyer and C. D. Anderson. “Note on the Nature of Cosmic Ray Particles”. In: *Phys. Rev.* 51 (1937), pages 884–886. DOI: 10.1103/PhysRev.51.884 (cited on page 24).
- [19] C. M. G. Lattes et al. “PROCESSES INVOLVING CHARGED MESONS”. In: *Nature* 159 (1947). [,42(1947)], pages 694–697. DOI: 10.1038/159694a0 (cited on page 24).
- [20] F. J. Hasert et al. “Observation of Neutrino Like Interactions Without Muon Or Electron in the Gargamelle Neutrino Experiment”. In: *Phys. Lett.* B46 (1973). [,5.15(1973)], pages 138–140. DOI: 10.1016/0370-2693(73)90499-1 (cited on page 24).
- [21] G. Arnison et al. “Experimental Observation of Isolated Large Transverse Energy Electrons with Associated Missing Energy at $s^{**}(1/2) = 540\text{-GeV}$ ”. In: *Phys. Lett.* B122 (1983). [,611(1983)], pages 103–116. DOI: 10.1016/0370-2693(83)91177-2 (cited on page 24).
- [22] G. Arnison et al. “Experimental Observation of Lepton Pairs of Invariant Mass Around 95-GeV/c $^{**}2$ at the CERN SPS Collider”. In: *Phys. Lett.* B126 (1983). [,7.55(1983)], pages 398–410. DOI: 10.1016/0370-2693(83)90188-0 (cited on page 24).
- [23] S. W. Herb et al. “Observation of a Dimuon Resonance at 9.5-GeV in 400-GeV Proton-Nucleus Collisions”. In: *Phys. Rev. Lett.* 39 (1977), pages 252–255. DOI: 10.1103/PhysRevLett.39.252 (cited on page 24).
- [24] F. Abe et al. “Observation of top quark production in $\bar{p}p$ collisions”. In: *Phys. Rev. Lett.* 74 (1995), pages 2626–2631. DOI: 10.1103/PhysRevLett.74.2626. arXiv: hep-ex/9503002 [hep-ex] (cited on page 24).
- [25] D. P. Barber et al. “Discovery of Three Jet Events and a Test of Quantum Chromodynamics at PETRA Energies”. In: *Phys. Rev. Lett.* 43 (1979), page 830. DOI: 10.1103/PhysRevLett.43.830 (cited on page 24).
- [26] S. Schael et al. “Precision electroweak measurements on the Z resonance”. In: *Phys. Rept.* 427 (2006), pages 257–454. DOI: 10.1016/j.physrep.2005.12.006. arXiv: hep-ex/0509008 [hep-ex] (cited on page 24).
- [27] Sabine Riemann. “Precision electroweak physics at high energies”. In: *Rept. Prog. Phys.* 73 (2010), page 126201. DOI: 10.1088/0034-4885/73/12/126201 (cited on page 24).
- [28] Kenji Abe et al. “A High precision measurement of the left-right Z boson cross-section asymmetry”. In: *Phys. Rev. Lett.* 84 (2000), pages 5945–5949. DOI: 10.1103/PhysRevLett.84.5945. arXiv: hep-ex/0004026 [hep-ex] (cited on page 24).

- [29] Koya Abe et al. “First direct measurement of the parity violating coupling of the Z0 to the s quark”. In: *Phys. Rev. Lett.* 85 (2000), pages 5059–5063. DOI: 10.1103/PhysRevLett.85.5059. arXiv: hep-ex/0006019 [hep-ex] (cited on page 24).
- [30] Koya Abe et al. “An Improved direct measurement of leptonic coupling asymmetries with polarized Z bosons”. In: *Phys. Rev. Lett.* 86 (2001), pages 1162–1166. DOI: 10.1103/PhysRevLett.86.1162. arXiv: hep-ex/0010015 [hep-ex] (cited on page 24).
- [31] K. Abe et al. “First measurement of the left-right charge asymmetry in hadronic Z boson decays and a new determination of $\sin^{**2} \theta(W)(\text{eff})$ ”. In: *Phys. Rev. Lett.* 78 (1997), pages 17–21. DOI: 10.1103/PhysRevLett.78.17. arXiv: hep-ex/9609019 [hep-ex] (cited on page 24).
- [32] Timo Antero Aaltonen et al. “Combination of CDF and D0 W-Boson Mass Measurements”. In: *Phys. Rev.* D88.5 (2013), page 052018. DOI: 10.1103/PhysRevD.88.052018. arXiv: 1307.7627 [hep-ex] (cited on page 24).
- [33] “Combination of CDF and D0 Results on the Width of the W boson”. In: (2010). arXiv: 1003.2826 [hep-ex] (cited on page 24).
- [34] Morad Aaboud et al. “Measurement of the W-boson mass in pp collisions at $\sqrt{s} = 7$ TeV with the ATLAS detector”. In: *Eur. Phys. J.* C78.2 (2018), page 110. DOI: 10.1140/epjc/s10052-017-5475-4. arXiv: 1701.07240 [hep-ex] (cited on page 24).
- [35] ATLAS. URL: cds.cern.ch/record/2285809/files/ATLAS-CONF-2017-071.pdf (cited on page 24).
- [36] CMS. URL: cds.cern.ch/record/2235162/files/TOP-15-012-pas.pdf (cited on page 24).
- [37] CMS. URL: cds.cern.ch/record/2284594/files/TOP-17-007-pas.pdf (cited on page 24).
- [38] NA62 collaboration. URL: <https://indico.cern.ch/event/714178/> (cited on page 24).
- [39] Cari Cesarotti et al. “Interpreting the Electron EDM Constraint”. In: (2018). arXiv: 1810.07736 [hep-ph] (cited on page 25).
- [40] M. G. Aartsen et al. “Measurement of the multi-TeV neutrino cross section with IceCube using Earth absorption”. In: *Nature* 551 (2017), pages 596–600. DOI: 10.1038/nature24459. arXiv: 1711.08119 [hep-ex] (cited on page 25).
- [41] Andrea Castro. “Recent Top Quark Mass Measurements from CMS”. In: *Proceedings, 10th International Workshop on Top Quark Physics (TOP2017): Braga, Portugal, September 17-22, 2017*. 2017. arXiv: 1712.01027 [hep-ex] (cited on page 25).
- [42] PDG. URL: <http://pdg.lbl.gov/2018/reviews/rpp2018-rev-standard-model.pdf> (cited on pages 25, 27, 42, 49, 57, 62).
- [43] P. A. R. Ade et al. “Planck 2015 results. XIII. Cosmological parameters”. In: *Astron. Astrophys.* 594 (2016), A13. DOI: 10.1051/0004-6361/201525830. arXiv: 1502.01589 [astro-ph.CO] (cited on page 26).
- [44] Evgige Corbelli and Paolo Salucci. “The Extended Rotation Curve and the Dark Matter Halo of M33”. In: *Mon. Not. Roy. Astron. Soc.* 311 (2000), pages 441–447. DOI: 10.1046/j.1365-8711.2000.03075.x. arXiv: astro-ph/9909252 [astro-ph] (cited on page 26).
- [45] S. M. Faber and R. E. Jackson. “Velocity dispersions and mass to light ratios for elliptical galaxies”. In: *Astrophys. J.* 204 (1976), page 668. DOI: 10.1086/154215 (cited on page 26).
- [46] Steven W. Allen, August E. Evrard, and Adam B. Mantz. “Cosmological Parameters from Observations of Galaxy Clusters”. In: *Ann. Rev. Astron. Astrophys.* 49 (2011), pages 409–470. DOI: 10.1146/annurev-astro-081710-102514. arXiv: 1103.4829 [astro-ph.CO] (cited on page 26).

- [47] Priyamvada Natarajan et al. “Mapping substructure in the HST Frontier Fields cluster lenses and in cosmological simulations”. In: *Mon. Not. Roy. Astron. Soc.* 468.2 (2017), pages 1962–1980. DOI: 10.1093/mnras/stw3385. arXiv: 1702.04348 [astro-ph.GA] (cited on page 26).
- [48] John F. Donoghue. “The effective field theory treatment of quantum gravity”. In: *AIP Conf. Proc.* 1483 (2012), pages 73–94. DOI: 10.1063/1.4756964. arXiv: 1209.3511 [gr-qc] (cited on page 26).
- [49] C. D. McCoy. “Does inflation solve the hot big bang model’s fine-tuning problems?” In: *Stud. Hist. Phil. Sci.* B51 (2015), pages 23–36. DOI: 10.1016/j.shpsb.2015.06.002 (cited on page 26).
- [50] R. D. Peccei. “The Strong CP problem and axions”. In: *Lect. Notes Phys.* 741 (2008). [,3(2006)], pages 3–17. DOI: 10.1007/978-3-540-73518-2_1. arXiv: hep-ph/0607268 [hep-ph] (cited on page 27).
- [51] C. Amsler et al. “Review of Particle Physics”. In: *Physics Letters B* 667.1 (2008). Review of Particle Physics, pages 1–6. ISSN: 0370-2693. DOI: <https://doi.org/10.1016/j.physletb.2008.07.018>. URL: <http://www.sciencedirect.com/science/article/pii/S0370269308008435> (cited on page 27).
- [52] Georges Aad et al. “Combined Measurement of the Higgs Boson Mass in pp Collisions at $\sqrt{s} = 7$ and 8 TeV with the ATLAS and CMS Experiments”. In: *Phys. Rev. Lett.* 114 (2015), page 191803. DOI: 10.1103/PhysRevLett.114.191803. arXiv: 1503.07589 [hep-ex] (cited on page 27).
- [53] Susanne Mertens. “Direct Neutrino Mass Experiments”. In: *J. Phys. Conf. Ser.* 718.2 (2016), page 022013. DOI: 10.1088/1742-6596/718/2/022013. arXiv: 1605.01579 [nucl-ex] (cited on page 27).
- [54] Ivan Esteban et al. “Updated fit to three neutrino mixing: exploring the accelerator-reactor complementarity”. In: *JHEP* 01 (2017), page 087. DOI: 10.1007/JHEP01(2017)087. arXiv: 1611.01514 [hep-ph] (cited on page 27).
- [55] NuFIT. URL: <http://www.nu-fit.org/?q=node/177> (cited on page 27).
- [56] nobel2004. URL: <https://www.nobelprize.org/prizes/physics/2004/popular-information/> (cited on page 28).
- [57] Xiao-Gang He, Girish C. Joshi, and B. H. McKellar. “The Quantization of the Electric Charge in Gauge Theories”. In: *Europhys. Lett.* 10 (1989), page 709. DOI: 10.1209/0295-5075/10/8/002 (cited on pages 28, 31).
- [58] Stefano Bertolini, Luca Di Luzio, and Michal Malinsky. “Intermediate mass scales in the non-supersymmetric SO(10) grand unification: A Reappraisal”. In: *Phys. Rev.* D80 (2009), page 015013. DOI: 10.1103/PhysRevD.80.015013. arXiv: 0903.4049 [hep-ph] (cited on page 28).
- [59] Hong-Wei Yu. “SU(8) GUT MODELS WITH STABLE PROTON, N ANTI-N OSCILLATIONS, FRACTIONAL CHARGES AND LOW MASS MONOPOLES”. In: *Phys. Lett.* 142B (1984), pages 42–46. DOI: 10.1016/0370-2693(84)91132-8 (cited on pages 28, 32).
- [60] Xiao-Gang Wen and Edward Witten. “Electric and Magnetic Charges in Superstring Models”. In: *Nucl. Phys.* B261 (1985), pages 651–677. DOI: 10.1016/0550-3213(85)90592-9 (cited on pages 28, 32).
- [61] Gregory G. Athanasiou et al. “Remarks on Wilson Lines, Modular Invariance and Possible String Relics in Calabi-yau Compactifications”. In: *Phys. Lett.* B214 (1988), pages 55–62. DOI: 10.1016/0370-2693(88)90451-0 (cited on pages 28, 32).
- [62] Stephen M. Barr, D. B. Reiss, and A. Zee. “Fractional Charges, Monopoles and Peculiar Photons”. In: *Phys. Rev. Lett.* 50 (1983), page 317. DOI: 10.1103/PhysRevLett.50.317 (cited on page 32).

- [63] P. H. Frampton and T. W. Kephart. “Fractionally Charged Particles as Evidence for Supersymmetry”. In: *Phys. Rev. Lett.* 49 (1982), page 1310. DOI: 10.1103/PhysRevLett.49.1310 (cited on page 32).
- [64] Katsuji Yamamoto. “Fractionally Charged Leptons in the SO(14) GUT”. In: *Phys. Lett.* 120B (1983), pages 157–160. DOI: 10.1016/0370-2693(83)90643-3 (cited on page 32).
- [65] Fang-xiao Dong et al. “Fractional Charges, Monopoles and Peculiar Photons in SO(18) GUT Models”. In: *Phys. Lett.* 129B (1983), pages 405–410. DOI: 10.1016/0370-2693(83)90129-6 (cited on page 32).
- [66] Xiang-Dong Jiang and Xian-Jian Zhou. “SO(10) X SO(8) MODEL WITH FRACTIONAL CHARGES, MONOPOLES AND PECULIAR PHOTONS. (IN CHINESE)”. In: *HEPNP* 9 (1985), pages 421–429 (cited on page 32).
- [67] K. Abe et al. “Search for proton decay via $p \rightarrow e^+ \pi^0$ and $p \rightarrow \mu^+ \pi^0$ in 0.31 megaton years exposure of the Super-Kamiokande water Cherenkov detector”. In: *Phys. Rev.* D95.1 (2017), page 012004. DOI: 10.1103/PhysRevD.95.012004. arXiv: 1610.03597 [hep-ex] (cited on page 32).
- [68] Ignatios Antoniadis and K. Benakli. “Fractionally charged particles and supersymmetry breaking in 4-D strings”. In: *Phys. Lett.* B295 (1992). [Erratum: *Phys. Lett.* B407,449(1997)], pages 219–224. DOI: 10.1016/S0370-2693(97)00755-7, 10.1016/0370-2693(92)91557-P. arXiv: hep-th/9209020 [hep-th] (cited on page 32).
- [69] Bob Holdom. “Two U(1)’s and Epsilon Charge Shifts”. In: *Phys. Lett.* 166B (1986), pages 196–198. DOI: 10.1016/0370-2693(86)91377-8 (cited on page 32).
- [70] Eder Izquierre and Itay Yavin. “New window to millicharged particles at the LHC”. In: *Phys. Rev.* D92.3 (2015), page 035014. DOI: 10.1103/PhysRevD.92.035014. arXiv: 1506.04760 [hep-ph] (cited on page 32).
- [71] David E. Brahm and Lawrence J. Hall. “U(1)-prime DARK MATTER”. In: *Phys. Rev.* D41 (1990), page 1067. DOI: 10.1103/PhysRevD.41.1067 (cited on page 32).
- [72] C. Boehm and Pierre Fayet. “Scalar dark matter candidates”. In: *Nucl. Phys.* B683 (2004), pages 219–263. DOI: 10.1016/j.nuclphysb.2004.01.015. arXiv: hep-ph/0305261 [hep-ph] (cited on page 32).
- [73] Maxim Pospelov, Adam Ritz, and Mikhail B. Voloshin. “Secluded WIMP Dark Matter”. In: *Phys. Lett.* B662 (2008), pages 53–61. DOI: 10.1016/j.physletb.2008.02.052. arXiv: 0711.4866 [hep-ph] (cited on page 32).
- [74] James D. Bjorken et al. “New Fixed-Target Experiments to Search for Dark Gauge Forces”. In: *Phys. Rev.* D80 (2009), page 075018. DOI: 10.1103/PhysRevD.80.075018. arXiv: 0906.0580 [hep-ph] (cited on page 32).
- [75] Gabriel Magill et al. “Millicharged particles in neutrino experiments”. In: (2018). arXiv: 1806.03310 [hep-ph] (cited on page 32).
- [76] R. Acciarri et al. “Long-Baseline Neutrino Facility (LBNF) and Deep Underground Neutrino Experiment (DUNE)”. In: (2015). arXiv: 1512.06148 [physics.ins-det] (cited on page 32).
- [77] M. Anelli et al. “A facility to Search for Hidden Particles (SHiP) at the CERN SPS”. In: (2015). arXiv: 1504.04956 [physics.ins-det] (cited on page 32).
- [78] Marco Battaglieri et al. “US Cosmic Visions: New Ideas in Dark Matter 2017: Community Report”. In: (2017). arXiv: 1707.04591 [hep-ph] (cited on page 32).
- [79] S. I. Alvis et al. “First Limit on the Direct Detection of Lightly Ionizing Particles for Electric Charge as Low as $e/1000$ with the Majorana Demonstrator”. In: *Phys. Rev. Lett.* 120.21 (2018), page 211804. DOI: 10.1103/PhysRevLett.120.211804. arXiv: 1801.10145 [hep-ex] (cited on page 32).

- [80] L. Lyons. “Quark Search Experiments at Accelerators and in Cosmic Rays”. In: *Phys. Rept.* 129 (1985), page 225. DOI: 10.1016/0370-1573(85)90011-0 (cited on page 33).
- [81] J. J. Aubert et al. “A Search for Free Quarks in Deep Inelastic Muon Scattering”. In: *Phys. Lett.* 133B (1983), page 461. DOI: 10.1016/0370-2693(83)90828-6 (cited on page 33).
- [82] A. E. Bondar et al. “SEARCH FOR LIGHT PARTICLES WITH CHARGE 2/3 IN e^+e^- ANNIHILATION”. In: *JETP Lett.* 40 (1984). [Pisma Zh. Eksp. Teor. Fiz. 40, 440 (1984)], pages 1265–1268 (cited on page 33).
- [83] H. Aihara et al. “Search for $q = 2/3e$ and $q = 1/3e$ particles produced in e^+e^- annihilations”. In: *Phys. Rev. Lett.* 52 (1984), page 2332. DOI: 10.1103/PhysRevLett.52.2332 (cited on page 33).
- [84] G. Abbiendi et al. “Search for stable and longlived massive charged particles in e^+e^- collisions at $s^{**}(1/2) = 130\text{-GeV}$ to 209-GeV ”. In: *Phys. Lett.* B572 (2003), pages 8–20. DOI: 10.1016/S0370-2693(03)00639-7. arXiv: hep-ex/0305031 [hep-ex] (cited on page 33).
- [85] P. Abreu et al. “Search for stable heavy charged particles in e^+e^- collisions at $s^{**}(1/2) = 130\text{-GeV}$ to 136-GeV , 161-GeV and 172-GeV ”. In: *Phys. Lett.* B396 (1997), pages 315–326. DOI: 10.1016/S0370-2693(97)00152-4 (cited on page 33).
- [86] R. Akers et al. “Search for heavy charged particles and for particles with anomalous charge in e^+e^- collisions at LEP”. In: *Z. Phys.* C67 (1995), pages 203–212. DOI: 10.1007/BF01571281 (cited on page 33).
- [87] D. Buskulic et al. “Search for particles with unexpected mass and charge in Z decays”. In: *Phys. Lett.* B303 (1993), pages 198–208. DOI: 10.1016/0370-2693(93)90066-Q (cited on page 33).
- [88] M. Banner et al. “A New Search for Relativistic Particles With Fractional Electric Charge at the CERN $p\bar{p}$ Collider”. In: *Phys. Lett.* 156B (1985), pages 129–133. DOI: 10.1016/0370-2693(85)91368-1 (cited on page 33).
- [89] F. Abe et al. “Limits on the production of massive stable charged particles”. In: *Phys. Rev.* D46 (1992), R1889–R1894. DOI: 10.1103/PhysRevD.46.R1889 (cited on page 33).
- [90] D. Acosta et al. “Search for long-lived charged massive particles in $\bar{p}p$ collisions at $\sqrt{s} = 1.8$ TeV”. In: *Phys. Rev. Lett.* 90 (2003), page 131801. DOI: 10.1103/PhysRevLett.90.131801. arXiv: hep-ex/0211064 [hep-ex] (cited on page 33).
- [91] Serguei Chatrchyan et al. “Search for fractionally charged particles in $p\bar{p}$ collisions at $\sqrt{s} = 7$ TeV”. In: *Phys. Rev.* D87.9 (2013), page 092008. DOI: 10.1103/PhysRevD.87.092008. arXiv: 1210.2311 [hep-ex] (cited on page 33).
- [92] M. Ambrosio et al. “Final search for lightly ionizing particles with the MACRO detector”. In: (2004). arXiv: hep-ex/0402006 [hep-ex] (cited on page 34).
- [93] M. Mori et al. “Search for fractionally charged particles in Kamiokande-II”. In: *Phys. Rev.* D43 (1991), pages 2843–2846. DOI: 10.1103/PhysRevD.43.2843 (cited on page 34).
- [94] G. Giacomelli and A. Margiotta. “The MACRO Experiment at Gran Sasso”. In: *Charles Peck Fest Pasadena, California, January 21, 2005*. 2007. arXiv: 0707.1691 [hep-ex] (cited on page 35).
- [95] Thomas K. Gaisser, Ralph Engel, and Elisa Resconi. *Cosmic Rays and Particle Physics*. Cambridge University Press, 2016. ISBN: 9780521016469, 9781316598917. URL: <http://www.cambridge.org/de/academic/subjects/physics/cosmology-relativity-and-gravitation/cosmic-rays-and-particle-physics-2nd-edition?format=HB> (cited on pages 37, 40, 46, 49).
- [96] The Nobel Prize. URL: <https://www.nobelprize.org/prizes/physics/1936/ceremony-speech/> (cited on page 37).

- [97] J. Clay. *Penetrating radiation*. Volume 30. 1927, pages 1115–1127 (cited on page 38).
- [98] R. A. Millikan and G. H. Cameron. “The Origin of the Cosmic Rays”. In: *Phys. Rev.* 32 (4 Oct. 1928), pages 533–557. DOI: 10.1103/PhysRev.32.533. URL: <https://link.aps.org/doi/10.1103/PhysRev.32.533> (cited on page 38).
- [99] M.H. Israel et al. “Isotopic Composition of Cosmic Rays: Results from the Cosmic Ray Isotope Spectrometer on the ACE Spacecraft”. In: *Nuclear Physics A* 758 (2005). Nuclei in the Cosmos VIII, pages 201–208. ISSN: 0375-9474. DOI: <https://doi.org/10.1016/j.nuclphysa.2005.05.038>. URL: <http://www.sciencedirect.com/science/article/pii/S037594740500686X> (cited on page 38).
- [100] Pasquale Blasi. “The Origin of Galactic Cosmic Rays”. In: *Astron. Astrophys. Rev.* 21 (2013), page 70. DOI: 10.1007/s00159-013-0070-7. arXiv: 1311.7346 [astro-ph.HE] (cited on page 39).
- [101] Thomas K. Gaisser, Todor Stanev, and Serap Tilav. “Cosmic Ray Energy Spectrum from Measurements of Air Showers”. In: *Front. Phys.(Beijing)* 8 (2013), pages 748–758. DOI: 10.1007/s11467-013-0319-7. arXiv: 1303.3565 [astro-ph.HE] (cited on pages 40, 41).
- [102] M A Malkov and L O’C Drury. “Nonlinear theory of diffusive acceleration of particles by shock waves”. In: *Reports on Progress in Physics* 64.4 (2001), page 429. URL: <http://stacks.iop.org/0034-4885/64/i=4/a=201> (cited on page 40).
- [103] “Detection of the Small Magellanic Cloud in gamma-rays with Fermi/LAT”. In: *Astron. Astrophys.* 523 (2010), A46. DOI: 10.1051/0004-6361/201014855. arXiv: 1008.2127 [astro-ph.HE] (cited on page 40).
- [104] M. Ackermann et al. “Detection of the Characteristic Pion-Decay Signature in Supernova Remnants”. In: *Science* 339 (2013), page 807. DOI: 10.1126/science.1231160. arXiv: 1302.3307 [astro-ph.HE] (cited on page 40).
- [105] W. D. Apel et al. “Kneelike structure in the spectrum of the heavy component of cosmic rays observed with KASCADE-Grande”. In: *Phys. Rev. Lett.* 107 (2011), page 171104. DOI: 10.1103/PhysRevLett.107.171104. arXiv: 1107.5885 [astro-ph.HE] (cited on page 41).
- [106] A. P. Garyaka et al. “All-particle primary energy spectrum in the 3–200 PeV energy range”. In: *J. Phys. G* 35 (2008), page 115201. DOI: 10.1088/0954-3899/35/11/115201. arXiv: 0808.1421 [astro-ph] (cited on page 41).
- [107] Kenneth Greisen. “End to the cosmic ray spectrum?” In: *Phys. Rev. Lett.* 16 (1966), pages 748–750. DOI: 10.1103/PhysRevLett.16.748 (cited on page 41).
- [108] G. T. Zatsepin and V. A. Kuzmin. “Upper limit of the spectrum of cosmic rays”. In: *JETP Lett.* 4 (1966). [*Pisma Zh. Eksp. Teor. Fiz.* 4, 114 (1966)], pages 78–80 (cited on page 41).
- [109] J. Bellido et al. “Proceedings of Science”. In: *ICRC* 301 (506 2017) (cited on page 42).
- [110] A. M. Hillas. “The Origin of Ultrahigh-Energy Cosmic Rays”. In: *Ann. Rev. Astron. Astrophys.* 22 (1984), pages 425–444. DOI: 10.1146/annurev.aa.22.090184.002233 (cited on page 42).
- [111] Pablo M. Bauleo and Julio Rodriguez Martino. “The dawn of the particle astronomy era in ultra-high-energy cosmic rays”. In: *Nature* 458N7240 (2009), pages 847–851. DOI: 10.1038/nature07948 (cited on page 43).
- [112] M. Nagano and Alan A. Watson. “Observations and implications of the ultrahigh-energy cosmic rays”. In: *Rev. Mod. Phys.* 72 (2000), pages 689–732. DOI: 10.1103/RevModPhys.72.689 (cited on page 42).
- [113] Alexander Aab et al. “Observation of a Large-scale Anisotropy in the Arrival Directions of Cosmic Rays above 8×10^{18} eV”. In: *Science* 357.6537 (2017), pages 1266–1270. DOI: 10.1126/science.aan4338. arXiv: 1709.07321 [astro-ph.HE] (cited on page 43).

- [114] E. Waxman. “IceCube’s Neutrinos: The beginning of extra-Galactic neutrino astrophysics?” In: *Proceedings, 9th Rencontres du Vietnam: Windows on the Universe: Quy Nhon, Vietnam, August 11-17, 2013.* 2013, pages 161–168. arXiv: 1312.0558 [astro-ph.HE] (cited on page 43).
- [115] P. O. Lagage and C. J. Cesarsky. “The maximum energy of cosmic rays accelerated by supernova shocks”. In: *Astron. Astrophys.* 125 (1983), pages 249–257 (cited on page 47).
- [116] T. Stanev. *High Energy Cosmic Rays*. Springer Praxis Books. Springer Berlin Heidelberg, 2010. ISBN: 9783540851486. URL: <https://books.google.be/books?id=1y9YEYHafBMC> (cited on page 47).
- [117] C. Megan Urry and Paolo Padovani. “Unified schemes for radio-loud active galactic nuclei”. In: *Publ. Astron. Soc. Pac.* 107 (1995), page 803. DOI: 10.1086/133630. arXiv: astro-ph/9506063 [astro-ph] (cited on page 47).
- [118] Robert Antonucci. “Unified models for active galactic nuclei and quasars”. In: *Ann. Rev. Astron. Astrophys.* 31 (1993), pages 473–521. DOI: 10.1146/annurev.aa.31.090193. 002353 (cited on page 47).
- [119] Demosthenes Kazanas et al. “Toward a Unified AGN Structure”. In: (2012). arXiv: 1206.5022 [astro-ph.HE] (cited on page 47).
- [120] J. Abraham et al. “Correlation of the highest-energy cosmic rays with the positions of nearby active galactic nuclei”. In: *Astropart. Phys.* 29 (2008). [Erratum: *Astropart. Phys.* 30,45(2008)], pages 188–204. DOI: 10.1016/j.astropartphys.2008.06.004, 10.1016/j.astropartphys.2008.01.002. arXiv: 0712.2843 [astro-ph] (cited on page 47).
- [121] Ray W. Klebesadel, Ian B. Strong, and Roy A. Olson. “Observations of Gamma-Ray Bursts of Cosmic Origin”. In: *Astrophys. J.* 182 (1973), pages L85–L88. DOI: 10.1086/181225 (cited on page 48).
- [122] C. A. Meegan et al. “Spatial distribution of gamma-ray bursts observed by BATSE”. In: *Nature* 355 (1992), pages 143–145. DOI: 10.1038/355143a0 (cited on page 48).
- [123] B. P. Abbott et al. “GW170817: Observation of Gravitational Waves from a Binary Neutron Star Inspiral”. In: *Phys. Rev. Lett.* 119.16 (2017), page 161101. DOI: 10.1103/PhysRevLett.119.161101. arXiv: 1710.05832 [gr-qc] (cited on page 48).
- [124] B. P. Abbott et al. “GW170814: A Three-Detector Observation of Gravitational Waves from a Binary Black Hole Coalescence”. In: *Phys. Rev. Lett.* 119.14 (2017), page 141101. DOI: 10.1103/PhysRevLett.119.141101. arXiv: 1709.09660 [gr-qc] (cited on page 48).
- [125] B.. P.. Abbott et al. “GW170608: Observation of a 19-solar-mass Binary Black Hole Coalescence”. In: *Astrophys. J.* 851.2 (2017), page L35. DOI: 10.3847/2041-8213/aa9f0c. arXiv: 1711.05578 [astro-ph.HE] (cited on page 48).
- [126] Benjamin P. Abbott et al. “GW170104: Observation of a 50-Solar-Mass Binary Black Hole Coalescence at Redshift 0.2”. In: *Phys. Rev. Lett.* 118.22 (2017). [Erratum: *Phys. Rev. Lett.* 121,no.12,129901(2018)], page 221101. DOI: 10.1103/PhysRevLett.118.221101, 10.1103/PhysRevLett.121.129901. arXiv: 1706.01812 [gr-qc] (cited on page 48).
- [127] B. P. Abbott et al. “GW151226: Observation of Gravitational Waves from a 22-Solar-Mass Binary Black Hole Coalescence”. In: *Phys. Rev. Lett.* 116.24 (2016), page 241103. DOI: 10.1103/PhysRevLett.116.241103. arXiv: 1606.04855 [gr-qc] (cited on page 48).
- [128] F. Acero. “Detection of Gamma Rays From a Starburst Galaxy”. In: *Science* 326 (2009), page 1080. DOI: 10.1126/science.1178826. arXiv: 0909.4651 [astro-ph.HE] (cited on page 48).
- [129] Niklas Karlsson. “Discovery of VHE Gamma-ray Emission from the Starburst Galaxy M82”. In: (2009). arXiv: 0912.3807 [astro-ph.HE] (cited on page 48).

- [130] Kohta Murase, Susumu Inoue, and Shigehiro Nagataki. “Cosmic Rays above the Second Knee from Clusters of Galaxies and Associated High-Energy Neutrino Emission”. In: *The Astrophysical Journal Letters* 689.2 (2008), page L105. URL: <http://stacks.iop.org/1538-4357/689/i=2/a=L105> (cited on page 48).
- [131] C. Grupen. *Astroparticle physics*. 2005. ISBN: 9783540253129. URL: <http://www.springer.com/book/3-540-25312-2> (cited on page 49).
- [132] U. F. Katz and Ch. Spiering. “High-Energy Neutrino Astrophysics: Status and Perspectives”. In: *Prog. Part. Nucl. Phys.* 67 (2012), pages 651–704. DOI: [10.1016/j.ppnp.2011.12.001](https://doi.org/10.1016/j.ppnp.2011.12.001). arXiv: [1111.0507 \[astro-ph.HE\]](https://arxiv.org/abs/1111.0507) (cited on page 51).
- [133] Morihiro Honda et al. “Calculation of atmospheric neutrino flux using the interaction model calibrated with atmospheric muon data”. In: *Phys. Rev. D* 75 (2007), page 043006. DOI: [10.1103/PhysRevD.75.043006](https://doi.org/10.1103/PhysRevD.75.043006). arXiv: [astro-ph/0611418 \[astro-ph\]](https://arxiv.org/abs/astro-ph/0611418) (cited on page 52).
- [134] M. G. Aartsen et al. “The IceCube Neutrino Observatory - Contributions to ICRC 2017 Part II: Properties of the Atmospheric and Astrophysical Neutrino Flux”. In: (2017). arXiv: [1710.01191 \[astro-ph.HE\]](https://arxiv.org/abs/1710.01191) (cited on page 53).
- [135] Kiyoshi Niu, Eiko Mikumo, and Yasuko Maeda. “A Possible Decay in Flight of a New Type Particle”. In: *Progress of Theoretical Physics* 46.5 (1971), pages 1644–1646. DOI: [10.1143/PTP.46.1644](https://doi.org/10.1143/PTP.46.1644). eprint: [/oup/backfile/content_public/journal/ptp/46/5/10.1143/ptp.46.1644/2/46-5-1644.pdf](http://oup/backfile/content_public/journal/ptp/46/5/10.1143/ptp.46.1644/2/46-5-1644.pdf). URL: <http://dx.doi.org/10.1143/PTP.46.1644> (cited on page 52).
- [136] Rikard Enberg, Mary Hall Reno, and Ina Sarcevic. “Prompt neutrino fluxes from atmospheric charm”. In: *Phys. Rev. D* 78 (2008), page 043005. DOI: [10.1103/PhysRevD.78.043005](https://doi.org/10.1103/PhysRevD.78.043005). arXiv: [0806.0418 \[hep-ph\]](https://arxiv.org/abs/0806.0418) (cited on page 53).
- [137] M. G. Aartsen et al. “Multimessenger observations of a flaring blazar coincident with high-energy neutrino IceCube-170922A”. In: *Science* 361.6398 (2018), eaat1378. DOI: [10.1126/science.aat1378](https://doi.org/10.1126/science.aat1378). arXiv: [1807.08816 \[astro-ph.HE\]](https://arxiv.org/abs/1807.08816) (cited on page 53).
- [138] Kate Scholberg. “Supernova Neutrino Detection”. In: *Ann. Rev. Nucl. Part. Sci.* 62 (2012), pages 81–103. DOI: [10.1146/annurev-nucl-102711-095006](https://doi.org/10.1146/annurev-nucl-102711-095006). arXiv: [1205.6003 \[astro-ph.IM\]](https://arxiv.org/abs/1205.6003) (cited on page 54).
- [139] Lutz Kopke. “Supernova Neutrino Detection with IceCube”. In: *J. Phys. Conf. Ser.* 309 (2011), page 012029. DOI: [10.1088/1742-6596/309/1/012029](https://doi.org/10.1088/1742-6596/309/1/012029). arXiv: [1106.6225 \[astro-ph.HE\]](https://arxiv.org/abs/1106.6225) (cited on page 54).
- [140] Aya Ishihara. “Diffuse Neutrino Fluxes and GZK Neutrinos with IceCube”. In: *JPS Conf. Proc.* 15 (2017), page 011008. DOI: [10.7566/JPSCP.15.011008](https://doi.org/10.7566/JPSCP.15.011008) (cited on page 54).
- [141] nobel1958. URL: <https://www.nobelprize.org/prizes/physics/1958/summary/> (cited on page 55).
- [142] “Design, Implementation and Test of a New Feature Extractor for the IceCube Neutrino Observatory”. In: (2010) (cited on page 58).
- [143] Paul H. Barrett et al. “Interpretation of Cosmic-Ray Measurements Far Underground”. In: *Rev. Mod. Phys.* 24.3 (1952), pages 133–178. DOI: [10.1103/RevModPhys.24.133](https://doi.org/10.1103/RevModPhys.24.133) (cited on page 60).
- [144] Dmitry Chirkin and Wolfgang Rhode. “Muon Monte Carlo: A High-precision tool for muon propagation through matter”. In: (2004). arXiv: [hep-ph/0407075 \[hep-ph\]](https://arxiv.org/abs/hep-ph/0407075) (cited on pages 61–64).
- [145] Dmitry Chirkin. “Study of South Pole ice transparency with IceCube flashers”. In: *Proceedings, 32nd International Cosmic Ray Conference (ICRC 2011): Beijing, China, August 11-18, 2011*. Volume 4, page 161. DOI: [10.7529/ICRC2011/V04/0333](https://doi.org/10.7529/ICRC2011/V04/0333) (cited on page 61).

- [146] S. R. Kelner, R. P. Kokoulin, and A. A. Petrukhin. “About cross-section for high-energy muon bremsstrahlung”. In: (1995) (cited on page 63).
- [147] AMANDA collaboration. URL: <http://amanda.uci.edu/> (cited on page 65).
- [148] E. Andres et al. “The AMANDA neutrino telescope: Principle of operation and first results”. In: *Astropart. Phys.* 13 (2000), pages 1–20. DOI: 10.1016/S0927-6505(99)00092-4. arXiv: astro-ph/9906203 [astro-ph] (cited on page 65).
- [149] J. Ahrens et al. “Observation of high-energy atmospheric neutrinos with the Antarctic Muon and Neutrino Detector Array”. In: *Phys. Rev.* D66 (2002), page 012005. DOI: 10.1103/PhysRevD.66.012005. arXiv: astro-ph/0205109 [astro-ph] (cited on page 65).
- [150] R. Abbasi et al. “The Design and Performance of IceCube DeepCore”. In: *Astropart. Phys.* 35 (2012), pages 615–624. DOI: 10.1016/j.astropartphys.2012.01.004. arXiv: 1109.6096 [astro-ph.IM] (cited on page 67).
- [151] Nicholas Choma et al. “Graph Neural Networks for IceCube Signal Classification”. In: (2018). arXiv: 1809.06166 [cs.LG] (cited on page 68).
- [152] M. G. Aartsen et al. “The IceCube Neutrino Observatory: Instrumentation and Online Systems”. In: *JINST* 12.03 (2017), P03012. DOI: 10.1088/1748-0221/12/03/P03012. arXiv: 1612.05093 [astro-ph.IM] (cited on pages 69, 71, 72).
- [153] R. Abbasi et al. “Calibration and Characterization of the IceCube Photomultiplier Tube”. In: *Nucl. Instrum. Meth.* A618 (2010), pages 139–152. DOI: 10.1016/j.nima.2010.03.102. arXiv: 1002.2442 [astro-ph.IM] (cited on page 69).
- [154] M. G. Aartsen et al. “Measurement of South Pole ice transparency with the IceCube LED calibration system”. In: *Nucl. Instrum. Meth.* A711 (2013), pages 73–89. DOI: 10.1016/j.nima.2013.01.054. arXiv: 1301.5361 [astro-ph.IM] (cited on pages 70, 76).
- [155] M. G. Aartsen et al. “The IceCube Realtime Alert System”. In: *Astropart. Phys.* 92 (2017), pages 30–41. DOI: 10.1016/j.astropartphys.2017.05.002. arXiv: 1612.06028 [astro-ph.HE] (cited on page 75).
- [156] Dariusz Góra. “High-Energy Gamma-Ray Follow-Up Program Using Neutrino Triggers from IceCube”. In: *Proceedings, 33rd International Cosmic Ray Conference (ICRC2013): Rio de Janeiro, Brazil, July 2-9, 2013*, page 0537. URL: <http://www.cbpf.br/%7Eicrc2013/papers/icrc2013-0537.pdf> (cited on page 75).
- [157] The IceCube collaboration. URL: https://wiki.icecube.wisc.edu/index.php/Pass2_Re-Processing (cited on page 76).
- [158] M. Ackermann et al. “Optical properties of deep glacial ice at the South Pole”. In: *J. Geophys. Res. Atmos.* 111.D13 (2006), page D13203. DOI: 10.1029/2005JD006687 (cited on page 76).
- [159] Dmitry Chirkin. “Evidence of optical anisotropy of the South Pole ice”. In: *Proceedings, 33rd International Cosmic Ray Conference (ICRC2013): Rio de Janeiro, Brazil, July 2-9, 2013*, page 0580. URL: <http://www.cbpf.br/%7Eicrc2013/papers/icrc2013-0580.pdf> (cited on page 77).
- [160] The IceCube Collaboration. URL: https://docushare.icecube.wisc.edu/dsweb/Get/Document-56552/dst_proposal_2011.pdf (cited on page 78).
- [161] M. G. Aartsen et al. “Search for steady point-like sources in the astrophysical muon neutrino flux with 8 years of IceCube data”. In: (2018). arXiv: 1811.07979 [hep-ph] (cited on page 78).
- [162] The IceCube Collaboration. URL: https://icecube.wisc.edu/~kjero/Bootcamp/2015/Notebooks/Reconstruction_Introduction.html (cited on page 79).

- [163] Samridha Kunwar et al. “The IceTop Scintillator Upgrade”. In: *PoS ICRC2017* (2018), page 401. DOI: 10.22323/1.301.0401 (cited on page 78).
- [164] Jan Auffenberg. “IceAct: Imaging Air Cherenkov Telescopes with SiPMs at the South Pole for IceCube-Gen2”. In: *PoS ICRC2017* (2018), page 1055. DOI: 10.22323/1.301.1055 (cited on page 78).
- [165] Satoshi Shimizu et al. “Overview and performance of the D-Egg optical sensor for IceCube-Gen2”. In: *PoS ICRC2017* (2018), page 1051. DOI: 10.22323/1.301.1051 (cited on page 79).
- [166] Lew Classen et al. “The mDOM - A multi-PMT digital optical module for the IceCube-Gen2 neutrino telescope”. In: *PoS ICRC2017* (2018), page 1047. DOI: 10.22323/1.301.1047 (cited on page 79).
- [167] M. Jeong and W. Kang. “A camera system for IceCube-Gen2”. In: *PoS ICRC2017* (2018), page 1040. DOI: 10.22323/1.301.1040 (cited on page 79).
- [168] Elisa Resconi, Kai Krings, and Kai Krings Martin Rongen. “The Precision Optical CAlibration Module for IceCube-Gen2: First Prototype”. In: *PoS ICRC2017* (2018), page 934. DOI: 10.22323/1.301.0934 (cited on page 79).
- [169] Erik Blaufuss, C. Kopper, and C. Haack. “The IceCube-Gen2 High Energy Array”. In: *PoS ICRC2015* (2016), page 1146. DOI: 10.22323/1.236.1146 (cited on page 80).
- [170] Markus Ahlers and Francis Halzen. “Pinpointing Extragalactic Neutrino Sources in Light of Recent IceCube Observations”. In: *Phys. Rev.* D90.4 (2014), page 043005. DOI: 10.1103/PhysRevD.90.043005. arXiv: 1406.2160 [astro-ph.HE] (cited on page 80).
- [171] Sebastian Euler, Javier Gonzalez, and Ben Roberts. “Simulation Studies for a Surface Veto Array to Identify Astrophysical Neutrinos at the South Pole”. In: *PoS ICRC2015* (2016), page 1070. DOI: 10.22323/1.236.1070 (cited on page 81).
- [172] Frank G. Schröder. “Radio detection of Cosmic-Ray Air Showers and High-Energy Neutrinos”. In: *Prog. Part. Nucl. Phys.* 93 (2017), pages 1–68. DOI: 10.1016/j.ppnp.2016.12.002. arXiv: 1607.08781 [astro-ph.IM] (cited on page 81).
- [173] P. Allison et al. “Performance of two Askaryan Radio Array stations and first results in the search for ultrahigh energy neutrinos”. In: *Phys. Rev.* D93.8 (2016), page 082003. DOI: 10.1103/PhysRevD.93.082003. arXiv: 1507.08991 [astro-ph.HE] (cited on page 81).
- [174] Christian Glaser. “ARIANNA: Measurement of cosmic rays with a radio neutrino detector in Antarctica”. In: *Acoustic and Radio EeV Neutrino Detection Activities (ARENA 2018) Catania, Italy, June 12-15, 2018*. 2018. arXiv: 1811.10661 [astro-ph.IM] (cited on page 81).
- [175] Don Colladay and V. Alan Kostelecky. “Lorentz violating extension of the standard model”. In: *Phys. Rev.* D58 (1998), page 116002. DOI: 10.1103/PhysRevD.58.116002. arXiv: hep-ph/9809521 [hep-ph] (cited on page 82).
- [176] M. G. Aartsen et al. “Neutrino Interferometry for High-Precision Tests of Lorentz Symmetry with IceCube”. In: *Nature Phys.* 14.9 (2018), pages 961–966. DOI: 10.1038/s41567-018-0172-2. arXiv: 1709.03434 [hep-ex] (cited on page 82).
- [177] R. Abbasi et al. “Search for a Lorentz-violating sidereal signal with atmospheric neutrinos in IceCube”. In: *Phys. Rev.* D82 (2010), page 112003. DOI: 10.1103/PhysRevD.82.112003. arXiv: 1010.4096 [astro-ph.HE] (cited on page 82).
- [178] M. G. Aartsen et al. “Search for Neutrinos from Dark Matter Self-Annihilations in the center of the Milky Way with 3 years of IceCube/DeepCore”. In: *Eur. Phys. J.* C77.9 (2017), page 627. DOI: 10.1140/epjc/s10052-017-5213-y. arXiv: 1705.08103 [hep-ex] (cited on page 83).

- [179] M. G. Aartsen et al. “Search for annihilating dark matter in the Sun with 3 years of IceCube data”. In: *Eur. Phys. J.* C77.3 (2017), page 146. DOI: 10.1140/epjc/s10052-017-4689-9. arXiv: 1612.05949 [astro-ph.HE] (cited on page 83).
- [180] R. Abbasi et al. “Limits on a muon flux from Kaluza-Klein dark matter annihilations in the Sun from the IceCube 22-string detector”. In: *Phys. Rev.* D81 (2010), page 057101. DOI: 10.1103/PhysRevD.81.057101. arXiv: 0910.4480 [astro-ph.CO] (cited on page 83).
- [181] M. G. Aartsen et al. “First search for dark matter annihilations in the Earth with the IceCube Detector”. In: *Eur. Phys. J.* C77.2 (2017), page 82. DOI: 10.1140/epjc/s10052-016-4582-y. arXiv: 1609.01492 [astro-ph.HE] (cited on page 83).
- [182] “Quantised singularities in the electromagnetic field,” in: *Proceedings of the Royal Society of London A: Mathematical, Physical and Engineering Sciences* 133.821 (1931), pages 60–72. ISSN: 0950-1207. DOI: 10.1098/rspa.1931.0130. eprint: <http://rspa.royalsocietypublishing.org/content/133/821/60.full.pdf>. URL: <http://rspa.royalsocietypublishing.org/content/133/821/60> (cited on page 83).
- [183] G.’t Hooft. “Magnetic monopoles in unified gauge theories”. In: *Nuclear Physics B* 79.2 (1974), pages 276–284. ISSN: 0550-3213. DOI: [https://doi.org/10.1016/0550-3213\(74\)90486-6](https://doi.org/10.1016/0550-3213(74)90486-6). URL: <http://www.sciencedirect.com/science/article/pii/0550321374904866> (cited on page 83).
- [184] Alexander M. Polyakov. “Particle Spectrum in the Quantum Field Theory”. In: *JETP Lett.* 20 (1974). [,300(1974)], pages 194–195 (cited on page 83).
- [185] M. G. Aartsen et al. “Search for non-relativistic Magnetic Monopoles with IceCube”. In: *Eur. Phys. J.* C74.7 (2014), page 2938. DOI: 10.1140/epjc/s10052-014-2938-8. arXiv: 1402.3460 [astro-ph.CO] (cited on page 84).
- [186] D Schultz. “IceProd 2: A Next Generation Data Analysis Framework for the IceCube Neutrino Observatory”. In: *Journal of Physics: Conference Series* 664.6 (2015), page 062056. URL: <http://stacks.iop.org/1742-6596/664/i=6/a=062056>.
- [187] Ralph Engel et al. “Towards the next generation of CORSIKA: A framework for the simulation of particle cascades in astroparticle physics”. In: (2018). arXiv: 1808.08226 [astro-ph.IM].
- [188] Giuseppe Battistoni et al. “Overview of the FLUKA code”. In: *Annals Nucl. Energy* 82 (2015), pages 10–18. DOI: 10.1016/j.anucene.2014.11.007.
- [189] Askhat Gazizov and Marek P. Kowalski. “ANIS: High energy neutrino generator for neutrino telescopes”. In: *Comput. Phys. Commun.* 172 (2005), pages 203–213. DOI: 10.1016/j.cpc.2005.03.113. arXiv: astro-ph/0406439 [astro-ph].
- [190] M. G. Aartsen et al. “Observation of High-Energy Astrophysical Neutrinos in Three Years of IceCube Data”. In: *Phys. Rev. Lett.* 113 (2014), page 101101. DOI: 10.1103/PhysRevLett.113.101101. arXiv: 1405.5303 [astro-ph.HE].
- [191] C. Andreopoulos et al. “The GENIE Neutrino Monte Carlo Generator”. In: *Nucl. Instrum. Meth.* A614 (2010), pages 87–104. DOI: 10.1016/j.nima.2009.12.009. arXiv: 0905.2517 [hep-ph].
- [192] Costas Andreopoulos et al. “The GENIE Neutrino Monte Carlo Generator: Physics and User Manual”. In: (2015). arXiv: 1510.05494 [hep-ph].
- [193] M. Honda et al. “Atmospheric neutrino flux calculation using the NRLMSISE-00 atmospheric model”. In: *Phys. Rev.* D92.2 (2015), page 023004. DOI: 10.1103/PhysRevD.92.023004. arXiv: 1502.03916 [astro-ph.HE].
- [194] Joerg R. Hoerandel. “On the knee in the energy spectrum of cosmic rays”. In: *Astropart. Phys.* 19 (2003), pages 193–220. DOI: 10.1016/S0927-6505(02)00198-6. arXiv: astro-ph/0210453 [astro-ph].

- [195] Thomas K. Gaisser. “Spectrum of cosmic-ray nucleons, kaon production, and the atmospheric muon charge ratio”. In: *Astropart. Phys.* 35 (2012), pages 801–806. DOI: 10.1016/j.astropartphys.2012.02.010. arXiv: 1111.6675 [astro-ph.HE].
- [196] G. D. Barr et al. “Three-dimensional calculation of atmospheric neutrinos”. In: *Phys. Rev. D* 70 (2 July 2004), page 023006. DOI: 10.1103/PhysRevD.70.023006. URL: <https://link.aps.org/doi/10.1103/PhysRevD.70.023006>.
- [197] Mario Dunsch et al. “Recent Improvements for the Lepton Propagator PROPOSAL”. In: (2018). arXiv: 1809.07740 [hep-ph].
- [198] Johan Lundberg et al. “Light tracking for glaciers and oceans: Scattering and absorption in heterogeneous media with Photonics”. In: *Nucl. Instrum. Meth.* A581 (2007), pages 619–631. DOI: 10.1016/j.nima.2007.07.143. arXiv: astro-ph/0702108 [ASTRO-PH].
- [199] K. J. Ma et al. “Time and Amplitude of Afterpulse Measured with a Large Size Photomultiplier Tube”. In: *Nucl. Instrum. Meth.* A629 (2011), pages 93–100. DOI: 10.1016/j.nima.2010.11.095. arXiv: 0911.5336 [physics.ins-det].
- [200] J. Ahrens et al. “Muon track reconstruction and data selection techniques in AMANDA”. In: *Nucl. Instrum. Meth.* A524 (2004), pages 169–194. DOI: 10.1016/j.nima.2004.01.065. arXiv: astro-ph/0407044 [astro-ph].
- [201] M. G. Aartsen et al. “Improvement in Fast Particle Track Reconstruction with Robust Statistics”. In: *Nucl. Instrum. Meth.* A736 (2014), pages 143–149. DOI: 10.1016/j.nima.2013.10.074. arXiv: 1308.5501 [astro-ph.IM].
- [202] IceCube collaboration. URL: https://internal-apps.icecube.wisc.edu/reports/data/icecube/2014/04/001/icecube_201404001_v1.pdf.
- [203] Stef Verpoest. URL: https://lib.ugent.be/fulltxt/RUG01/002/479/620/RUG01-002479620_2018_0001_AC.pdf.
- [204] Till Neunhoffer. “Estimating the angular resolution of tracks in neutrino telescopes based on a likelihood analysis”. In: *Astropart. Phys.* 25 (2006), pages 220–225. DOI: 10.1016/j.astropartphys.2006.01.002. arXiv: astro-ph/0403367 [astro-ph].
- [205] URL: https://wiki.icecube.wisc.edu/index.php/SLC_hit_cleaning.
- [206] URL: <https://www.dissertations.se/dissertation/fef1f8e4ba/>.
- [207] Yoav Freund and Robert E Schapire. “A Decision-Theoretic Generalization of On-Line Learning and an Application to Boosting”. In: *Journal of Computer and System Sciences* 55.1 (1997), pages 119–139. ISSN: 0022-0000. DOI: <https://doi.org/10.1006/jcss.1997.1504>. URL: <http://www.sciencedirect.com/science/article/pii/S00220009791504X>.
- [208] S. Fink C. Böser and S. Röcker. *Introduction to boosted decision trees: A multivariate approach to classification problems*. Presented at the KSETA Doctoral Workshop, Berlin, Germany. July 2014.
- [209] Hanchuan Peng, Fuhui Long, and C. Ding. “Feature selection based on mutual information criteria of max-dependency, max-relevance, and min-redundancy”. In: *IEEE Transactions on Pattern Analysis and Machine Intelligence* 27.8 (Aug. 2005), pages 1226–1238. ISSN: 0162-8828. DOI: 10.1109/TPAMI.2005.159.
- [210] The IceCube collaboration. URL: <https://docushare.icecube.wisc.edu/dsweb/Get/Document-56551/VEFproposal.pdf>.
- [211] The IceCube collaboration. URL: https://docushare.icecube.wisc.edu/dsweb/Get/Document-59303/lowup_2012_proposal.pdf.
- [212] The IceCube collaboration. URL: https://docushare.icecube.wisc.edu/dsweb/Get/Document-59906/MuonFilter2012_v3_with_addendum.pdf.

- [213] The IceCube collaboration. URL: <https://docushare.icecube.wisc.edu/dsweb/Get/Document-59728/onlinel2proposal2012.pdf>.
- [214] The IceCube collaboration. URL: <https://docushare.icecube.wisc.edu/dsweb/Get/Document-59397/DeepCoreFilterProposal.pdf>.
- [215] IceCube collaboration. URL: https://wiki.icecube.wisc.edu/index.php/Effects_of_DOM_Mainboard_Release_443.
- [216] S. Verpoest. “Search for particles with fractional charges in IceCube based on anomalous energy loss”. Master’s thesis. UGent, 2018.
- [217] J. Künnen. “A Search for Dark Matter in the Center of the Earth with the IceCube Neutrino Detector”. Master’s thesis. VUB, 2015.
- [218] R. J. Britto, B. S. Acharya, and G. C. Anupama. “Data analysis method for the search of point sources of gamma rays with the HAGAR telescope array”. In: *Proceedings, 32nd International Cosmic Ray Conference (ICRC 2011): Beijing, China, August 11-18, 2011*. Volume 9, page 142. DOI: 10.7529/ICRC2011/V09/0943.
- [219] M. G. Aartsen et al. “Searches for Relativistic Magnetic Monopoles in IceCube”. In: *Eur. Phys. J.* C76.3 (2016), page 133. DOI: 10.1140/epjc/s10052-016-3953-8. arXiv: 1511.01350 [astro-ph.HE].
- [220] F. Scheriau. “Data-Mining in der Astroteilchenphysik”. Master’s thesis. University of Dortmund, 2014.
- [221] Gary J. Feldman and Robert D. Cousins. “A Unified approach to the classical statistical analysis of small signals”. In: *Phys. Rev.* D57 (1998), pages 3873–3889. DOI: 10.1103/PhysRevD.57.3873. arXiv: physics/9711021 [physics.data-an].
- [222] Gary C. Hill and Katherine Rawlins. “Unbiased cut selection for optimal upper limits in neutrino detectors: The Model rejection potential technique”. In: *Astropart. Phys.* 19 (2003), pages 393–402. DOI: 10.1016/S0927-6505(02)00240-2. arXiv: astro-ph/0209350 [astro-ph].
- [223] Aaron Roodman. “Blind analysis in particle physics”. In: *eConf* C030908 (2003). [,166(2003)], TUIT001. arXiv: physics/0312102 [physics.data-an].